Spatiotemporal variability of fugitive gas migration emissions around a petroleum well

Neil Fleming[1], Tiago Morais[1], Ulrich Mayer[2], and M. Cathryn Ryan[1]

[1]University of Calgary
[2]University of British Colombia

November 23, 2022

Abstract

Well integrity failure resulting in migration of natural gas outside of the surface casing can cause atmospheric greenhouse gas emissions and groundwater quality impacts from existing and historic energy wells. Spatial and temporal variability in gas migration can result in errors in detection (i.e., presence/absence) and efflux estimations. This field-based case study used automated dynamic closed chambers to record repeated (˜ every 18 minutes) CO2 and CH4 efflux measurements over a two-week period around a single petroleum production well in Alberta, Canada. Long-term efflux measurements supplemented soil gas compositional and isotopic characterization, along with surface concentration measurements. Effluxes were spatially concentrated around the wellhead and only occasionally detectable more than a few meters away. Estimated total emissions attributable to gas migration ranged from 48 - 466 g CH4 d-1 (or 0.07 - 0.7 m3 CH4 d-1). Methane effluxes and concentrations were temporally variable on second-to-hourly and diel scales. Multivariate stepwise regression analysis indicates that multiple meteorological factors, particularly wind speed and air temperature, were related to the temporal variability. Despite temporal variability, elevated concentrations and effluxes were consistently detectable around the well. Major soil gas composition suggests that gas migration near the wellhead causes advective displacement of soil gas, while more distal measurements are indicative of episodic and diffusion-dominated transport. Values of 13C-CO2 and 13C-CH4 samples were consistent with CH4¬ oxidation within the unsaturated zone. Although these results reflect a single well, the findings are salient to gas migration detection and emission estimation efforts.

Spatiotemporal variability of fugitive gas migration emissions around a petroleum well

N.A. Fleming, * T.A. Morais, K.U. Mayer, M.C. Ryan

N.A. Fleming, * T.A. Morais, and M.C. Ryan, Geoscience, Univ. of Calgary, 2500 University Drive NW, Calgary AB, T2N 1N4, Canada; K.U. Mayer Earth, Ocean and Atmospheric Sciences, Univ. of British Colombia, 2007 Main Mall, Vancouver BC, V6T 1Z4, Canada. *Corresponding author (naflemin@ucalgary.ca)

ABSTRACT

Well integrity failure resulting in migration of natural gas outside of the surface casing can cause atmospheric greenhouse gas emissions and groundwater quality impacts from existing and historic energy wells. Spatial and temporal variability in gas migration can result in errors in detection (i.e., presence/absence) and efflux estimations. This field-based case study used automated dynamic closed chambers to record repeated (~ every 18 minutes) CO_2 and CH_4 efflux measurements over a two-week period around a single petroleum production well in Alberta, Canada. Long-term efflux measurements supplemented soil gas compositional and isotopic characterization, along with surface concentration measurements. Effluxes were spatially concentrated around the wellhead and only occasionally detectable more than a few meters away. Estimated total emissions attributable to gas migration ranged from 48 - 466 g CH_4 d^{-1} (or 0.07 - 0.7 m^3 CH_4 d^{-1}). Methane effluxes and concentrations were temporally variable on second-to-hourly and diel scales. Multivariate stepwise regression analysis indicates that multiple meteorological factors, particularly wind speed and air temperature, were related to the temporal variability. Despite temporal variability, elevated concentrations and effluxes were consistently detectable around the well. Major soil gas composition suggests that gas migration near the wellhead causes advective displacement of soil gas, while more distal measurements are indicative of episodic and diffusion-dominated transport. Values of ^{13}C-CO_2 and ^{13}C-CH_4

 https://doi.org/10.1016/j.apr.2021.101094

samples were consistent with CH_4 oxidation within the unsaturated zone. Although these results reflect a single well, the findings are salient to gas migration detection and emission estimation efforts.

KEYWORDS

Gas Migration; Methane; Well Integrity; Stray Gas; Fugitive Emissions; Meteorological Effects

1. INTRODUCTION

Energy well integrity issues are a topic of increasing focus among government and industry practitioners, spurred in part by increased drilling activity in regions now accessible due to multi-stage hydraulic fracturing and concern of the growing environmental and economic liability of inactive and abandoned wells (Alboiu & Walker 2019; Jackson et al., 2013; Schiffer et al., 2020). Well integrity issues include gas migration outside the surface casing (GM), where a subsurface source of natural gas typically migrates from a shallow or intermediate gas-charged stratigraphic interval to ground surface (Figure 1; Rowe & Muehlenbachs, 1999, Tilley & Muehlenbachs, 2012). The "surface casing" of energy wells is generally installed to a depth below the base of non-saline groundwater protection (typically 100-300 m; Dusseault and Jackson, 2014). The annulus between progressively smaller diameter casings is typically cemented between the casing and the borehole (e.g., Alberta Energy Regulator, 2020; Bachu, 2017). Leakage pathways which result in gas migration are generally understood to be due either to defects in the cement itself, or between the cement and the borehole or one of the casings (Bachu, 2017; Dusseault and Jackson, 2014). Fugitive, or migrating, gases are typically primarily methane (CH_4), often with minor amounts of ethane, propane, and other volatile hydrocarbons (Tilley & Muehlenbachs, 2012; Szatowski et al., 2002).

Gas migration impacts can include atmospheric emissions, groundwater water quality perturbations, and land use interference. Methane is a greenhouse gas with a global warming potential 25 times more potent by mass than carbon dioxide over a period of 100 years (and 84 times that of CO_2 over a 20-year period; IPCC, 2013). Specific focus on decreasing methane emissions from the upstream petroleum sector is included in global efforts to decrease anthropogenic greenhouse gas emissions (IPCC 2013). For example, the Alberta oil and gas

industry intends to reduce 2012 methane emission rates by 45% by 2025 (Government of Alberta). Specific concern for GM also arises since, in some instances, gases migrate through non-saline (i.e., total dissolved solids less than 4000 mg L^{-1}; Alberta Energy Regulator 2021) groundwater. Dissolved methane can alter chemical conditions of groundwater, specifically its redox state, perturbing the indigenous microbial community, potentially altering pH, mobilizing metals, forming hydrogen-sulfide gas, or later exsolving when groundwater is pumped to the surface for residential or commercial use (Cahill et al., 2017; Gorody, 2012; Kelly et al., 1985; Roy et al., 2016). Should these exsolved gases accumulate in pumphouses, residences, or other facilities, explosive or asphyxiating atmospheres may develop (Engelder & Zevenbergen, 2018). Finally, GM may cause impacts or limitations on land usage since excess methane and/or carbon dioxide may displace oxygen in soil gas and impact plant or crop health. GM also has the potential for generating a dangerous or explosive atmosphere, necessitating setbacks for built structures (Noomen et al., 2012; Sihota et al., 2013; Williams & Aitkenhead, 1991). Although gas migration has only been reported for 0.73% of all wells in the province of Alberta (n > 450,000 wells in total; Bachu, 2017), a recent review concluded gas migration testing has only been required in 3.5% of Alberta's energy wells (Abboud et al., 2020). Methane emission distributions are often heavily skewed by a small number of 'super-emitter' sources that comprise a large proportion of the total emissions (Brandt et al., 2014; Saint-Vincent et al., 2020; Zavala-Araiza et al., 2015). Previous work suggests that emissions specific to GM in Alberta follow this same distribution, where a smaller number of wells have the highest GM emission rates and contribute disproportionately to total emission volumes (Erno & Schmitz, 1996).

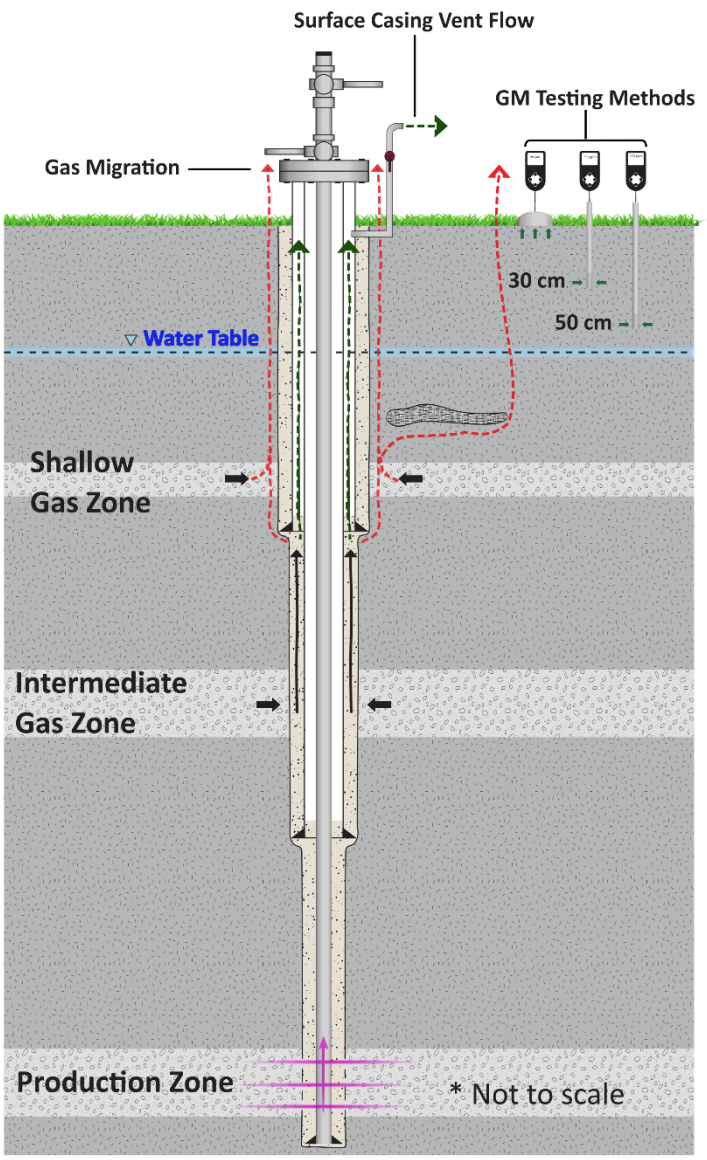

Figure 1 Conceptual model of gas migration (GM) and surface casing vent flow (SCVF) (After Bachu, 2017). Migrating gases (CH_4 and other light hydrocarbons) originate from an intermediate or shallow gas producing formation and travel to the surface either wholly outside the casing (GM; red) or also within the outermost casing annulus (SCVF; green). Common testing depths for detecting the presence of GM through combustible gas and/or CH_4 concentration measurements include ground-surface detection, or at a specified depth (usually > 30 cm threshold requiring ground disturbance permitting despite the 'recommended' 50 cm depth (Alberta Energy Regulator, 2021; Fleming et al., 2019).

A significant fraction of Alberta's energy wells will require GM testing before they can be abandoned (Abboud et al., 2020). If GM is found, repair is required prior to legal abandonment,

presenting an economic liability to industry (Alberta Energy Regulator, 2021). While requirements vary depending on jurisdiction, an effective and reliable approach to measure presence/absence of GM and estimate emission rates is needed to manage GM around petroleum wells. Tests for the presence/absence of GM are often conducted by sequential snapshot measurement of near-surface combustible gas concentrations at multiple points around a well, over a total GM test duration of less than one hour (Alberta Energy Regulator, 2021; Szatowski et al., 2002). The recommended test point spacing by the Alberta Energy Regulator includes a total of 14 measurement points, with two within 30 cm of the wellbore and then at 2, 4, and 6 m away in a cross pattern. Measurement depths are recommended as 50 cm, though measurements are often completed at ground surface or some intermediate subsurface depth (< 30 cm) that does not require ground disturbance permitting (Figure 1; Alberta Energy Regulator, 2021; Fleming et al., 2019; Province of Alberta, 2020). The efficacy of the recommended gas migration testing method has not been fully validated (Abboud et al., 2020). Recent surveys of methane efflux measurements around industry gas wells (Forde et al., 2019a; Lyman et al., 2020; Riddick et al., 2020), and in field injection experiments (Cahill et al., 2017; Forde et al., 2018) have revealed substantial variability of measured concentrations and effluxes, both spatially and temporally on seasonal, diel, and short-term (30 minute) time scales, potentially complicating reliable detection and emission rate estimations.

Several causal mechanisms explain the spatiotemporal variability of migrating gases. Within the saturated zone, subsurface heterogeneity and the presence of capillary barriers will trap buoyant free gas and cause fingered lateral and vertical movement and eventual episodic release when free gas pressure and buoyancy forces overcomes viscous forces and capillary entry pressures (Gorody, 2012; Steelman et al., 2017; Van de Ven et al., 2020; Woods & Norris 2016).

Dissolution and oxidation decrease migrating free phase gas quantities reaching the water table, to varying degrees depending on geochemical conditions and free-gas interfacial area (Cahill et al., 2017; Roy et al., 2016; Van de Ven et al., 2020). Heterogeneity in the unsaturated zone also leads to variable advective and diffusive gas effluxes (Ulrich et al., 2019). Barometric pressure decreases cause a pressure differential between the soil gas and atmosphere and therefore increased gas efflux across the soil-atmosphere interface, especially in thicker unsaturated zones (Forde et al., 2019b; Kovach, 1945). Wind-induced soil gas transport can be significant, where higher wind speeds (and related turbulence-induced pressure fluctuations) induce short-term variations in advective efflux (Poulsen & Møldrup, 2006; Poulsen et al., 2017; Redeker et al., 2015). Advective or diffusive mixing of migrating gases of deep subsurface origin (such as CH_4, C_2H_6, He) and gases of primarily atmospheric origin (O_2, Ar), produce identifiable soil gas mixtures (Frederick et al., 2017). Particularly in a thick unsaturated zone, microbial oxidation can consume enough methane to decrease or entirely obscure the GM surface expression, resulting in diagnostic carbon isotope fractionation (Forde et al., 2018; McMahon et al. 2018; Rowe & Muehlenbachs, 1999; Schout et al., 2019).

In summary, spatially and temporally variable CH_4 efflux and concentrations have been observed around energy wells, and field injection and laboratory studies have revealed some of the causal mechanisms. While episodic subsurface migration and varying meteorological factors such as barometric pressure, wind speed, and temperature can explain some of the variation, there is limited temporal and spatial discretization of measurements of gas migration effluxes and concentrations around energy wells. In addition, temporal variability is not assessed in the context of the standard of practice for GM testing. Industry tests for the presence of GM and further quantification of emissions, as well as the need to quantify the GM contribution to

atmospheric emissions, water quality perturbations, and land use impacts, will benefit from field-validation of the conceptual understanding of the behavior and spatiotemporal variability of migrating gases.

We present findings of spatiotemporal efflux and concentration variability around an established petroleum well known to have gas migration, with a view to recommending an effective field test for GM detection and efflux estimation. High-resolution efflux and concentration data and statistical analysis results relate external factors that may be driving changes in measured CH_4 efflux and concentration. Spatial efflux surveys and soil gas samples establish relationships and spatial trends in migrating gases and in-soil processes of oxidation, atmospheric mixing, and atmospheric displacement. The implications of these findings are discussed in terms of atmospheric methane emissions and the standard of practice for GM detection using currently practiced and proposed techniques.

2. MATERIALS AND METHODS

2.1 Field site description

An industry partner provided access to an anonymous site with known gas migration outside the outermost casing, at a conventional (non-thermal) petroleum production well that was drilled and completed using standard practices for non-horizontal wells after 1995. The status of this well is 'suspended' (i.e., idle, not actively producing oil or gas but with no decommissioning work completed). No additional methane emission sources beyond those attributed to GM are expected at the site. No SCVF was measured by the well operator, and no other surface and subsurface methane leakage sources are located near the well (verified through site inspection and spot concentration measurements performed by the authors). The well is located within Alberta Energy Regulator's 'Required Test Area' where a high instance of GM has been identified

(Alberta Energy Regulator, 2021; Figure 3a). Historic gas migration test results were provided by the operator for 14 GM testing events conducted by the site operator (8 tests) and service providers (6 tests) using industry-accepted methods (Alberta Energy Regulator, 2021) over >10 years (Figure 2). The GM measurement spacings generally followed the Alberta Energy Regulator's 'recommended' method (described above). Specific details of historic sampling, including sampling equipment and measurement depth, were not provided, and may have differed depending on testing party (Alberta Energy Regulator, 2021; Fleming et al., 2019). The maximum methane concentration measured across all (n = 14) historic GM testing events averaged 18,000 ppm (std. dev. = 30,000 ppm), demonstrating substantial variation in maximum concentrations between test occasions.

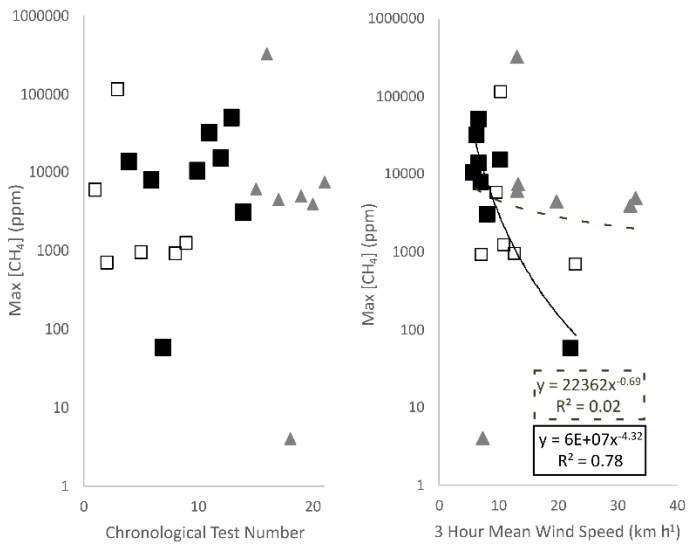

Figure 2 The maximum recorded combustible gas concentration as ppm CH_4 (log scale) from all available gas migration testing conducted at the study well. Historic tests conducted by one individual field operator are indicated as filled squares, and tests conducted by various service companies are empty squares. Tests conducted by the authors are shown as gray triangles. Results are shown in chronological order of testing date (left) and as a function of wind speed (using mid-day (11:00 to 14:00 hrs) data from the nearest weather station 10-20 km from study site; right). Trendlines are shown on all tests conducted (R^2=0.02; dashed line) and for those conducted by the same individual well operator (R^2= 0.78; black line).

A shallow water table ~0.6 m below ground surface (BGS; with +/- 0.3 m seasonal fluctuations) was identified by water monitoring wells hand-installed by the authors. The water table slope was consistent with an approximately southward groundwater flow direction. Slug and permeameter testing yielded a hydraulic conductivity at shallow depth (< 2 m) of $3x10^{-6}$ m s^{-1}. Fine silty-sand was observed down to two meters (the depth at which hand auger lithology samples were collected). Nearby water well records suggest unconsolidated sediments are present to about 10m depth, below which sedimentary bedrock occurs. Additional site details are reserved to protect site anonymity.

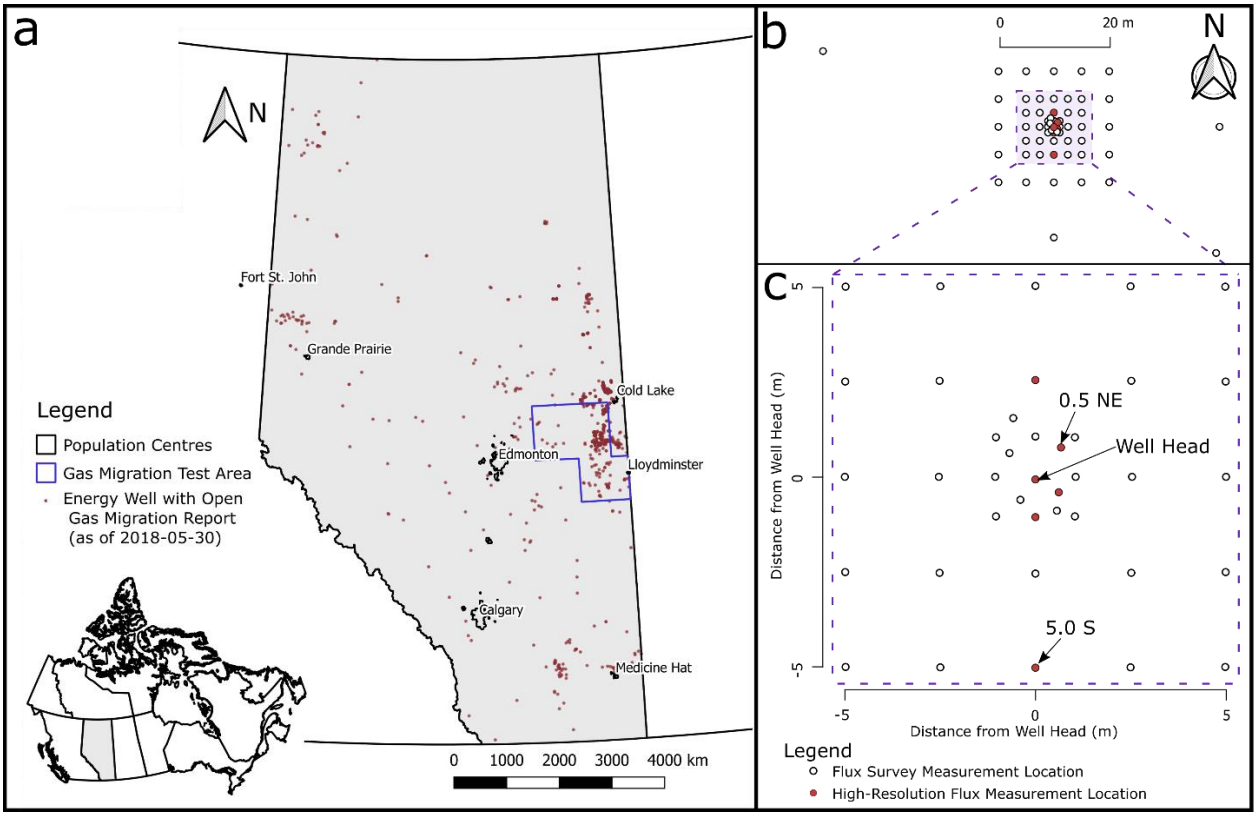

Figure 3 a) Overview of Alberta with all petroleum wells with open (i.e., detected but not repaired) reports of external gas migration as of 2018-05-30 (n = 1186), with the majority of these reported cases located on the eastern side of central Alberta in the region around Lloydminster and Cold Lake. The Alberta Energy Regulator Directive 20 gas migration Required Test Area outlined in blue is the only location provincially in which gas migration testing is currently mandated on all wells (Alberta Energy Regulator, 2021). Data from Alberta Energy Regulator (2018) and Statistics Canada (2016). b) Full scale and c) close-up plan view

schematic of the efflux monitoring network at the study well pad, showing locations of flux survey chambers (open circles). The location of repeat sampling and high-resolution efflux measurements over a two-week period (October 11th-27th 2019 are shown as red circles, labelled by distance and direction from the wellhead).

2.2 Methane concentration measurements using standard industry practices

Combustible gas concentrations were surveyed with a handheld detector (GT-43, Gas Measurement Instruments Ltd.) on soil surface (using a bell probe) and at 30 cm depth (with a slide-hammer gas vapor probe; Retract-A-Tip Gas Vapor Probe, AMS Inc.) on five separate occasions at recommended spacings (Alberta Energy Regulator, 2021). The handheld detector is representative of commonly available portable gas detectors in use, where multiple integrated sensors (thermal conductivity, semiconductor, catalytic bead) detect combustible hydrocarbon gases (CH_4, C_2H_6, etc.) across a wide range of concentrations (Szatowski et al., 2002). The sensors are calibrated to CH_4, and the sensor response to all combustible gases is reported in concentrations of CH_4 by ppm, % of the Lower-Explosive Limit (LEL) of methane (~5% v/v), or % gas by volume depending on sensed concentration (Gas Measurement Instruments, 2016). Using the three integrated sensors, the reported measurement resolution for CH_4 is 1 ppm in the <10,000 ppm range, 1% LEL in the <100% LEL range, and 1% gas by volume in the 1% to 100% volume range (Gas Measurement Instruments, 2016).

2.3 Soil gas sampling and analysis

Soil gas samples were collected from shallow soil vapor wells on five occasions (Feb 22, Jul 11, Aug 22-23, Sep 25, Oct 27, 2019). The soil vapor wells were constructed using 6.4 mm (1/4”) ID polyethylene plastic tubing with a Luer stopcock-valve fitting (Masterflex) and geotextile filter cloth covering a 10 cm perforated screen at the bottom. Vapor wells were installed at depths of 10 cm and 30 cm below ground surface by insertion of pre-constructed soil vapor wells into

diagonally drilled holes with soil allowed to collapse around the tubing. The 10 and 30 cm depths was selected based on inferred applicability to commercial gas migration testing procedures, with 30 cm being the maximum depth of observation permitted for subsurface sampling without the added expense of ground disturbance permitting (Province of Alberta, 2020). Previous attempts at installation of deeper soil vapor wells (0.5 and 1.0 m) resulted in saturation and clogging due to the shallow (0.3 to 0.8 m BGS over the observation period) water-table at the site. Prior to sampling, 20 mL of stale gas was purged from the vapor well tubing using a syringe (representing more than 3 tubing volumes removed). Following purging, a 60 mL soil gas sample was collected and injected through the butyl septa of a 30 mL helium-flushed and partially evacuated glass vial until the vial was overpressured. Syringe withdrawal rates were < 2 mL s^{-1} to limit atmospheric contamination and influx along the tubing. Soil gas samples were also obtained on Oct 21, 2018 using a slide-hammer probe (Retract-A-Tip Gas Vapor Probe, AMS Inc.) and stored in fully evacuated vials (in contrast to helium-flushed vials in other sampling events), permitting analysis of the He content of soil gas).

Major gas species were analysed by injecting a 5 mL gas sample aliquot into a Scion 450/456 four-channel gas chromatograph fitted with four separate sample loops, analytical columns, and detectors. The dedicated fourth channel separated and quantified argon-oxygen, with a lower detection limit of 50 ppm argon. The fourth channel used an MXT-Molsieve 5A analytical column (30m x 0.53mm, 50um film thickness) held at a constant temperature of 30°C, a 50µl sample loop, hydrogen carrier gas (constant flow 1.0 mL/min), and a Thermal Conductivity Detector (Filament Temperature 250 °C). Certified gas standards were used to calibrate the gas chromatograph immediately prior to analyses. Analytical precision and accuracy for all gases is typically better than ±2.5% of the reported concentration, and the reported lower detection limit

for alkanes (C1 to C5) is approximately 0.5 ppm. Isotope composition was measured using gas chromatography-isotope ratio mass spectrometry methods to determine $\delta^{13}C$ on CO_2, CH_4, and C_2H_6 (C2; ethane) on nine selected soil gas samples and six dissolved gas samples that met concentration thresholds (0.1% of the gas species of interest) (Humez et al., 2016). Two samples were analysed for $\delta^{2}H$ on CH_4 for additional gas source identification. Analyses were performed on a ThermoFisher MAT 253 isotope ratio mass spectrometer coupled to Trace GC Ultra + GC Isolink (ThermoFisher). All samples are reported in ‰ notation with respect to VPDB for $\delta^{13}C$ and VSMOW for $\delta^{2}H$. Lab reported accuracies are ±0.5 ‰ $\delta^{13}C$ and ±2 ‰ $\delta^{2}H$. All compositional and isotopic analyses were conducted at the University of Calgary Applied Geochemistry and Isotope Science Laboratories.

The composition and isotopic signatures of soil gases have previously been used to interpret the origins and near-surface interactions of migrating gases. Helium is routinely used as a noble trace gas associated with deep geologic origin, such as around natural CO_2 and CH_4 seeps, fault zones, and in gas migration leakage scenarios (Annunziatellis et al., 2008; Frederick et al., 2017; Wen et al., 2016). Similarly, elevated concentrations of higher alkanes (ethane, C2; propane, C3; etc.), are indicative of deeper gas origins since these gases are not considered to be co-produced during microbial methanogenesis that might occur in wetlands or surface aquifers (Bachu, 2017; Kang et al., 2014; Whiticar, 1999). Isotope ratios of $\delta^{13}C$ on CH_4, C2¸and CO_2 can also all be used to distinguish gas sources since diagnostic isotopic fractionation will occur during the source formation of these gases (Tilley & Muehlenbachs, 2012; Szatowski et al., 2002; Whiticar, 1999) and during their transport over geologic time (Hendry et al., 2017). In shallow groundwater and soil gas, argon can originate from both atmospheric sources, and the ultimate geogenic source of most argon on Earth, where ^{40}Ar is produced in the subsurface through the

radioactive decay of ^{40}K. However, any Ar in younger groundwater and soil gas systems (<20,000 years) can be presumed to originate from atmospheric sources due to the negligibly low abundance and long half life of the ^{40}K source (Almon and Magaritz, 1990). Therefore, Ar is used here as a noble gas tracer in shallow soil and groundwater systems, alongside other primarily atmospheric gases such as N_2 and O_2 (Almon and Magaritz, 1990; Martin et al., 1995; Frederick et al., 2017). Carbon dioxide can co-occur with CH_4 as a component of migrating subsurface natural gas, be produced during the microbial oxidation of methane, or during natural biologic respiration in soils (Romanak et al., 2014; Whiticar, 1999). Isotopic $\delta^{13}C_{CO2}$ values, and soil gas compositional trends, are used here to infer CO_2 origins (Risk et al., 2013; Romanak et al., 2014; Sandau et al., 2019).

2.4 Soil gas efflux measurements

Near-surface gas concentrations and effluxes were measured in two efflux survey and sampling events (Aug 20, 2019 and Sep 25, 2019) and one high-resolution long-term sampling event (Oct 11-27, 2019). Automated long-term and survey chambers measured spatial and temporal distributions of carbon dioxide and methane effluxes using the same equipment and approach previously described (Forde et al., 2018; Sihota et al., 2013). Soil efflux collars (20 cm tall, 200 mm internal-diameter SDR pipe segments) were installed in the soil to approximately 15 cm depth more than 24 hours before the initial survey measurements. During the two-week intensive measurements, a multiplexer (LI-8150, LI-COR Inc) switched between six long-term dynamic closed chambers (LI-8100-104, LI-COR Inc.) with chamber concentrations analyzed at 1 Hz with an infra-red gas analyzer (Li-8100, LI-COR Inc.) and an ultra-portable greenhouse gas analyzer (model 915-0011, Los Gatos Research Inc.). During each survey event, an efflux survey chamber (LI-8100-103, LI-COR Inc.) connected to the same two analysers was manually moved

between 51 different collar locations (Figure 3b). A custom wellhead collar (16 cm radius from the outermost well casing, total ground surface area 0.44 m^2) measured GM effluxes in the previously identified high-efflux zone immediately outside the surface casing (Figure S1). This custom collar fully encircled the well and was sealed against the intermediate casing below the wellhead. The long-term chamber closure times ranged from 15 to 90 seconds, switching sequentially between all 6 chambers with appropriate pre- and post-purge times, at around 18 minutes per cycle (Table S1).

Conservative CH_4 and CO_2 effluxes were calculated with linear curve fitting of chamber closure time vs. concentration in SoilFluxPro (LI-COR Biosciences; Forde et al., 2018; Sihota et al., 2013). The minimum detectable efflux (MDF) was calculated with conservative detector analytical accuracies taken to be $\Delta C = 0.2$ ppm for CH_4 and $\Delta C = 1$ ppm for CO_2, which is consistent with similar measurements at controlled injection gas migration study sites (Table S1; Christiansen et al., 2015; Forde et al., 2019a, 2019b). Manufacturer-reported instrumental accuracies are < 2 ppb for CH_4 (Los Gatos Research) and <1 ppm for CO_2 (LI-COR Inc).

The pre-closure concentrations of CH_4 and CO_2 within each chamber during each efflux measurement were taken as conservative estimates of the ground-surface concentrations at that moment and location. Use of these concentration 'initial values' from each automated efflux measurement as a proxy for measured concentrations using standard GM detection methods was validated by direct comparison between the two approaches using the same analyser. Immediately before each Aug 20, 2019 efflux survey measurement, the pre-closure concentrations were recorded within the chamber, and using the same gas analysers with a custom-fit bell-probe held against the soil surface adjacent to the outside of the collar. This procedure imitates standard industry practice for ground-surface concentration measurement

(e.g., DP-IR, Gas Measurement Instruments Ltd.; Irwin, INFICON; etc.). The moderately good positive correlation between the two methods (Spearman Rank R^2 = 0.48, m=0.85 on n= 48 measurement) at concentrations of < 3 ppm, validates use of initial chamber concentrations as a conservative estimate of ground-surface concentrations that would be obtained with industry-practiced detection techniques.

2.5 Environmental measurements

Soil moisture sensors (HydraProbe, Stevens Water Monitoring Systems Inc.) recorded hourly averaged temperature, electrical conductivity, water content, and apparent dielectric content to a datalogger (CR1000, Campbell Scientific Inc.) between July and November 2019 at six locations (depths of 5 and 30 cm, and distances of 1.0, 2.5, and 6.0 m East of the wellhead). Soil temperatures were also monitored using small sensors (TidbiT, Onset Computer Corporation) affixed with wire into countersunk holes in a softwood post at soil depths of 0, 0.1, 0.3, 0.5, 1.0 and 1.5 m BGS at locations 1.0 m East, and 6.0 m East of the wellhead between July 9 and November 18, 2019. Three additional temperature sensors were installed at 0.25 m North of the wellhead (immediately outside the wellhead efflux chamber) at depths of 0, 0.1 and 0.3 m for the duration of the October 11-27 measurement period. Water levels were recorded hourly in two piezometers with screens centered 1.0 m BGS, located 1.25 and 10 m South of the wellhead.

Precipitation and wind speed data were retrieved from the nearest public weather station (10 to 20 km away; exact distance withheld for confidentiality reasons) (Alberta Agriculture and Forestry). During this period, there was good regional correlation (averaging 0.86) between the 2 m height average wind speeds for the five nearest publicly available weather stations within a 50 km radius of the study site. Atmospheric pressures and temperatures were recorded hourly on-site (Barologger Edge, Solinst Canada Ltd.). Earth tide data (cm vertical displacement) over the

measurement period was estimated with site-specific coordinates using open software (Milbert, 2018). Change rates of water level and barometric pressure were calculated using a weighted five-hour central difference with three-hour rolling median smoothing (selected as the shortest window that eliminated hour-to-hour noise and produced visually smooth change rates).

2.6 Descriptive statistics of CH_4 and CO_2 concentration and efflux analysis

2.6.1 Regression modelling

Data processing and statistical analysis were conducted in the software package R (R Project version 4.0.2) with figures generated primarily using the ggplot2 package (R Core Team, Wickham, 2016). Linear interpolation was used to match the environmental data (typically recorded hourly) to times of efflux measurement. Thirteen environmental factors from the auxiliary data were considered for potential explanation of temporal variation in effluxes and concentration at each of the six chamber locations. These factors included: relative humidity, absolute barometric pressure, atmospheric temperature, approximate barometric pressure change rate, piezometer water level, approximate water level change rate, soil temperature at 0.05 m and 0.3 m BGS, soil water content at 0.05 m and 0.3 m BGS, temperature difference between the atmosphere and 0.3 m soil depth, vertical earth tide displacement, and wind speed.

Stepwise generalized additive regression models were used to identify the most important environmental predictors of temporal efflux and concentration variation by assessing the statistical relationships to the explanatory environmental factors (Hastie, 2019; Hastie & Tibshirani, 1990; Oliveira et al., 2018). Generalised additive regression models consider the combined (i.e., additive) linear or nonlinear (i.e., generalised) statistical relationships between multiple predictor variables (e.g., wind speed, atmospheric temperature, barometric pressure) and a response variable such as CH_4 efflux (Hastie & Tibshirani, 1990). In contrast to multivariate

linear regression, this method is advantageous for natural systems since it allows for nonlinear relationships between predictor and response variables to be described by a smooth function (Chen et al., 2019). In this analysis, parameter relationships could be represented as either linear, or a 2nd or 3rd order smoothed curve.

The relative statistical importance of each explanatory variable was assessed by building the model sequentially (i.e., in a forward stepwise fashion), with a single predictor variable being added at each step (Oliveira et al., 2018). Beginning with no explanatory factors, at each step the chosen algorithm sequentially added the single predictor variable which caused the largest increase to model performance. Continuous addition of all predictor variables may eventually lead to addition of irrelevant variables, overfitted models of excessive complexity, and weaker general predictive capacity. Excess model complexity was prevented here by optimising model performance towards the lowest possible Akaike Information Criterion (AIC) at each step (Akaike, 1974). A decreased AIC is produced by a model with better fit to the data, analogous to an increase in the model R^2. An increased AIC is produced by a model with greater complexity, such as a model with extraneous parameters or a statistical relationship described with a 2nd order curve when a linear fit is adequate (Hastie, 2019). Following this algorithm, the stepwise addition of model parameters stopped when further model fit would be achieved at the expense of excessive complexity. This type of statistical model analysis allows for identification of relationships between explanatory and response variables in complex data series with multiple potential interactions, however the results must be compared to existing scientific literature to ensure they are sensible (Chen et al., 2019).

2.6.2 Geostatistical interpolation

The relationship between flux magnitude and distance from the wellhead was first assessed through the Spearman rank correlation coefficient. The Spearman correlation describes non-linear relationships by correlating the relative rank rather than absolute magnitude. Total methane gas emissions from gas migration were then estimated by interpolating the CH_4 effluxes from August and September spatial surveys across the 20 m by 20 m measurement grid using Empirical Bayesian Kriging and Inverse Distance Weighting methods in ArcMap (ESRI). These two methods of spatial efflux interpolation were chosen for comparison based on their previous application in the related field of landfill gas emissions (Abichou et al., 2006; Börjesson et al., 2000; Spokas et al., 2003;), and elsewhere in the environmental geosciences (Annunziatellis et al., 2008; Cardellini et al., 2003). In this application, both kriging and IDW methods rely on the assumption that locations more closely spaced will have more similar effluxes than locations further apart (Börjesson et al., 2000). Inverse distance weighting is a deterministic method where the flux value at each interpolation location is calculated based on nearby measured values, weighted directly by the distance to the measurement points. Kriging can more optimally relate a predicted value to nearby measured points using a semi-variogram that most closely describes the site-specific distance-efflux relationship for all measured data. The predicted values in the kriged interpolation are based on both the distance and direction to the measured points, which may account for anisotropy and a non-uniform relationship between distance and efflux (Spokas et al., 2003).

The geospatial mean of the interpolated surfaces were used to generate an estimate of total methane emissions related to gas migration across the gridded area (Abichou et al., 2006), and the error associated with the interpolation using a 95% CI in the case of the kriged interpolation.

Emissions attributable to gas migration were also estimated with the previously published practice using the arithmetic mean efflux of all points measured within a 3 m radius of the wellhead, applied to the area within this radius (Erno & Schmitz, 1996). Finally, total emissions from directly within the wellhead chamber were calculated using the ground-surface area of the wellhead chamber, 0.42 m^2, multiplied by the mean efflux rate.

3. RESULTS

3.1 Methane concentration surveys:

Combustible gas concentrations measured using the handheld sensor were highest, and generally consistently detected, at ground surface only within one meter of the wellhead (Figure S. 2), while subsurface (30 cm depth) combustible gas was detected at higher concentrations and further distances (Figure S3). These gas concentrations had a similar spatial distribution and concentration range to the industry-provided GM test results (Figure 2), which also showed highest concentrations near the wellhead. Concentration measurements indicated that the only source of elevated combustible gas was from within the soil, with no indication of emissions from SCVF or other internal well integrity failure. During repeated site visits, there were no consistent sensory indications of the presence of GM, including an absence of visually obvious vegetation stress such as stunted, dead or discolored plants.

3.2 Gas efflux survey result

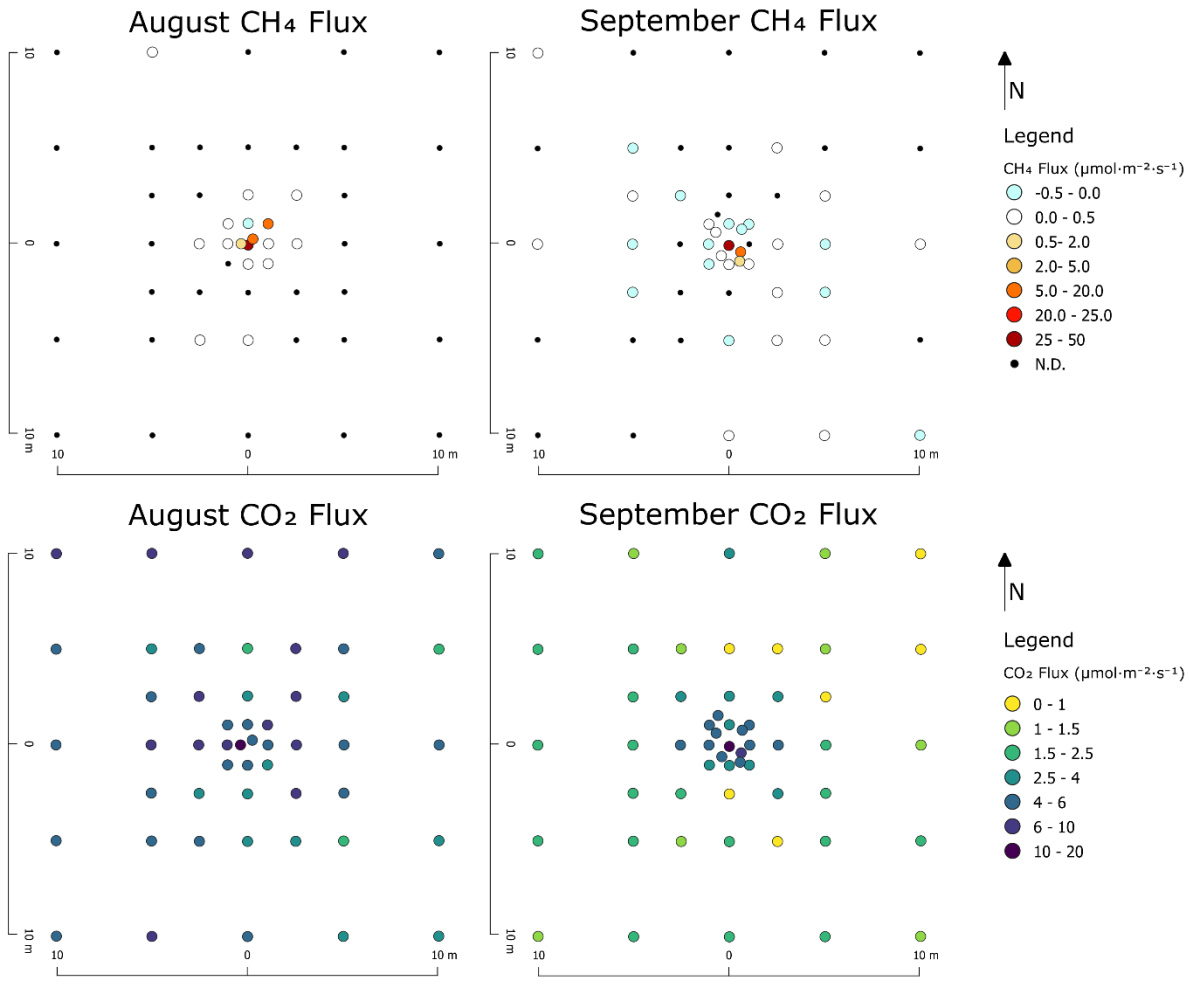

Figure 4 Plan view of efflux survey results for CH_4 (top row) and CO_2 (bottom row) measured in μmol m^2 s^{-1} on Aug 20, 2019 (PM; left hand side) and Sep 25. 2019 (AM; right hand side). Detection limits are generally 0.08 μmol m^2 s^{-1} CO_2 and 0.02 μmol m^2 s^{-1} CH_4. The horizontal distance from the wellhead is shown in scale bars.

Higher CO_2 effluxes were also observed around the wellhead, especially during the September efflux survey (Figure 4). Methane effluxes were substantially greater immediately around the wellhead, and some positive effluxes (emitting CH_4 from the soil into the atmosphere) were detected up to 10 m from the wellhead. Many effluxes (66% and 36% of measurements in August and September respectively), including some within meters of the wellhead, were less

than the detection limit (0.02 µmol CH_4 m^{-2} s^{-1}). Several sampling locations in September registered low-rate negative effluxes indicating CH_4 consumption occurred in the soil zone.

Considering data from both surveys, there was an inverse Spearman rank correlation with distance from the wellhead and CH_4 efflux across the entire measurement grid, and poor inverse correlation with distance and CO_2 efflux (r = -0.73, -0.17 for CH_4 and CO_2 respectively). Spearman correlation analyses were preferred to Pearson correlations since the former more appropriately described the nonlinear decline in effluxes with radial distance from the well. The estimated total CH_4 emissions from gas migration varied depending on measurement period and the method used (Table 4). There was a 62% increase in mean GM-related methane efflux in the wellhead chamber between the October dataset considering all measurements across the two-week measurement period (n=1215) and a subset when only considering times with wind speeds less than 3 km h^{-1} (< 0.83 m s^{-1}, thus reducing the observations to n =243; Table 4; Figure S12).

3.3 High frequency efflux measurement

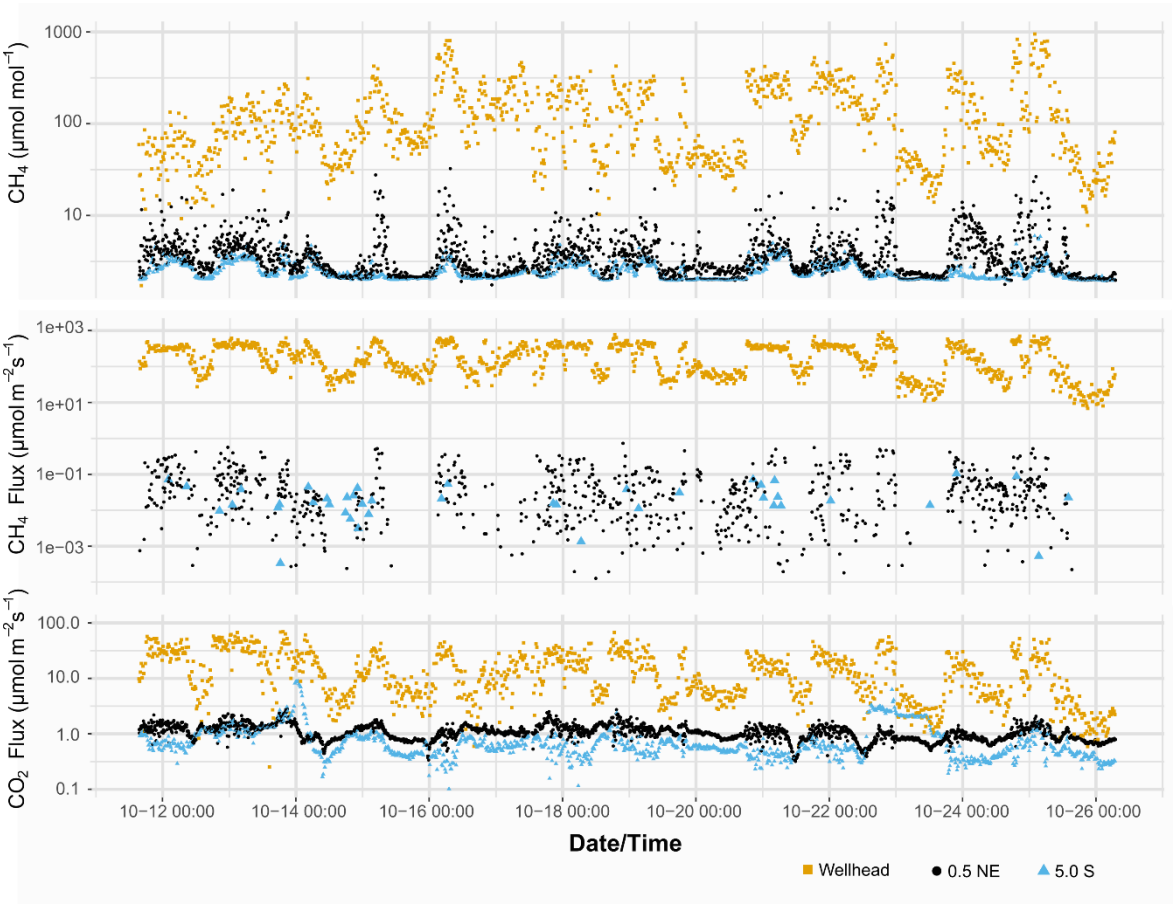

Figure 5 Time series of measured chamber pre-closure CH_4 concentrations (µmol mol^{-1}), CH_4 effluxes (µmol m^{-2} s^{-1}), and CO_2 effluxes (µmol m^{-2} s^{-1}) for three locations with high resolution measurement: at the wellhead (yellow squares), 0.5 m NE (black circles) and 5.0 m South of the wellhead (blue triangles).

The initial CH_4 concentrations at the wellhead chamber were always above the values at 5.0 m South of the wellhead, though the difference fluctuated from 10 to > 100 ppm CH_4 and the distinction was less clear during some periods (e.g. mid-day; Figure 5). Initial concentrations of CH_4 for other long-term chambers, including two located only 0.5 m from the wellhead, were approximately similar to the 5.0 South location, though slightly higher during peak flux periods (Table 1). Initial CH_4 concentrations at 5.0 South ranged between minimum and maximum values of 2.0 and 5.5 ppm CH_4, (5th percentile 2.07 ppm, 95th 4.33 ppm). Despite the higher CO_2

efflux at the wellhead, the pre-closure CO_2 concentration was not substantially different between chambers, ($R^2 > 0.9$) (Figure S5).

Table 1 Descriptive statistics of Oct 11-27th, 2019 high resolution efflux measurement series with chamber locations described in distance (m) and direction from the gas migration petroleum well. Confidence intervals calculated at 95% with bootstrapping methods and presented as (lower, upper).

	---------- CH_4 Efflux---------- ---			-- CO_2 Efflux --	CO_2 Efflux: CH_4 Efflux Linear Correl. Coeff (R)	CH_4 Concentration	Total Obs.
Chamber Location	Mean	SD	Detectable Obs.	Mean		Mean	n
	------- µmol m^{-2} s^{-1} ------		%	- µmol m^{-2} s^{-1} -	--	--- ppm ---	---
Wellhead	219 (210, 230)	197.2	100	16.4 (15.5, 17.3)	0.86	146 (138, 153)	1212
0.5 SE	1.25 (1.14, 1.35)	2.3	93	1.97 (1.93, 2.02)	0.51	6.22 (6.00, 6.42)	1216
0.5 NE	0.04 (0.04, 0.05)	0.8	47	1.08 (1.06, 1.09)	0.15	3.72 (3.62, 3.82)	2431
1.0 S	0.07 (0.06, 0.08)	1.0	40	1.27 (1.24, 1.30)	0.12	3.94 (3.74, 4.14)	1215
2.5 N	0.01 (0.00, 0.01)	0.3	11	0.87 (0.85, 0.89)	0.12	2.65 (2.60, 2.69)	1215
5.0 S	0.00 (0.00, 0.01)	0.3	8	0.84 (0.79, 0.89)	-0.19	2.48 (2.45, 2.51)	1214

3.4 Multivariate regression modelling of high-resolution methane efflux and concentration measurements

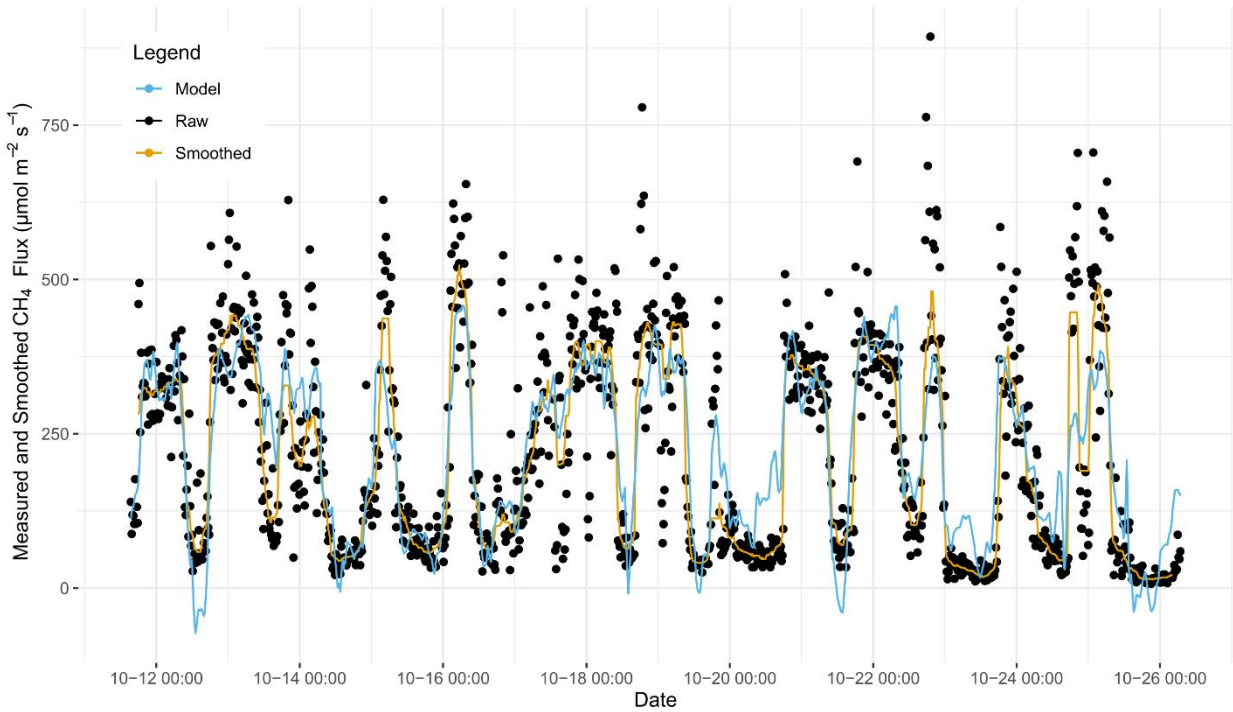

Figure 6 Wellhead chamber time series of CH_4 efflux from Oct 11-27th, 2019 with raw data (black dots), 20-point rolling median smoothing (yellow line) and multivariate regression modelling results (blue).

The two-week high resolution efflux monitoring period showed strong temporal variability, including diel variation with higher measured pre-closure concentrations and effluxes generally occurring overnight (Figure 5), and differences between consecutive measurements and stepped efflux behavior during chamber closure (Figure S6). Stepwise multivariate regression modelling results indicate that the quasi-diel patterns in observed gas migration concentrations and effluxes at the wellhead over the October 11-27th measurement period were most strongly related to varying wind speed and atmospheric temperature. Minor model contributions by other factors, including temperature at 30 cm depth, were considered in a final regression model including eight of the 13 possible environmental factors that explained 63% of the temporal variation in

wellhead CH_4 efflux (and 81% of smoothed efflux; Figure 6, Table S3). Wind speed was the most important parameter, and could explain 44% of the variation in measured CH_4 efflux at the wellhead (59% of smoothed efflux). Wellhead chamber CH_4 efflux was negatively correlated with wind speed (Pearson Correlation R = -0.72) and atmospheric temperatures (Pearson Correlation R = -0.49).

At all chamber locations, wind speed was the most important single predictor of temporal variation in CH_4 pre-closure concentration, and therefore first added factor to the stepwise model (Table 2). Wind speed was also the most important single addition to model R^2 at four out of the six chamber locations (Table S5). Other common relevant factors for CH_4 concentration models included change in barometric pressure, atmospheric temperature, and shallow soil water content or temperature. Compared to the CH_4 concentration regression models, the CH_4 efflux regression models (Table S3, Table S4) had less consistency in significant factors across all modelled chamber locations. However, wind speed and atmospheric temperature, or the differential in temperature between the atmosphere and soil, were assigned the highest priority by the model at 5 of 6 locations. Other lower priority (but statistically significant) factors included in the regression models for CH_4 efflux included groundwater levels and soil water contents (Table S4).

Table 2 Parameters most influencing the statistical model for the first three steps of forward stepwise multivariate generalized additive modelling of pre-closure CH_4 chamber concentrations at each long-term location. Model formulae are in the form: $[CH_4]$ = Parameter$_1$ + Parameter$_2$ …. The Akaike information criterion (AIC) is listed below the formulae at each step, with a decreasing AIC indicating an incrementally increasing goodness of fit. Environmental parameters abbreviations are: U_wind (windspeed), Wat.Cont_0.3 (30 cm depth soil water content), T_soil_0.05 (soil temperature at 5 cm depth), Baro_dP_dt (approximated barometric pressure change rate), T_atm (atmospheric temperature), E_tide (vertical component earth tide displacement).

Chamber Location	Model Step:1	Model Step:2	Model Step:3
Wellhead	U_wind ; 15200	Wat.Cont_0.3 + U_wind ; 15059	Baro_dP_dt + Wat.Cont_0.3 + U_wind ; 14985
0.5 SE	U_wind ; 6451	Baro_dP_dt + U_wind ; 6423	Baro_dP_dt + s(U_wind, df* = 2) ; 6405
0.5 NE	U_wind ; 11258	T_soil_0.05 + U_wind ; 11139	Baro_dP_dt + T_soil_0.05 + U_wind ; 11112
1.0 S	U_wind ; 6368	s(U_wind, df = 2) ; 6326	E_tide + s(U_wind, df = 2) ; 6308
2.5 N	U_wind ; 2816	T_soil_0.05 + U_wind ; 2708	T_soil_0.05 + s(U_wind, df = 2) ; 2676
5.0 S	U_wind ; 1789	T_atm + U_wind ; 1542	T_atm + Wat.Cont_0.3 + U_wind ; 1480

*df refers to the degrees of freedom of the smooth fitting function (1 if not indicated)

3.5 Soil Gas analysis results

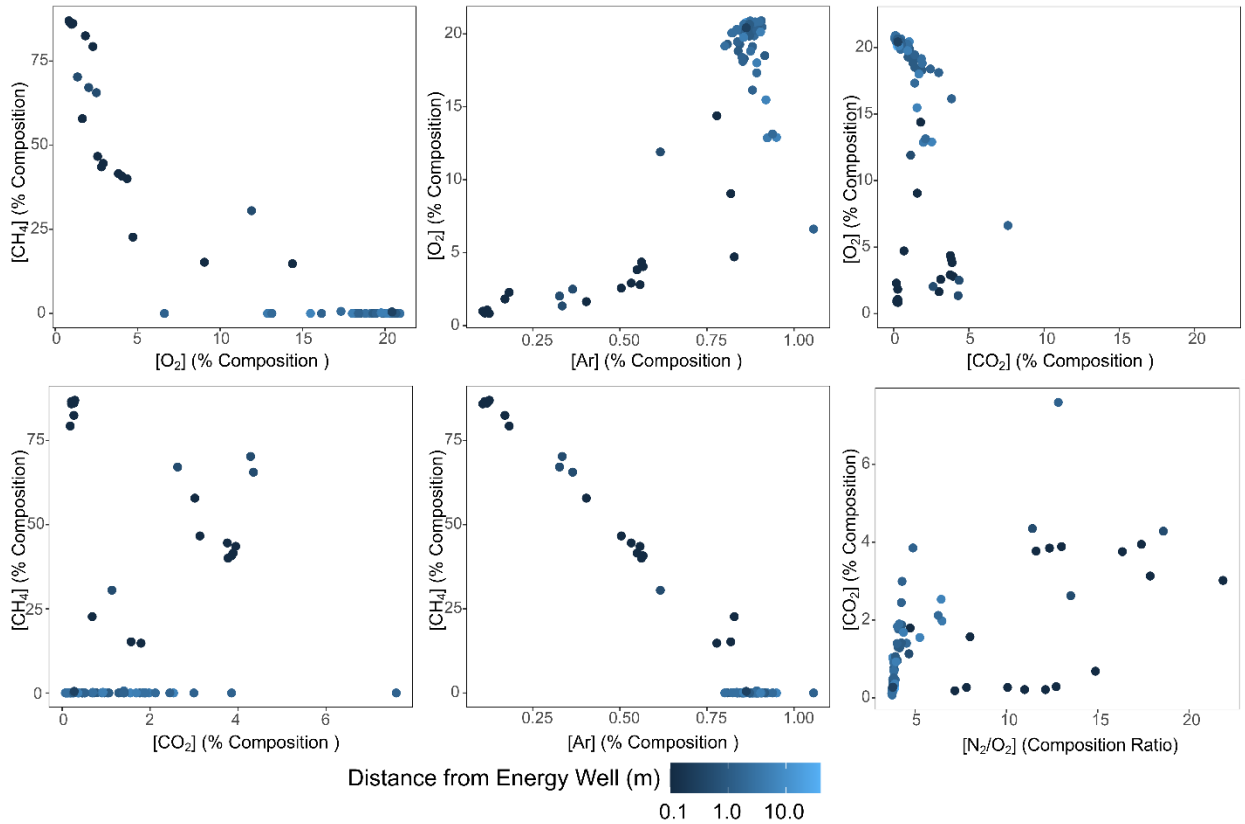

Figure 7 Selected scatterplot distributions of soil gas results at the 30 cm depth across five sampling events (% composition by volume), with lighter colors corresponding to increasing radial distance from the energy well.

Table 3 Pearson correlation matrix of soil gas compositions at the 30 cm depth around the gas migration test well.

	Ar	*N_2*	*O_2*	*CO_2*	*CH_4*
Ar	1	0.99	0.85	-0.12	-0.99
N_2		1	0.87	-0.15	-1.00
O_2			1	-0.51	-0.91
CO_2				1	0.21

The highest CH_4 concentration measured was 87% v/v, collected immediately outside the surface casing at a depth of 30 cm in November (i.e., early winter); this sample also contained CO_2 at 0.289 % v/v and He at 306 ppm. Across all samples, there was a relatively linear negative relationship between CH_4 and Ar (Figure 7). The O_2-Ar and O_2-CH_4 relationship was non-linear, with proportionally lower O_2 concentrations in most samples relative to direct mixtures of atmospheric and migrating gases. Further from the well, the soil gases contained generally lower concentrations of CH_4 and trace He, and higher concentrations of Ar, O_2, and N_2. Moderately positively correlations between CH_4 and CO_2 (Table 3) indicate CO_2 may be associated with migrating gases; however, the highest concentration CH_4 samples have lower concentrations of both CO_2 and Ar in comparison to samples with slightly lower CH_4 concentrations (Table S2). Several samples of soil CH_4 concentrations within < 5 m from the wellhead were as low as < 5 ppm CH_4. Some subsurface gas samples with deep gas signatures (including elevated CH_4, C2 and higher alkanes, and He) were detected up to 10 m from the well. Near the wellhead, soil gas samples had a high CH_4 content and low N_2 and Ar. CH_4 correlated very well with He (R^2 = 0.99) and the total concentration of higher alkanes, sum C_2-C_5, (R^2 = 0.87). Isotopic analyses of high concentration CH_4 samples nearest the wellhead had signatures of $\delta^{13}C_{CH4}$ = -60.7 ‰, $\delta^{13}C_{C2H6}$ = -45.0 ‰, $\delta^{2}H_{CH4}$ = -232 ‰, consistent with previous soil gas analyses conducted by the well owner (not shown). All soil gas samples (n=9) with CH_4 concentrations high enough for isotopic analysis (> 0.1% v/v CH_4) were within 0.5 m from the wellhead (Table S2). Analyses of $\delta^{13}C_{CO2}$ on these same gas samples ranged from -64.2 to -42.7 ‰. The $\delta^{13}C_{CH4}$ value rose as the concentration of CH_4 decreased relative to CO_2 (Figure S7).

4. DISCUSSION

4.1 Gas source and mixing implications

Trends and ratios in the isotopic composition and concentration of fixed gas indicators can be combined to infer mixing between two end-members soil gas sources and redox processes (Frederick et al., 2017; Romanak et al., 2014; Sandau et al., 2019). The presence of He and higher alkanes with methane, in addition to the carbon isotope ratios of $\delta^{13}C_{CH4}$, $\delta^{13}C_{C2}$ and $\delta^{2}H_{CH4}$, are diagnostic of migrating deeper or intermediate-zone thermogenic gases (Annunziatellis et al., 2008; Frederick et al., 2017). Isotopic and compositional 'fingerprints' of SCVF or GM gases can be compared with compositional depth profiles of gases sampled during drilling in nearby wells to estimate the stratigraphic source of the gas. Comparison of the isotope values of methane and ethane at this study well to four published isotope depth profiles in the region (Rowe & Muehlenbachs, 1999; Szatowski et al., 2002), indicate that the source of migrating gases at this study well may be ~300-400 m BGS.

While the saturated soils observed at the site provide conditions suitable for shallow natural (biogenic) CH_4 production (Romanak et al., 2014; Tokida et al., 2007; Whiticar, 1999), several results suggest there is not a significant biogenic CH_4 source at this site. Firstly, ethane, propane, higher alkanes, and helium are indicative of a deeper thermogenic methane, and gases are not co-produced during biogenic methane production (Kang et al., 2014). Similarly, the carbon isotope composition of CH_4 (and CO_2 near the wellbore) indicate a non-biogenic source (Kang et al., 2014; Szatowski et al., 2002; Romanak et al., 2014; Whiticar, 1999). Though the well pad is located near wetland areas, the maximum recorded methane efflux rates are higher than previously published rates in natural wetland settings (Tokida et al., 2007; Kang et al., 2014).

Considering the above observations and findings by previous authors, at this site CH_4, C2-C5, and He are interpreted to originate from a deeper gas migration source, while N_2, Ar and O_2 are interpreted to have primarily atmospheric origins (Annunziatellis et al., 2008; Frederick et al., 2017; Sandau et al., 2019). Since Ar is biologically inert, it provides a 'tracer' of atmospheric gases. The generally linear Ar-CH_4 relationship suggests a two end-member mixing model between methane and Ar, with dilution and displacement of atmospheric gas near the wellhead (Frederick et al., 2017). The non-linear correlations between O_2 and other gas species reflects its biological consumption and production.

4.2 Spatial distribution of migrating gases

Elevated CH_4 concentrations and efflux around the wellhead indicated a preferential migration zone. During the long-term measurements, the average CH_4 efflux at the 0.44 m^2 chamber encircling the wellhead was approximately two orders of magnitude greater than the next highest measured location at 0.5 m SE (Table 1). While the wellhead chamber extended > 15 cm beyond the edge of the surface casing, concentration surveys repeatedly indicated that the highest measured surface CH_4 concentrations (and therefore likely also the highest efflux) occurred immediately outside the casing (Figure S2). The observed spatial distribution supports the dominance of vertically acting buoyancy forces on gas transport in the saturated zone, and a higher gas permeability near the well in both the saturated and unsaturated zones (Van de Ven et al., 2020). Fracturing or disturbance of the rock within the formation during drilling, and the subsequent cementation challenges, are generally understood to result in micro-annuli between the cement and casing or cement and formation, causing the zone along the well casing to be a preferential migration pathway with lower capillary entry pressure to migrating free-phase gas (D'Aniello et al., 2020; Dusseault & Jackson, 2014).

Excluding the subset of highest effluxes and concentrations immediately adjacent to the wellhead, effluxes at ground surface, and surface and in-soil gas concentrations, were not uniformly lower with increasing radial distance (0.5 to 5 m) from the interpreted preferential migration pathway immediately outside the outermost casing. Spatial variability in gas effluxes and concentrations measured at the soil surface are known to exist due to subsurface heterogeneity and lateral migration underneath capillary barriers in the saturated zone (Forde et al., 2019a; Steelman et al., 2017; Van de Ven & Mumford, 2020) as well as preferential gas movement in the unsaturated zone (Chamindu Deepagoda et al., 2016; Mitton, 2018). This spatially variable distribution of migrating gases, with higher effluxes and concentrations closer to the well, rapidly decreasing to low or intermittently non-detectable values, confirms findings by several previous authors (Erno & Schmitz, 1996; Forde et al., 2019a; Lyman et al., 2020; Smith et al., 2019).

The rate and shape of concentration increase curves within the closed efflux chambers over time (Figure S6) varied spatially. Advective efflux was suggested by rapid linear concentration increases at high efflux locations, regardless of concentration gradients, while a low-rate exponential concentration increase indicative of diffusive efflux was observed at collars more distal to the preferential migration pathway (similar to finding by Forde et al., 2019a; Sihota et al., 2013). Occasional stepwise concentration increases suggest ebullition events (Figure S6).

The total number of CH_4 efflux measurements above the minimum detectable efflux ranged from 100% at the wellhead chamber down to 8% at 5.0 South (Table 1), suggesting that the gas migration pathway outside the outermost casing can be characterized as a relatively continuous transport pathway, while further away the transport of gas through the saturated zone shifted to a transitional or discontinuous flow regime, as was observed by Van de Ven et al. (2020) in lab

experiments. The spatial distribution of soil gas composition, detectable effluxes, and efflux curve behavior indicates primarily advection-driven gas transport from the gas source depth, along the well-casing preferential migration pathway to the atmosphere, with more intermittent and diffusive flow at greater distances from the wellhead (similar to observations by Chamindu Deepagoda et al., 2016).

Both heterogeneity in efflux patterns and short-term variation in effluxes over the two-hour spatial survey may have also introduced some apparent spatial variation since individual 90 second closures may have captured ebullition events or periods of higher efflux at some locations but not others. This spatial heterogeneity resulted in a poor spatial autocorrelation of CH_4 effluxes which introduced a large degree of uncertainty in the interpolated effluxes used to estimate total emissions (Table 4).

4.3 Total CH_4 emissions and other impacts

Total gas migration CH_4 emissions across the full measurement grid was estimated to be 466 g d^{-1} (non-detectable to 2590 g d^{-1} at 95% CI) in August and 229 g d^{-1} (non-detectable to 1750 g d^{-1} at 95% CI) in September using Bayesian kriging interpolation methods. Emissions averaged 129 g d^{-1} from the wellhead chamber over the 15-day high resolution measurement period (Table 4). While multi-day emissions directly around the wellhead reasonably predicted GM emission magnitude, the sum of low-rate diffusive effluxes applied across the 20 m by 20 m measurement area centered on the well did contribute significantly to the total estimated emissions from GM. Poor spatial autocorrelation of CH_4 effluxes resulted in substantial uncertainty in interpolation and therefore large total emissions estimate error through kriging methods (Figure S8). Emission estimates at the lower and upper 95% confidence intervals were non-detectable to 2590 and non-detectable to 1750 g CH_4 d^{-1} for August and September, respectively. This uncertainty indicates

the potential for error in estimates of total GM emissions at other sites when using point efflux measurements. Total GM emission estimates compared similarly when using Inverse Distance Weighting interpolation or the mean efflux applied to a three-meter radius around the well (after Erno & Schmitz, 1996), while Bayesian kriging estimates were higher (Table 4). High-resolution multi-day measurements were more likely than single sampling events to capture higher magnitude GM methane effluxes, which tended to occur over night during periods with low wind velocities, resulting in order of magnitude higher estimated effluxes for long-term chamber measurements compared to the snapshot survey measurements (Table 4).

Despite the uncertainty in emission estimates, the average of the two kriged spatial survey estimates, at 350 g CH4 d^{-1} (or 0.5 m^3 d^{-1}, 3.6 t CO2e y^{-1}), is within the range of values reported for energy wells with gas migration and comparable to other sources of anthropogenic methane emissions (Table 5). Direct comparison between these results and emission values presented in previous studies are complicated by differences in study design, since emissions measured through full-wellhead enclosures (e.g., Kang et al., 2014) or at cut-and-capped wells (Schout et al., 2019) may not be entirely due to GM, but also SCVF or other well integrity failures. There is also an expected variation between wells due to differences in geology and well design, and jurisdictional differences in wellhead configuration (where surface casings in Alberta are vented to the atmosphere; Dusseault & Jackson, 2014).

Table 4 Estimated total GM-related CH_4 emissions at this study site. Values are average effluxes (with upper, lower 95% confidence interval where available).

Data Description	Average Emissions		Method	Comments
	g d^{-1}	m^3 d^{-1}		
STUDY WELL				
August efflux survey	23	0.03	a	
	104	0.15	b	n=10 detectable efflux locations
	466 (0, 2590)	0.7 (0, 3.8)	c	
	118	0.17	d	
September efflux survey	15	0.03	a	
	84	0.12	b	n=8 detectable efflux locations
	229 (0, 1748)	0.34 (0, 2.6)	c	
	48	0.07	d	
October long-term measurement	129 (123, 135)	0.19 (0.18, 0.20)	a	Bootstrapped mean on n=1215 ground-surface emission measurements over 14 days
	1733	2.55	b	Mean of n=5 14-day long-term chamber mean efflux rates
Wind speed < 3 km h^{-1}	208 (199, 217)	0.31 (0.29, 0.32)	a	Mean wellhead ground-surface emissions, subset to times with wind speed < 3 km h^{-1}

[a] Ground-surface efflux in chamber directly around wellhead, [b] Arithmetic mean of all efflux measurements applied to a 3 m radius around the well (non-detectable and < 0 efflux treated as zero), [c] Bayesian Kriging Interpolation, [d] Inverse Distance Weighting Interpolation

Table 5 Previously reported literature values for emissions resulting from well integrity failure, and comparison with other anthropogenic and natural CH_4 sources/sinks. Unless otherwise stated, values are mean emissions (with upper, lower 95% confidence interval where available).

Data Description	Emissions		Method	Comments	Source
	g d^{-1}	m^3 d^{-1}			
GAS MIGRATION AROUND PETROLEUM WELLS					
Mean ground-surface emissions (Western Canada)	2350	3.5	b	N =29 shallow oil and gas wells in Eastern Alberta and Western Saskatchewan. Average 3 m CH_4 emission for all measurements at each well across n=29 wells reported in their Table 2. Median = 1052 g d^{-1}, 1.55 m^3 d^{-1}.	Erno & Schmitz, 1996
Mean ground-surface emission, natural gas storage wells (Utah)	100 (0, 300)	0.15 (0, 0.4)	b	Measurements conducted by Lyman et al., 2020. Dynamic efflux chamber measurement method	Smith et al., 2019
Mean wellhead emissions (Pennsylvania)	264	0.390	e	Measurements from 19 abandoned Pennsylvanian wells with existing above-ground wellhead. Median = 1.3 g d^{-1}, 0.0020 m^3d^{-1}	Kang et al., 2014
1 abandoned well (Netherlands)	10392		e	Only one of 29 abandoned (cut-and-capped) wells surveyed was leaking. Efflux at 2 m depth in soil.	Schout et al., 2018
Mean abandoned onshore oil and gas well (UK)	43 (35, 51)	0.06 (0.05, 0.08)	-	Emissions based on diffusive modelling of methane concentration measurements. Mean of 104 wells.	Boothroyd et al., 2015
SURFACE CASING VENT FLOWS IN PETROLEUM WELLS IN ALBERTA					
Mean Surface Casing Vent Flow (Alberta)	8860	013	-	April 2018 database records on n= 9493 open reports. Median = 136 g d^{-1}, 0.2 m^3 d^{-1}	Alberta Energy Regulator, 2018
NON-PETROLEUM SOURCES/SINKS					
Replacement/growing heifers/steers	183	0.27	-	Per-head direct emission through enteric fermentation, North America	IPCC 2019
Dairy cow	268	0.40			
Canadian landfill emissions to atmosphere, per capita	35	0.05	-	Based on the 2018 estimate of 12 Mt CO2e emitted to the atmosphere as CH4, with per-capita values calculated using July 1st, 2019 population of 37,589,262	Environment and Climate Change Canada, 2020.
Alberta soil consumption capacity	-124	-0.2	-	Per m^2 ground area. Ideal laboratory conditions. Up to 40-50% oxidation efficiency	Stein & Hetteriatchi 2001
Methane biofiltration	-1900	-2.8	-	Per m^3 bulk substrate. Actively aerated system	Gunasekera et al., 2018

[b] Arithmetic mean of all efflux measurements applied to a 3 m radius around the well (non-detectable and < 0 efflux treated as zero), [c] Bayesian Kriging Interpolation, [d] Inverse Distance Weighting Interpolation, [e] All efflux at and around the wellhead

Gas migration emissions are thought to typically represent only a small contribution of total emissions in the perspective of other vented and fugitive methane emission sources at the well pad scale, and more broadly within the upstream oil and gas industry (Schiffner et al., 2020; Schout et al., 2019; Smith et al., 2019). For example, an estimated 3.9 % of average per-well emissions at a gas storage facility measured by Smith et al. (2019) were due to emissions from

gas migration outside the surface casing. While likely comparatively low in the perspective of other sources within the upstream oil and gas industry, relatively poor quantification of the absolute number of wells with GM complicates quantification of industry-wide contributions of methane emissions through GM (Abboud et al., 2020). In addition, representative emission averages are difficult to obtain from limited measurements in an emission distribution that is characteristically heavily skewed by a small number of 'super emitters' (Brandt et al., 2014; Erno & Schmitz, 1996; Saint-Vincent et al., 2020; Zavala-Araiza et al., 2015). Nonetheless, GM at this study well was repeatably detectable using efflux and concentration-based approaches at varying time scales, despite a comparatively low emission rate in perspective of industry-wide sources. This indicates that 'super-emitting' GM wells most significant from an emissions standpoint will be reliably detected in similar field settings. Placed within the larger context of anthropogenic emissions, the annual methane emissions from this study well were equivalent to the operation of ~1 Canadian passenger vehicles (at 3.26 t CO_2e y^{-1}) or the direct emissions through enteric fermentation over the full-life of < 2 North American beef cattle (IPCC 2019; Natural Resources Canada).

Legal requirements for well decommissioning (abandonment) in Western Canada stipulate that GM (and other well integrity failures such as surface casing vent flow; SCVF) are repaired to non-detectable rates, at expense averaging at least $150 000 per well, and with an anecdotally high rate of unsuccessful repair attempts (Alberta Energy Regulator 2021; Dusseault et al., 2014). This repair cost is an economic disincentive for operators to repair and decommission non-producing wells with GM, therefore contributing to a backlog of suspended energy wells that may otherwise be decommissioned (Abboud et al., 2020; Alboiu & Walker, 2019; Schiffner et al., 2020). More widespread and increasingly rigorous testing approaches may provide insight

into the liability of suspended wells with GM, while remediation of all but super-emitter wells may contribute proportionally low reductions in overall methane emissions in the broader perspective of anthropogenic emissions.

From a GM detection perspective, surface efflux and concentration measurements most easily detect those wells which are more significant sources of atmospheric emissions, such that the highest impact wells will be most readily detected. This, however, may not be true of subsurface and groundwater impacts due to the complexity of subsurface migration pathways and geochemistry, and the potential for greater methane dissolution with lower rate or more episodic gas migration due to greater interfacial area between free phase gas and groundwater (Cahill et al., 2017; Van De Ven et al., 2020). The desired testing sensitivity and future standards of GM testing must consider desired risk mitigation, be it atmospheric emissions, groundwater impacts, or simply any presence of GM.

4.4 Temporal variability in measured effluxes and concentrations:

Measured CH_4 and CO_2 efflux and pre-closure concentrations of CH_4 at locations < 1 m from the well varied by up to 50% between individual measurements (taken ~18 minutes apart; Figure 5). Previous authors have found, both conceptually and experimentally, that the interaction of buoyancy and capillary forces of migrating free-phase gas in porous media will result in fingered and continuous or discontinuous migration pathways, causing spatially variable and potentially intermittent gas emission at the surface despite a continuous gas source at depth (Ahlfeld & Dahamani, 1994; Gorody, 2012; Van de Ven et al., 2020). This conceptual and laboratory understanding is supported by these field data of intermittently detectable observations, ‘stepped’ closed chamber concentration increases (Figure S6), and substantial variations in efflux

magnitude between measurements < 1h apart, as has been observed by other authors (Sihota et al., 2013; Forde et al., 2019a; Lyman et al., 2020).

In addition to this described irregular variation attributed to episodic ebullition and gas movement in the saturated zone, a quasi-diel cycle in efflux and concentration by up to one order of magnitude was identified with higher measured CH_4 and CO_2 initial chamber concentrations and effluxes occurring at night, and greater magnitude of variation nearest the wellhead (Figure 5). Decreased initial chamber concentrations during the daytime were correlated with periods of higher wind speeds, as suggested by the stepwise regression modeling results (Table 2), and as observed in previous gas migration studies at the well pad scale, and field-scale vadose zone gas injection experiments (Yin et al., 2014; Ulrich et al., 2019). Wind speed was also inversely correlated with historic gas migration concentration tests (Figure 1Figure 2) suggesting it has a similar effect in efflux chambers and the industry standard of practices. Increased wind velocity has been shown to erode the methane concentration boundary layer, thereby decreasing measured methane concentrations at and near the ground surface (Chamindu Deepagoda et al., 2016; Ulrich et al., 2019).

Regression models suggest multiple other factors were also related to varying initial CH_4 concentrations, including soil temperature and barometric pressure change for chambers near the well, and air temperature and absolute barometric pressure for chambers further away (Table 2). Despite the relatively thin vadose zone, the regression model also indicated a moderate relationship to changes in barometric pressure, particularly for suppressing higher modelled effluxes and higher concentrations during periods with the highest rate of barometric pressure increase, leading to a modest increase in the model R^2 for the CH_4 concentrations at several locations (Table S3, Table S5). This observation is consistent with pressure-differential induced

movements of soil gas within the unsaturated zone, as previously observed in multiple fields of research including artificial gas migration experiments, landfill gas emission, and natural methane-producing ecosystems such as peatlands (Börjesson, & Svensson, 1997; Forde et al., 2019b; Nachshon et al., 2011). There was no indication that falling barometric pressure triggered ebullition events as observed by Tokida et al. (2007).

Other observed statistical relationships to methane efflux and concentrations were to the water level and rate of water level change, and the related variable of soil water content. This is consistent with advective movement of gas during filling and emptying of pores, and altered gas movement pathways and lower effective gas permeability in the soil at higher soil water contents. Temperature-related factors included the atmospheric temperature, potentially leading to greater diffusion rates at higher temperatures, and the differential between soil and atmospheric temperatures since this may induce a convectively driven advective efflux (Nachshon et al., 2011).

4.5 Wind influences on variations in measured efflux

Regression modelling results also indicate that variation in wind speed was the most important predictor for the variation in the measured CH_4 efflux at the wellhead chamber, where it contributed to 11% of the final model R^2 fit. Measured CH_4 and CO_2 efflux and wind speed are negatively correlated at multiple chamber locations (Figure S11), where lower measured effluxes occur during times of higher wind speeds. These observations are similar to previous studies using dynamic closed chambers (e.g., Oliveira et al., 2018; Seo et al., 2020). This trend of lower measured efflux at higher wind speeds largely conflicts with conceptual understandings of greater ground-surface gas exchange at higher wind speeds caused by pressure pumping and a Bernoulli effect of reduced pressure (Poulsen & Møldrup, 2006; Poulsen et al., 2017; Redeker et

al., 2015). While these reported data may be due to a strong correlation to some unconsidered factor accounting for true variation in efflux at this site, lower observed efflux is most likely explained by measurement bias with site infrastructure and the equipment used (Maier et al., 2019). Experimental error involving flushing of gases within the chamber due to an imperfect isolation during chamber closure is considered unlikely. This wind-efflux relationship was observed across all six independent chambers, and spot-checked concentration increase curves did not indicate any air flushing during chamber closure (Figure S6; Figure S11).

Firstly, winds may flush soil gases around structures, removing the migrating soil gases from within the collars (5 cm depth at the wellhead, 15 cm depth elsewhere). Previous authors suggested that higher wind caused lower measured radon efflux and radon entry into structures due to flushing of the soil with atmospheric air, especially around above-ground structures that will induce pressure gradients within the soil (Kovach, 1945; Riley et al., 1996). This may present a potential problem for future use of chamber-based methods of CH_4 emissions through well pad soils. Larger flux collars (as used here), or larger or custom chambers or tents may be necessary to encircle the surface facilities (including the well casing or full wellhead) that are expected to represent preferential gas movement pathways (e.g., Kang et al., 2014; Lebel et al., 2020; Riddick et al., 2020).

Another explanation for the observed wind-efflux relationship is a bias towards under-estimating effluxes during high-wind periods due to more rapid breakthrough times at higher wind speeds and the closed chamber's attenuation of atmospheric pressure variations. In a laboratory experiment of gas breakthrough with varying wind speeds, Poulsen et al. (2017) noted that the breakthrough times of soil gas during windy periods was as low as 1 to 2% of wind-free conditions. Episodic arrivals of methane and other gases through ebullition at the water table will

therefore break through to the ground-surface boundary layer more rapidly in times of higher wind speed, increasing the chance that an ebullition event will not be captured by the discrete 90 second chamber measurements during higher-wind periods. At a shallow peatland, Redeker et al. (2015) observed that a high wind event of less than 10 minutes caused substantial gas exchange that temporarily raised peatland CO_2 effluxes until the soil had been flushed with atmospheric air, at which point the efflux was suppressed for several tens of minutes until pre-wind efflux rates re-established. The vents on the dynamic closed efflux chambers used in this study are specifically designed to limit any pressure fluctuations caused by wind under the intent to limit measured effluxes to those caused by diffusive mechanisms while avoiding the over-estimation of effluxes caused by a venturi-induced pressure drop within a chamber with open vents (Xu et al., 2006). Therefore, the vented chambers used in this study inhibit one of the primary modes of gas exchange across the ground surface. Since the effluxes at sites with shallow water tables are decreased after a higher wind event, the chamber measurements at this site may have been biased towards under-estimating the effluxes during periods of higher winds (Maier et al., 2019). This bias may have contributed to the 62% increase in average wellhead CH_4 efflux for low-wind (< 3 km h^{-1}) periods compared to the full time series (Table 4).

4.6 Methane oxidation in the unsaturated zone

Several previous authors have also suggested quasi-diel variations in CH_4 efflux may be explained by the strong, exponential dependence of CH_4 oxidation rates on higher temperatures, even when the magnitude of temperature variation in some previous studies were relatively small (Börjesson, & Svensson., 1997; Mikkelä et al., 1995; Stein & Hettiaratchi, 2001; Tang et al., 2008). During this field experiment, the magnitude of daily atmospheric temperature variation was up to 15 °C (from -5 to +10 °C), leading to soil temperatures variations of up to 4 °C (from 2

to 6 °C) at the 5 cm depth and <1 °C (around an average 3 °C) at the 30 cm depth (Figure S9). Variable oxidation rates caused by these diurnally fluctuating soil temperatures were unlikely to have caused a substantial proportion of the variation in observed efflux at the wellhead. The regression model fit indicated that soil temperature variation gave a relatively limited contribution to model performance at most chamber locations (Table S3, Table S5). In addition, there was no indication of increased CO_2 efflux coinciding with decreased CH_4 efflux at higher temperatures, as would be expected if the soil microbes were producing CO_2 at higher rates during higher daytime temperatures. This observed oxidation effect is expected to be more prevalent away from the primary gas transport zone. The relative importance of oxidation in decreasing measured concentrations would be lower along the high-efflux preferential flow pathway due to less contact time, lower surface area, and lower soil O_2 where atmospheric gases have been displaced (Forde et al., 2018; Gunasekera et al., 2018).

Although variable oxidation rates do not appear to contribute substantially to the diel variation in effluxes, there is good evidence that some CH_4 is being oxidized to CO_2 within the unsaturated zone, in support of observations of previous research at gas migration sites (Erno & Schmitz, 1996; Forde et al., 2018, Schout et al., 2018). Soil $\delta^{13}C_{CO2}$ averaged -53 ‰, indicating some CO_2 was being formed through biodegradation of thermogenically sourced CH_4, or a mixed thermogenic-biogenic source (Table S2, Figure S7; Risk et al., 2013; Romanak et al., 2014). Higher CO_2 effluxes and soil CO_2 concentrations are observed within meters of the wellhead preferential flow pathway (Figure 4; Figure 7). At the elevated concentrations observed, this CO_2 may be derived from some combination of natural in-soil biologic respiration, production of CO_2 during oxidation of CH_4, and transport of deeper CO_2 as a component of the migrating gases (Romanak et al., 2014). The samples with highest migrating gas concentrations of CH_4 and He,

collected from immediately outside the well casing, did not have the highest concentration of CO_2. In addition, the N_2/O_2 ratio is commonly higher than ten for samples near the well, compared to the atmospheric value of 3.7, which is consistent with the consumption of atmospheric O_2 (Figure 7; Romanak et al., 2014). Samples with O_2 concentrations that are depleted relative to atmospheric concentrations also have higher CO_2 concentrations. At the lower O_2 concentrations, the trend between O_2 and CO_2 is steeper than -1, indicating that methane oxidation is more important than natural biologic respiration in the production of CO_2 near the wellhead. More distal to the well, the N_2/O_2 ratio and the trend of O_2 to CO_2, are more consistent with a biologic respiration source (Figure 7; Sandau et al., 2019; Romanak et al., 2014). Biologic respiration is likely contributing to measured CO_2 concentrations and effluxes with a mixed or natural source, with increasing importance of biologic respiration further from the well. These combined compositional and isotopic indicators suggest that CH_4 oxidation within the unsaturated zone is leading to the elevated CO_2 concentrations and effluxes within meters of the wellhead.

While perturbations to the natural geochemical conditions, including anaerobic soils and inhibition of plant growth may develop, microbially mediated oxidation of CH_4 is favorable from an explosion hazard and emissions standpoint since these reactions will eventually yield CO_2, with substantially lower global warming potential (Hoeks, 1972; IPCC 2013). Systems to enhance this microbial methane oxidation may therefore be exploited as one potential option to decrease emissions from low-rate gas migration sources. Passively or actively managed in-soil oxidation or biofiltration systems could therefore be investigated as a medium or long-term strategy to address low-rate emission sources. However, the capacity of natural, actively, and passively managed systems to continue oxidizing CH_4 during soil conditions sub-optimal for

microbial growth (including low temperatures or low moisture contents) will need to be investigated further (Stein and Hettiaratchi. 2001; Gunasekera et al., 2018).

4.7 Implications for gas migration testing and future scientific study

Potential sensory indications of GM may include visual observations of bubbling through ponded water, vegetation impacts (including discolored, stunted, or dead plants), and "auditory, olfactory, or other evidence of possible gas migration" (BCOGC, 2019; Nooman et al., 2012). In Alberta, GM impacts on vegetation have been recorded historically and additional GM test points are recommended at locations of apparent vegetation stress surrounding a well (Alberta Energy Regulator, 2021; Bachu, 2017). Other sensory indications are not formally referenced by Alberta's provincial regulator. Throughout the field campaigns at this study site, conclusive sensory indications of GM were absent. Vegetation impacts were not observed despite soil oxygen contents at the 30 cm depth routinely approaching < 5% v/v O_2 (Figure 7). This may be explained in part by lessened requirements of soil O_2 by willow (Salix sp.) and other wetland vegetation at this site, with relevance to other sites with shallow water tables (Jackson & Attwood, 1996). These observations support previous arguments by Forde et al. (2019a) and Sandl et al. (2021) that reliance on sensory GM indications may be unreliable or insufficiently conclusive (especially at lower emission rates in similar field settings), and likely lead to under-quantification of the total number of wells with GM.

These high-resolution and survey efflux data document increased episodicity and less advection-driven gas movement further from the well casing, leading to increasingly lower and more irregularly detectable concentrations and effluxes (Figure S6; Chamindu Deepagoda et al., 2016; Van de Ven et al., 2020). Preferential flow pathways have often been observed along the well casing, as in this study, though Forde et al. (2019a) suggest that soil heterogeneity may, in some

cases, lead to undetectable GM nearby the well while gas is detectable at further distances. Spatiotemporal variability at this site caused intermittently non-detectable values of both surface concentration and measured efflux within meters of the casing. With application to GM detection, both efflux and concentration measurements were highly sensitive to measurement location, requiring measurement at sufficient spatial density to capture any preferential gas flow pathways both close to and further from the wellhead. Surface CH_4 concentrations, despite being in the % gas range in the shallow subsurface, were at times limited to 10's of ppm in the wellhead chamber, indicating that sensitive detectors in the ppm range are vital to distinguish the presence of wells with GM, especially if using surface detection methods (Ulrich et al., 2019). Wind speed was shown to be strongly inversely related to temporally variable pre-closure chamber CH_4 concentrations, a conservative proxy for ground-surface concentrations, and historic GM survey results. This suggests withholding GM testing during times of high wind speeds may increase the likelihood of detecting GM, especially if using ground surface measurements. The observed temporal change in maximum methane concentrations may also have implications for risk assessments of sites with GM near public structures or surface developments, such as where urbanisation has encroached on legacy infrastructure (Alberta Energy Regulator, 2014). Risk assessments could be improved by performing concentration-based measurements during circumstances that are expected to produce the highest possible concentrations at a site (e.g., low wind speeds), or through long-term measurements. Geological factors and soil heterogeneity may drive spatial variations at this site (e.g., Forde et al., 2019a; Steelman et al., 2017). Differences in well construction and operating practices, and local geology, may drive differences in spatiotemporal gas migration behavior and emission rates between this site and at other sites (Bachu, 2017; Forde et al., 2019b; Kang et al., 2014). Short-

term temporal variability in measured concentrations may have been caused by some combination of variable wind, temperature, episodic gas migration, and other factors, leading to a range in measured values of concentration or efflux at any one location over time. Despite this variation, methane concentration as a screening tool (i.e., pass/fail) for the presence of GM was resilient to temporal variability at this well with a thin unsaturated zone. Therefore, the concentration or efflux value from any 'snapshot' measurement may be a good indication of the presence of gas migration and relative magnitude of emissions only. Attempts, whether in industry or academia, to attribute a single efflux or concentration value to a well for the purposes of total emission quantification, risk classification, or assessment of trends in leakage rate over multiple years, must consider the error associated with estimates based on short-term measurements. In addition, the reported total emission rate depends substantially on the estimation method used (Table 4). Effluxes, like concentration measurements, were also shown to be spatiotemporally variable and impacted by a variety of environmental factors.

Accurate measurement of total gas migration emission rates may require multi-day measurements to account for variation induced by episodic gas movement and meteorological factors, including the apparent decrease in observed effluxes at higher wind speeds when using the dynamic closed chamber approach. While not considered in this work, soil frost and recent strong rainfall are currently listed in legislation as complicating factors for gas migration detection in Alberta, showing a precedent in regulations for recommending consideration of other environmental factors significant to gas migration detection work such as wind speed and barometric pressure change (Forde et al., 2019b; Alberta Energy Regulator, 2021). We recommend future work directly comparing the influences on measured gas efflux and

concentration by these various environmental factors, as well as assessing the resiliency of different testing methodologies to the observed spatiotemporal variation.

5. CONCLUSIONS

This study recorded multi-day shallow subsurface transport dynamics, and instances of spatial and temporal concentration and efflux variations for established conditions of gas migration around a petroleum well, where:

i) Efflux and concentration values varied spatially, with the highest CH_4 effluxes and concentrations focused within < 1 m of the wellhead. Gas species and isotopic composition, and efflux patterns, suggested deep gas (including thermogenic CH_4, C2-C5, and He) displaced atmospheric air and soil gas.

ii) Compared to measurements around the casing, detectable methane effluxes and concentrations as near as 0.5 m away from the wellhead were more temporally irregular. Methane effluxes 5 m South of the preferential migration pathway were routinely below detection limits.

iii) Two-week high-resolution efflux data recorded moderate temporal variability among individual measurements at a single location, and a diel variation with higher CH_4 and CO_2 initial concentrations and effluxes occurring at night. Multi-component stepwise regression modelling results show wind speed and atmospheric temperature were important predictors of temporal variation in surface concentration and measured efflux around the wellhead. Multiple factors were related to the observed temporal variation, and the correlated factors changed depending on measurement location.

Spatial variability, and short and medium-term temporal variability, may introduce error in estimates of total emissions and surface concentrations around sites with migrating gases. Although the presence of gas migration could be reliably determined at this site, despite observed spatiotemporal variability, quantifying the efflux rate was challenging. The range of total GM-related emissions at this site was 48-466 g CH_4 d^{-1} (0.07-0.69-m^3 CH_4 d^{-1}) using different emission estimation methods, with a mean efflux of 129 g CH_4 d^{-1}; (0.19 m^3 CH_4 d^{-1}) from the preferential migration zone encircling the well casing. At this site, total emissions from gas migration were largest around the well casing, though effluxes at this location also varied temporally. Variation in emission estimates introduced by different estimation methods, and spatiotemporal emission variability, suggests that measurement and estimation methods to account for spatiotemporal variation may need to be considered for accurate GM emission estimation. This well had comparatively low methane emission rates in the broader context of the upstream petroleum industry. Reliable detectability of migrating gas at this site indicates that higher-rate GM sources most important from an emissions standpoint will be detectable using common GM test methods in similar field settings. Relative gas species composition and shifts in the $\delta^{13}C$ value of CH_4 and CO_2 were consistent with near-surface methane oxidation, suggesting this process could be enhanced to further decrease emissions. Consideration of factors causing spatial and temporal variability of migrating gases may lead to more representative measurements of surface concentrations and effluxes, and therefore improved detection and quantification of the risks and impacts associated with migrating gases around energy wells.

We conclude that at this case-study site, short-term concentration or efflux surveys at sufficient spatial density will be resilient to temporal variability for the purposes of detecting the presence

of gas migration. GM detection surveys could be optimized by considering meteorological factors, and long-term assessment is required for accurate estimation of total emissions.

CREDIT AUTHOR STATEMENT

All authors contributed to study conceptualization. Cathy Ryan and Ulrich Mayer shared funding acquisition and supervision. Neil Fleming led the data acquisition and data analysis and wrote the initial draft. Tiago Morais assisted with data acquisition, visualization, and initial draft authorship. All authors contributed to editing and reviewing drafts.

DECLARATION OF COMPETING INTERESTS

The authors declare no competing personal or financial external interests that would have impacted the outcomes of this study.

ACKNOWLEDGMENTS

This work was co-funded by the Alberta Upstream Petroleum Research Fund (AUPRF), administered by the Petroleum Technology Alliance of Canada (PTAC), and the National Science and Engineering Research Council of Canada (NSERC), Grant no. CRDPJ/503367-2016, with additional funding by the Canada First Research Excellence Fund (CFREF). Funding for equipment utilized in this study was provided by the Canadian Foundation for Innovation (CFI), the BCKDF, the BCOGC, and NSERC through an RTI grant. We give thanks to the energy company that provided access to the study well, historic gas migration test data, and logistical support in field work.

APPENDIX A. SUPPLEMENTARY MATERIALS

Supplementary data for this article can be found as a separate document.

REFERENCES

Abboud, J. M., Watson, T. L., Ryan, M. C., 2020. Fugitive methane gas migration around Alberta's petroleum wells. Greenh. Gases: Sci. Technol. https://doi.org/10.1002/ghg.2029

Abichou, T., Powelson, D., Chanton, J., Escoriaza, S., Stern, J., 2006. Characterization of methane flux and oxidation at a solid waste landfill. J. Environ. Eng. 132(2), 220-228. https://doi.org/10.1061/(ASCE)0733-9372(2006)132:2(220)

Ahlfeld, D. P., Dahmani, A., & Ji, W., 1994. A conceptual model of field behavior of air sparging and its implications for application. Groundw. Monit. Remediat. 14(4), 132-139. https://doi.org/10.1111/j.1745-6592.1994.tb00491.x

Akaike, H., 1974. A new look at the statistical model identification. IEEE transactions on automatic control, 19(6), 716-723.

Alberta Agriculture and Forestry, Alberta Climate Information Service (ACIS) https://agriculture.alberta.ca/acis (retrieved January 2020)

Alberta Energy Regulator. 2014. Directive 79: Surface Development in Proximity to Abandoned Wells. Alberta, Canada. https://static.aer.ca/prd/2020-07/Directive079_0.pdf

Alberta Energy Regulator. 2020. Directive 009: Casing Cementing Minimum Requirements. Alberta, Canada. https://static.aer.ca/prd/2020-10/Directive009.pdf

Alberta Energy Regulator. 2021. Directive 20: Well Abandonment. Alberta, Canada. https://static.aer.ca/prd/documents/directives/Directive020.pdf

Alberta Energy Regulator. 2018. Vent Flow/ Gas Migration Report. Alberta, Canada. Accessed 2018-05-30 from http://www1.aer.ca/ProductCatalogue/365.html

Alboiu, V., & Walker, T. R., 2019. Pollution, management, and mitigation of idle and orphaned oil and gas wells in Alberta. Canada. Environ. Monit. Assess, 191(10), 611. https://doi.org/10.1007/s10661-019-7780-x

Almon, E., Magaritz, M, 1990. Dissolved common gases in groundwaters of the Appalachian region. J. Hydrol. 121(1-4), 21-32. https://doi.org/10.1016/0022-1694(90)90222-J

Annunziatellis, A., Beaubien, S. E., Bigi, S., Ciotoli, G., Coltella, M., Lombardi, S., 2008. Gas migration along fault systems and through the vadose zone in the Latera caldera (central Italy): Implications for CO2 geological storage. Int. J. Greenh. Gas Con. 2(3), 353-372. https://doi.org/10.1016/j.ijggc.2008.02.003

Bachu, S., 2017. Analysis of gas leakage occurrence along wells in Alberta, Canada, from a GHG perspective – Gas migration outside well casing. Int. J. Greenh. Gas Con. 61, 146-154. https://doi.org/10.1016/j.ijggc.2017.04.003

BCOGC. 2019. Oil & Gas Operations Manual. Chapter 9 Well Activity: Completion, Maintenance and Abandonment. Version 1.29. https://www.bcogc.ca/node/13316/download

Boothroyd, I, M, Almond, S, Qassim, S, M, Worrall, F, Davies, R, J, 2015. Fugitive emissions of methane fromabandoned, decommissioned oil and gas wells. Science of the Total Environment 547, 461–469. doi:https://doi.org/10.1016/j.scitotenv.2015.12.096.

Börjesson, G., Danielsson, Å., Svensson, B. H., 2000. Methane fluxes from a Swedish landfill determined by geostatistical treatment of static chamber measurements. Environ. Sci. Technol. 34(18), 4044-4050. https://doi.org/10.1021/es991350s

Börjesson, G., Svensson, B., 1997. Seasonal and diurnal methane emissions from a landfill and their regulation by methane oxidation. Waste Manag. Res. 15(1) 33-54. https://doi.org/10.1177/0734242X9701500104.

Brandt, A.R., Heath, G.A., Kort, E.A., O'sullivan, F., Pétron, G., Jordaan, S.M., Tans, P.,Wilcox, J., Gopstein, A.M., Arent, D., Wofsy, S., Brown, N.J., Bradley, R., Stucky, G.D., Eardley, D., Harris, R., 2014. Energy and environment methane leaks from North American natural gas systems. Sci. 343(6172), 733–735. https://doi.org/10.1126/science.1247045

Cahill, A., Steelman, C., Forde, O., Kuloyo, O., Ruff, S., Mayer, B., Mayer, K.U., Strous, M., Ryan, M.C., Cherry, J.A., Parker, B.L., 2017. Mobility and persistence of methane in groundwater in a controlled-release field experiment. Nat. Geosci. 10, 289.

Cardellini, C., Chiodini, G., Frondini, F., Granieri, D., Lewicki, J., Peruzzi, L., 2003. Accumulation chamber measurements of methane fluxes: application to volcanic-geothermal areas and landfills. Appl. Geochem. 18(1), 45-54. https://doi.org/10.1016/S0883-2927(02)00091-4

Chamindu Deepagoda, T.K.K., Smits, K. Oldenburg, C., 2016. Effect of subsurface soil moisture variability and atmospheric conditions on methane gas migration in shallow subsurface. Int. J. Greenh. Gas Con. 55:105–117. https://doi.org/10.1016/j.ijggc.2016.10.016

Chen, K., O'Leary, R. A., Evans, F. H., 2019. A simple and parsimonious generalised additive model for predicting wheat yield in a decision support tool. Agric. Syst. 173, 140-150. https://doi.org/10.1016/j.agsy.2019.02.009

Christiansen, J., Outhwaite J., Smukler, S., 2015. Comparison of CO2, CH4 and N2O soil-atmosphere exchange measured in static chambers with cavity ring-down spectroscopy and gas chromatography. Agric. For. Meteorol. 211, 48-57. https://doi.org/10.1016/j.agrformet.2015.06.004

D'Aniello, A., Fabbricino, M., Ducci, D., Pianese, D., 2020. Numerical Investigation of a Methane Leakage from a Geothermal Well into a Shallow Aquifer. Groundw. 58(4), 598-610. doi:10.1111/gwat.12943

Dusseault, M., Jackson, R., 2014., Seepage pathway assessment for natural gas to shallow groundwater during well stimulation, in production, and after abandonment. Environ. Geosci. 21(3), 107-126. doi: 10.1306/eg.04231414004

Dusseault, M., Jackson., R., MacDonald, D. 2014., Towards a Road Map for Mitigating the Rates and Occurrences of Long-Term Wellbore Leakage. University of Waterloo & Geofirma Engineering Ltd. (2014). http://geofirma.com/wp-content/uploads/2015/05/lwp-final-report_compressed.pdf.

Engelder, T., Zevenbergen, J., 2018. Analysis of a gas explosion in Dimock PA (USA) during fracking operations in the Marcellus gas shale. Process Saf. Environ. Prot. 117, 61-66. https://doi.org/10.1016/j.psep.2018.04.004

Environment and Climate Change Canada. 2020. National inventory report: greenhouse gas sources and sinks in Canada: executive summary. http://publications.gc.ca/pub?id=9.816345&sl=0

Erno, B., Schmitz, R. 1996. Measurements of soil gas migration around oil and gas wells in the Lloydminster area. J. Can. Pet. Tech. 35(07).

Fleming, N., Morais, T., Kennedy, C., Ryan, M.C., 2019. Evaluation of SCVF and GM measurement approaches to detect fugitive gas migration around energy wells. Presented at Geoconvention 2019. Calgary, Canada. May 13-17 2019.

Forde, O., Mayer, K., Cahill, A., Mayer, B., Cherry, J., Parker, B., 2018. Vadose zone gas migration and surface effluxes after a controlled natural gas release into an unconfined shallow aquifer. Vadose Zone J. 17, 1-16.

Forde, O. N., Mayer, K. U., & Hunkeler, D. 2019a. Identification, spatial extent and distribution of fugitive gas migration on the well pad scale. Sci. Total Environ. 652, 356–366.

Forde, O. N., Cahill, A. G., Beckie, R. D., & Mayer, K. U. 2019b. Barometric-pumping controls fugitive gas emissions from a vadose zone natural gas release. Sci. Rep. 9, 1-9.

Frederick, G., Wolfram, K., Eric, P., Gaëtan, B., Pierrick, D., Bernhard, M., & Eric, C. G., 2017. Natural CH4 gas seeps in the French Alps: characteristics, typology and contribution to CH4 natural emissions to the atmosphere. Energy Procedia, 114, 3020-3032. https://doi.org/10.1016/j.egypro.2017.03.1430

Gas Measurement Instruments Ltd. 2016. GT series user handbook. Accessed November 2020 from: https://www.manualslib.com/manual/1680676/Gmi-Gt-Series.html?page=2#manual

Gorody, A. W., 2012. Factors affecting the variability of stray gas concentration and composition in groundwater. Environ. Geosci. 19(1), 17-31. https://doi.org/10.1306/eg.12081111013

Government of Alberta. Reducing methane emissions. Accessed November 2020 from: https://www.alberta.ca/climate-methane-emissions.aspx

Gunasekera, S. S., Hettiaratchi, J. P., Bartholameuz, E. M., Farrokhzadeh, H., Irvine, E., 2018. A comparative evaluation of the performance of full-scale high-rate methane biofilter (HMBF) systems and flow-through laboratory columns. Environ. Sci. Pollut. Res. 25, 35845-35854. https://doi.org/10.1007/s11356-018-3100-1

Hastie, T., 2019. gam: Generalized Additive Models. R package version 1.16.1.

Hastie, T. J., Tibshirani, R. J., 1990. Generalized additive models, Vol. 43. CRC press.

Hendry, M. J., Schmeling, E. E., Barbour, S. L., Huang, M., Mundle, S. O., 2017. Fate and transport of shale-derived, biogenic methane. Sci. Rep. 7(1), 1-9. https://doi.org/10.1038/s41598-017-05103-8

Hoeks, J., 1972. Effect of leaking natural gas on soil and vegetation in urban areas. Report published by the Centre for Agricultural Publishing and Documentation, Wageningen, Netherlands.

Humez, P., Mayer, B., Ing, J., Nightingale, M., Becker, V., Kingston, A., ... Taylor, S., 2016. Occurrence and origin of methane in groundwater in Alberta (Canada): Gas geochemical and isotopic approaches. Sci. Total Environ. 541, 1253-1268.

IPCC. 2013. Climate Change 2013: The Physical Science Basis. Contribution of Working Group I to the Fifth Assessment Report of the Intergovernmental Panel on Climate Change [Stocker, T.F., D. Qin, G.-K. Plattner, M. Tignor, S.K. Allen, J. Boschung, A. Nauels, Y. Xia, V. Bex and P.M. Midgley (eds.)]. Cambridge University Press, Cambridge, United Kingdom and New York, NY, USA, 1535 pp.

IPCC. 2019. 2019 Refinement to the 2006 IPCC Guidelines for National Greenhouse Gas Inventories. Volume 4, Chapter 10. Accessed August 2020 from https://www.ipcc-nggip.iges.or.jp/public/2019rf/vol4.html.

Jackson, M., Attwood, P., 1996. Roots of willow (Salix viminalis L.) show marked tolerance to oxygen shortage in flooded soils and in solution culture. Plant and Soil, 187(1), 37-45.

Jackson, R. E., Gorody, A. W., Mayer, B., Roy, J. W., Ryan, M. C., Van Stempvoort, D. R., 2013. Groundwater protection and unconventional gas extraction: The critical need for field-based hydrogeological research. Groundw 51 (4), 488–510. https://doi:10.1111/gwat.12074.

Kang, M., Kanno, C. M., Reid, M. C., Zhang, X., Mauzerall, D. L., Celia, M. A., Chen, Y., Onstott, T. C., 2014. Direct measurements of methane emissions from abandoned oil and gas wells in Pennsylvania. Proc. Natl. Acad. Sci. 111(51), 18173-18177. https://doi.org/10.1073/pnas.1408315111

Kelly, W. R., Matisoff, G., Fisher, J. B., 1985. The effects of a gas well blow out on groundwater chemistry. Environ. Geol. Water Sci. 7(4), 205-213. https://doi.org/10.1007/bf02509921

Kovach, E. M., 1945. Meteorological influences upon the radon-content of soil-gas. Eos, Trans. Am. Geophys. Union, 26(2), 241-248. https://doi.org/10.1029/TR026i002p00241

Lebel, E. D., Lu, H. S., Vielstädte, L., Kang, M., Banner, P., Fischer, M. L., Jackson, R. B. 2020. Methane Emissions from abandoned oil and gas wells in California. Environ. Sci. Technol. 54(22), 14617-14626. https://doi.org/10.1021/acs.est.0c05279

Lyman, S. N., Tran, H. N., Mansfield, M. L., Bowers, R., Smith, A., 2020. Strong temporal variability in methane effluxes from natural gas well pad soils. Atmos. Pollut. Res. 11(8), 1386-1395. https://doi.org/10.1016/j.apr.2020.05.011

Maier, M., Mayer, S., Laemmel, T., 2019. Rain and wind affect chamber measurements. Agric. For. Meteorol. 279, 107754. https://doi.org/10.1016/j.agrformet.2019.107754

Martin, G. E., Snow, D. D., Kim, E., Spalding, R. F., 1995. Simultaneous determination of argon and nitrogen. Groundw. 33(5), 781-785. https://doi.org/10.1111/j.1745-6584.1995.tb00024.x

McMahon, P. B., Thomas, J. C., Crawford, J. T., Dornblaser, M. M., Hunt, A. G., 2018. Methane in groundwater from a leaking gas well, Piceance Basin, Colorado, USA. Sci. Total Environ., 634, 791-801. https://doi.org/10.1016/j.scitotenv.2018.03.371

Mikkelä, C., Sundh, I., Svensson, B. H., Nilsson, M., 1995. Diurnal variation in methane emission in relation to the water table, soil temperature, climate and vegetation cover in a Swedish acid mire. Biogeochem. 28(2), 93-114. https://doi.org/10.1007/BF02180679

Milbert, D., 2018. Solid Earth Tide. Accessed 2020 from: https://geodesyworld.github.io/SOFTS/solid.htm#link2

Mitton, M., 2018. Subsurface methane migration from natural gas distribution pipelines as affected by soil heterogeneity: field scale experimental and numerical study (Doctoral dissertation, Colorado School of Mines. Arthur Lakes Library)

Nachshon, U., Weisbrod, N., Dragila, M. I., & Ganot, Y., 2011. The importance of advective fluxes to gas transport across the earth-atmosphere interface: the role of thermal

convection. Planet Earth 2011-Global Warming Challenges and Opportunities for Policy and Practice. IntechOpen.

Natural Resources Canada. Greenhouse Gases Equivalencies Calculator- Calculations and References. Accessed 08-2020 from https://oee.nrcan.gc.ca/corporate/statistics/neud/dpa/calculator/refs.cfm

Noomen, M. F., van der Werff, H. M., Van der Meer, F., 2012. Spectral and spatial indicators of botanical changes caused by long-term hydrocarbon seepage. Ecol. Inform. 8, 55-64. https://doi.org/10.1016/j.ecoinf.2012.01.001

Oliveira, S., Viveiros, F., Silva, C., & Pacheco, J. E., 2018. Automatic Filtering of Soil CO2 Flux Data; Different Statistical Approaches Applied to Long Time Series. Front. Earth Sci. 6, 208. https://doi.org/10.3389/feart.2018.00208

Poulsen, T. G., Møldrup, P., 2006. Evaluating effects of wind-induced pressure fluctuations on soil-atmosphere gas exchange at a landfill using stochastic modelling. Waste Manag. Res. 24(5), 473-481. https://doi.org/10.1177/0734242X06066363

Poulsen, T. G., Pourber, A., Furman, A., Papadikis, K., 2017. Relating wind-induced gas exchange to near-surface wind speed characteristics in porous media. Vadose Zone J. 16(8), 1-13. https://doi.org/10.2136/vzj2017.02.0039

Province of Alberta. 2020. Pipeline Act. Accessed September 2020 from https://www.qp.alberta.ca/documents/Acts/p15.pdf Redeker, K. R., Baird, A. J., Teh, Y. A., 2015. Quantifying wind and pressure effects on trace gas effluxes across the soil-atmosphere interface. Biogeosci. 12(24), 7423-7434. doi:10.5194/bg-12-7423-2015

Riddick, S. N., Mauzerall, D. L., Celia, M. A., Kang, M., & Bandilla, K. 2020. Variability observed over time in methane emissions from abandoned oil and gas wells. Intern.J. Greenh. Gas Control. 100, 103116. https://doi.org/10.1016/j.ijggc.2020.103116

Riley, W. J., Gadgil, A. J., Bonnefous, Y. C., Nazaroff, W. W., 1996. The effect of steady winds on radon-222 entry from soil into houses. Atmos. Environ. 30(7), 1167-1176. https://doi.org/10.1016/1352-2310(95)00248-0

Risk, D., McArthur, G., Nickerson, N., Phillips, C., Hart, C., Egan, J., Lavoie, M., 2013. Bulk and isotopic characterization of biogenic CO2 sources and variability in the Weyburn injection area. Int. J. Greenh. Gas Control. 16, S263-S275. https://doi.org/10.1016/j.ijggc.2013.02.024

Romanak, K.D., Wolaver, B., Yang, C., Sherk, G.W., Dale, J., Dobeck, L.M., Spangler, L.H., 2014. Process-based soil gas leakage assessment at the Kerr Farm: comparison of results to leakage proxies at ZERT and Mt. Etna. Int. J. Greenh. Gas Control. 30, 42-57. https://doi.org/10.1016/j.ijggc.2014.08.008

Rowe, D., Muehlenbachs, K., 1999. Isotopic fingerprints of shallow gases in the Western Canadian sedimentary basin: tools for remediation of leaking heavy oil wells. Org. Geochem. 30(8), 861-871. https://doi.org/10.1016/S0146-6380(99)00068-6

Roy, N., Molson, J., Lemieux, J. M., Van Stempvoort, D., Nowamooz, A., 2016. Three-dimensional numerical simulations of methane gas migration from decommissioned hydrocarbon production wells into shallow aquifers. Water Resour. Res. 52(7), 5598-5618. https://doi.org/10.1002/2016WR018686

Saint-Vincent, P. M., Reeder, M. D., Sams III, J. I., Pekney, N. J., 2020. An analysis of abandoned oil well characteristics affecting methane emissions estimates in the Cherokee Platform in Eastern Oklahoma. Geophys. Res Lett. 47(23). https://doi.org/10.1029/2020GL089663

Sandau, C. D., Prokipchuk, M., Dominato, K. R., Mundle, S. O., 2019. Soil gas investigation of an alleged gas migration issue on a residential farm located above the Weyburn-Midale CO2 enhanced oil recovery project. Int. J. Greenh. Gas Control. 81, 11-20. https://doi.org/10.1016/j.ijggc.2013.02.024

Sandl, E., Cahill, A. G., Welch, L., & Beckie, R. 2021. Characterizing oil and gas wells with fugitive gas migration through Bayesian multilevel logistic regression. Sci. Total Environ. 769, 144678. https://doi.org/10.1016/j.scitotenv.2020.144678

Schiffner, D., 2020. Methane Emissions from Suspended Wells: Can Internalizing the Cost of Methane Leaks Incentivize Plugging and Reclamation of Petroleum Wells in Alberta? Proc. World Geothermal Congress, April 26 – May 2, 2020, Reykjavik, Iceland.

Schout, G., Griffioen, J., Hassanizadeh, S. M., de Lichtbuer, G. C., Hartog, N., 2019. Occurrence and fate of methane leakage from cut and buried abandoned gas wells in the Netherlands. Sci. Total Environ. 659, 773-782. https://doi.org/10.1016/j.scitotenv.2018.12.339

Seo, D., Han, W., Park, E., Jeong, J., Oh, Y. Y., Kim, H. J., ...Yun, S., 2020. Analyses and numerical evaluation of integrated time-series monitoring datasets including CO2 concentration and effluxes at controlled CO2 release site in South Korea. J. Hydro. 590, 125213. https://doi.org/10.1016/j.jhydrol.2020.125213

Sihota, N. J., Mayer, K. U., Toso, M. A., Atwater, J., 2013. Methane emissions and contaminant degradation rates at sites affected by accidental releases of denatured fuel-grade ethanol. J. Contam. Hydrol. 151, 1-15. https://doi.org/10.1016/j.jconhyd.2013.03.008

Smith, Ann P., Bowers, Richard L., Boyd, Victoria H., Lyman, S., 2019. Long-Term Methane Emissions Quantification and Alert System for Natural Gas Storage Wells and Fields. GSI Environmental, Inc., Austin, Texas. https://www.osti.gov/biblio/1526753

Spokas, K., Graff, C., Morcet, M., Aran, C., 2003. Implications of the spatial variability of landfill emission rates on geospatial analyses. Waste Manag. 23(7), 599-607. https://doi.org/10.1016/S0956-053X(03)00102-8

Statistics Canada, 2016. 2016 Census- Boundary Files. Accessed From: https://www12.statcan.gc.ca/census-recensement/2011/geo/bound-limit/bound-limit-2016-eng.cfm

Steelman, C. M., Klazinga, D. R., Cahill, A. G., Endres, A. L., Parker, B. L., 2017. Monitoring the evolution and migration of a methane gas plume in an unconfined sandy aquifer using time-lapse GPR and ERT. J. Contam. Hydrol. 205, 12-24. https://doi.org/10.1016/j.jconhyd.2017.08.011

Stein, V., Hettiaratchi, J. P., 2001. Methane oxidation in three Alberta soils: influence of soil parameters and methane efflux rates. Environ. Technol. 22(1), 101-11. https://doi.org/10.1080/09593332208618315

Szatkowski, B., Whittaker, S., Johnston, B., 2002. Identifying the source of migrating gases in surface casing vents and soils using stable Carbon Isotopes, Golden Lake Pool, West-

central Saskatchewan. Summary of Investigations 2002, Volume 1 Saskatchewan Geological Survey, Regina, SK, Canada. 2002(4.1) pp.118-125.

Tang, J., Bao, Z., Xiang, W., Gou, Q., 2008. Geological emission of methane from the Yakela condensed oil/gas field in Talimu Basin, Xinjiang, China. J. Environ. Sci. 20(9), 1055-1062. https://doi.org/10.1016/S1001-0742(08)62149-X

Tilley, B., Muehlenbachs, K., 2011. Fingerprinting of gas contaminating groundwater and soil in a petroliferous region, Alberta, Canada. Presented at Proceedings from International Network of Environmental Forensics Conference, 2011, Cambridge (UK) (2011) pp. 115-125.

Tokida, T., Miyazaki, T., Mizoguchi, M., Nagata, O., Takakai, F., Kagemoto, A., Hatano, R., 2007. Falling atmospheric pressure as a trigger for methane ebullition from peatland. Glob. Biogeochem. Cycles, 21(2). https://doi.org/10.1029/2006GB002790

Ulrich, B. A., Mitton, M., Lachenmeyer, E., Hecobian, A., Zimmerle, D., Smits, K. M., 2019. Natural gas emissions from underground pipelines and implications for leak detection. Environ. Sci. Technol. Lett. 6(7), 401-406. https://doi.org/10.1021/acs.estlett.9b00291

Van De Ven, C., Abraham, J., Mumford, K., 2020. Laboratory investigation of free-phase stray gas migration in shallow aquifers using modified light transmission. Adv. Water Resour. 103543.

Van De Ven, C., Mumford, K., 2020. Intermediate-Scale Laboratory Investigation of Stray Gas Migration Impacts: Methane Source Architecture and Dissolution. Environ. Sci. Technol. 54(10), 6299-6307.

Wen, T., Castro, M. C., Nicot, J. P., Hall, C. M., Larson, T., Mickler, P., Darvari, R., 2016. Methane sources and migration mechanisms in shallow groundwaters in Parker and Hood Counties, Texas- A heavy noble gas analysis. Environ. Sci. Technol, 50(21), 12012-12021. https://doi.org/10.1021/acs.est.6b01494

Whiticar, M. J., 1999. Carbon and hydrogen isotope systematics of bacterial formation and oxidation of methane. Chem. Geo. 161(1-3), 291-314. https://doi.org/10.1016/S0009-2541(99)00092-3

Wickham, H., 2016. ggplot2: Elegant Graphics for Data Analysis. Springer-Verlag New York.

Williams, G. M., Aitkenhead, N., 1991. Lessons from Loscoe: the uncontrolled migration of landfill gas. Q. J. Eng. Geol. Hydrogeol., 24(2), 191-207. https://doi.org/10.1144/GSL.QJEG.1991.024.02.03

Woods, A. W., Norris, S., 2016. Dispersion and dissolution of a buoyancy driven gas plume in a layered permeable rock. Water Resour. Res. 52(4), 2682-2697. https://doi.org/10.1002/2015WR018159

Xu, L., Furtaw, M., Madsen, R., Garcia, R., Anderson, D., McDermitt, D., 2006. On maintaining pressure equilibrium between a soil CO2 efflux chamber and the ambient air. J. Geophys. Res: Atmos. 111(D8). https://doi.org/10.1029/2005JD006435

Yin, J, Mayer, K.U., Sihota, N., 2014. Evaluation of gas migration near production wells in Northeastern BC- Results of a preliminary field survey. The University of British Colombia

Zavala-Araiza, D., Lyon, D. R., Alvarez, R. A., Davis, K. J., Harriss, R., Herndon, S. C., ... Hamburg, S. P., 2015. Reconciling divergent estimates of oil and gas methane

emissions. Proc. Natl. Acad. Sci. 112(51), 15597-15602. https://doi.org/10.1073/pnas.1522126112

2020. 4.02. https://www.R-project.org/.

Spatiotemporal variability of fugitive gas migration emissions around a petroleum well

N.A. Fleming, * T.A. Morais, K.U. Mayer, M.C. Ryan

N.A. Fleming, * T.A. Morais, and M.C. Ryan, Geoscience, Univ. of Calgary, 2500 University Drive NW, Calgary AB, T2N 1N4, Canada; K.U. Mayer Earth, Ocean and Atmospheric Sciences, Univ. of British Colombia, 2007 Main Mall, Vancouver BC, V6T 1Z4, Canada. *Corresponding author (naflemin@ucalgary.ca)

ABSTRACT

Well integrity failure resulting in migration of natural gas outside of the surface casing can cause atmospheric greenhouse gas emissions and groundwater quality impacts from existing and historic energy wells. Spatial and temporal variability in gas migration can result in errors in detection (i.e., presence/absence) and efflux estimations. This field-based case study used automated dynamic closed chambers to record repeated (~ every 18 minutes) CO_2 and CH_4 efflux measurements over a two-week period around a single petroleum production well in Alberta, Canada. Long-term efflux measurements supplemented soil gas compositional and isotopic characterization, along with surface concentration measurements. Effluxes were spatially concentrated around the wellhead and only occasionally detectable more than a few meters away. Estimated total emissions attributable to gas migration ranged from 48 - 466 g CH_4 d^{-1} (or 0.07 - 0.7 m^3 CH_4 d^{-1}). Methane effluxes and concentrations were temporally variable on second-to-hourly and diel scales. Multivariate stepwise regression analysis indicates that multiple meteorological factors, particularly wind speed and air temperature, were related to the temporal variability. Despite temporal variability, elevated concentrations and effluxes were consistently detectable around the well. Major soil gas composition suggests that gas migration near the wellhead causes advective displacement of soil gas, while more distal measurements are indicative of episodic and diffusion-dominated transport. Values of ^{13}C-CO_2 and ^{13}C-CH_4

 https://doi.org/10.1016/j.apr.2021.101094

samples were consistent with CH_4 oxidation within the unsaturated zone. Although these results reflect a single well, the findings are salient to gas migration detection and emission estimation efforts.

KEYWORDS

Gas Migration; Methane; Well Integrity; Stray Gas; Fugitive Emissions; Meteorological Effects

1. INTRODUCTION

Energy well integrity issues are a topic of increasing focus among government and industry practitioners, spurred in part by increased drilling activity in regions now accessible due to multi-stage hydraulic fracturing and concern of the growing environmental and economic liability of inactive and abandoned wells (Alboiu & Walker 2019; Jackson et al., 2013; Schiffer et al., 2020). Well integrity issues include gas migration outside the surface casing (GM), where a subsurface source of natural gas typically migrates from a shallow or intermediate gas-charged stratigraphic interval to ground surface (Figure 1; Rowe & Muehlenbachs, 1999, Tilley & Muehlenbachs, 2012). The "surface casing" of energy wells is generally installed to a depth below the base of non-saline groundwater protection (typically 100-300 m; Dusseault and Jackson, 2014). The annulus between progressively smaller diameter casings is typically cemented between the casing and the borehole (e.g., Alberta Energy Regulator, 2020; Bachu, 2017). Leakage pathways which result in gas migration are generally understood to be due either to defects in the cement itself, or between the cement and the borehole or one of the casings (Bachu, 2017; Dusseault and Jackson, 2014). Fugitive, or migrating, gases are typically primarily methane (CH_4), often with minor amounts of ethane, propane, and other volatile hydrocarbons (Tilley & Muehlenbachs, 2012; Szatowski et al., 2002).

Gas migration impacts can include atmospheric emissions, groundwater water quality perturbations, and land use interference. Methane is a greenhouse gas with a global warming potential 25 times more potent by mass than carbon dioxide over a period of 100 years (and 84 times that of CO_2 over a 20-year period; IPCC, 2013). Specific focus on decreasing methane emissions from the upstream petroleum sector is included in global efforts to decrease anthropogenic greenhouse gas emissions (IPCC 2013). For example, the Alberta oil and gas

industry intends to reduce 2012 methane emission rates by 45% by 2025 (Government of Alberta). Specific concern for GM also arises since, in some instances, gases migrate through non-saline (i.e., total dissolved solids less than 4000 mg L^{-1}; Alberta Energy Regulator 2021) groundwater. Dissolved methane can alter chemical conditions of groundwater, specifically its redox state, perturbing the indigenous microbial community, potentially altering pH, mobilizing metals, forming hydrogen-sulfide gas, or later exsolving when groundwater is pumped to the surface for residential or commercial use (Cahill et al., 2017; Gorody, 2012; Kelly et al., 1985; Roy et al., 2016). Should these exsolved gases accumulate in pumphouses, residences, or other facilities, explosive or asphyxiating atmospheres may develop (Engelder & Zevenbergen, 2018). Finally, GM may cause impacts or limitations on land usage since excess methane and/or carbon dioxide may displace oxygen in soil gas and impact plant or crop health. GM also has the potential for generating a dangerous or explosive atmosphere, necessitating setbacks for built structures (Noomen et al., 2012; Sihota et al., 2013; Williams & Aitkenhead, 1991). Although gas migration has only been reported for 0.73% of all wells in the province of Alberta (n > 450,000 wells in total; Bachu, 2017), a recent review concluded gas migration testing has only been required in 3.5% of Alberta's energy wells (Abboud et al., 2020). Methane emission distributions are often heavily skewed by a small number of 'super-emitter' sources that comprise a large proportion of the total emissions (Brandt et al., 2014; Saint-Vincent et al., 2020; Zavala-Araiza et al., 2015). Previous work suggests that emissions specific to GM in Alberta follow this same distribution, where a smaller number of wells have the highest GM emission rates and contribute disproportionately to total emission volumes (Erno & Schmitz, 1996).

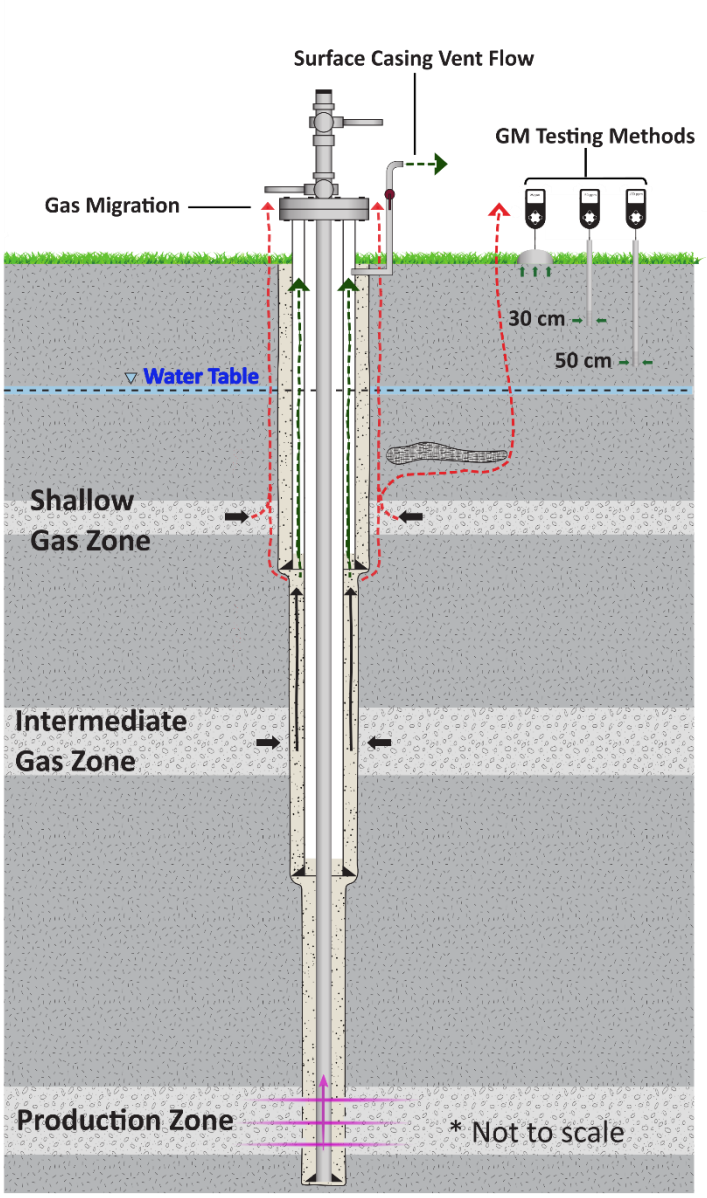

Figure 1 Conceptual model of gas migration (GM) and surface casing vent flow (SCVF) (After Bachu, 2017). Migrating gases (CH_4 and other light hydrocarbons) originate from an intermediate or shallow gas producing formation and travel to the surface either wholly outside the casing (GM; red) or also within the outermost casing annulus (SCVF; green). Common testing depths for detecting the presence of GM through combustible gas and/or CH_4 concentration measurements include ground-surface detection, or at a specified depth (usually > 30 cm threshold requiring ground disturbance permitting despite the 'recommended' 50 cm depth (Alberta Energy Regulator, 2021; Fleming et al., 2019).

A significant fraction of Alberta's energy wells will require GM testing before they can be abandoned (Abboud et al., 2020). If GM is found, repair is required prior to legal abandonment,

presenting an economic liability to industry (Alberta Energy Regulator, 2021). While requirements vary depending on jurisdiction, an effective and reliable approach to measure presence/absence of GM and estimate emission rates is needed to manage GM around petroleum wells. Tests for the presence/absence of GM are often conducted by sequential snapshot measurement of near-surface combustible gas concentrations at multiple points around a well, over a total GM test duration of less than one hour (Alberta Energy Regulator, 2021; Szatowski et al., 2002). The recommended test point spacing by the Alberta Energy Regulator includes a total of 14 measurement points, with two within 30 cm of the wellbore and then at 2, 4, and 6 m away in a cross pattern. Measurement depths are recommended as 50 cm, though measurements are often completed at ground surface or some intermediate subsurface depth (< 30 cm) that does not require ground disturbance permitting (Figure 1; Alberta Energy Regulator, 2021; Fleming et al., 2019; Province of Alberta, 2020). The efficacy of the recommended gas migration testing method has not been fully validated (Abboud et al., 2020). Recent surveys of methane efflux measurements around industry gas wells (Forde et al., 2019a; Lyman et al., 2020; Riddick et al., 2020), and in field injection experiments (Cahill et al., 2017; Forde et al., 2018) have revealed substantial variability of measured concentrations and effluxes, both spatially and temporally on seasonal, diel, and short-term (30 minute) time scales, potentially complicating reliable detection and emission rate estimations.

Several causal mechanisms explain the spatiotemporal variability of migrating gases. Within the saturated zone, subsurface heterogeneity and the presence of capillary barriers will trap buoyant free gas and cause fingered lateral and vertical movement and eventual episodic release when free gas pressure and buoyancy forces overcomes viscous forces and capillary entry pressures (Gorody, 2012; Steelman et al., 2017; Van de Ven et al., 2020; Woods & Norris 2016).

Dissolution and oxidation decrease migrating free phase gas quantities reaching the water table, to varying degrees depending on geochemical conditions and free-gas interfacial area (Cahill et al., 2017; Roy et al., 2016; Van de Ven et al., 2020). Heterogeneity in the unsaturated zone also leads to variable advective and diffusive gas effluxes (Ulrich et al., 2019). Barometric pressure decreases cause a pressure differential between the soil gas and atmosphere and therefore increased gas efflux across the soil-atmosphere interface, especially in thicker unsaturated zones (Forde et al., 2019b; Kovach, 1945). Wind-induced soil gas transport can be significant, where higher wind speeds (and related turbulence-induced pressure fluctuations) induce short-term variations in advective efflux (Poulsen & Møldrup, 2006; Poulsen et al., 2017; Redeker et al., 2015). Advective or diffusive mixing of migrating gases of deep subsurface origin (such as CH_4, C_2H_6, He) and gases of primarily atmospheric origin (O_2, Ar), produce identifiable soil gas mixtures (Frederick et al., 2017). Particularly in a thick unsaturated zone, microbial oxidation can consume enough methane to decrease or entirely obscure the GM surface expression, resulting in diagnostic carbon isotope fractionation (Forde et al., 2018; McMahon et al. 2018; Rowe & Muehlenbachs, 1999; Schout et al., 2019).

In summary, spatially and temporally variable CH_4 efflux and concentrations have been observed around energy wells, and field injection and laboratory studies have revealed some of the causal mechanisms. While episodic subsurface migration and varying meteorological factors such as barometric pressure, wind speed, and temperature can explain some of the variation, there is limited temporal and spatial discretization of measurements of gas migration effluxes and concentrations around energy wells. In addition, temporal variability is not assessed in the context of the standard of practice for GM testing. Industry tests for the presence of GM and further quantification of emissions, as well as the need to quantify the GM contribution to

atmospheric emissions, water quality perturbations, and land use impacts, will benefit from field-validation of the conceptual understanding of the behavior and spatiotemporal variability of migrating gases.

We present findings of spatiotemporal efflux and concentration variability around an established petroleum well known to have gas migration, with a view to recommending an effective field test for GM detection and efflux estimation. High-resolution efflux and concentration data and statistical analysis results relate external factors that may be driving changes in measured CH_4 efflux and concentration. Spatial efflux surveys and soil gas samples establish relationships and spatial trends in migrating gases and in-soil processes of oxidation, atmospheric mixing, and atmospheric displacement. The implications of these findings are discussed in terms of atmospheric methane emissions and the standard of practice for GM detection using currently practiced and proposed techniques.

2. MATERIALS AND METHODS

2.1 Field site description

An industry partner provided access to an anonymous site with known gas migration outside the outermost casing, at a conventional (non-thermal) petroleum production well that was drilled and completed using standard practices for non-horizontal wells after 1995. The status of this well is 'suspended' (i.e., idle, not actively producing oil or gas but with no decommissioning work completed). No additional methane emission sources beyond those attributed to GM are expected at the site. No SCVF was measured by the well operator, and no other surface and subsurface methane leakage sources are located near the well (verified through site inspection and spot concentration measurements performed by the authors). The well is located within Alberta Energy Regulator's 'Required Test Area' where a high instance of GM has been identified

(Alberta Energy Regulator, 2021; Figure 3a). Historic gas migration test results were provided by the operator for 14 GM testing events conducted by the site operator (8 tests) and service providers (6 tests) using industry-accepted methods (Alberta Energy Regulator, 2021) over >10 years (Figure 2). The GM measurement spacings generally followed the Alberta Energy Regulator's 'recommended' method (described above). Specific details of historic sampling, including sampling equipment and measurement depth, were not provided, and may have differed depending on testing party (Alberta Energy Regulator, 2021; Fleming et al., 2019). The maximum methane concentration measured across all (n = 14) historic GM testing events averaged 18,000 ppm (std. dev. = 30,000 ppm), demonstrating substantial variation in maximum concentrations between test occasions.

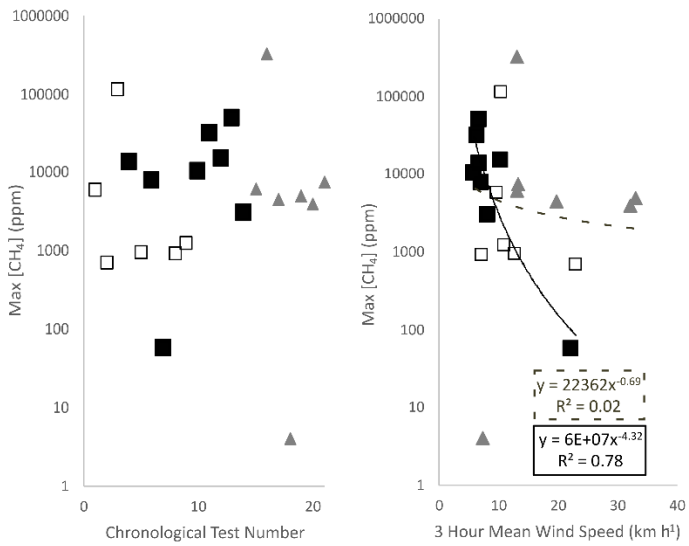

Figure 2 The maximum recorded combustible gas concentration as ppm CH_4 (log scale) from all available gas migration testing conducted at the study well. Historic tests conducted by one individual field operator are indicated as filled squares, and tests conducted by various service companies are empty squares. Tests conducted by the authors are shown as gray triangles. Results are shown in chronological order of testing date (left) and as a function of wind speed (using mid-day (11:00 to 14:00 hrs) data from the nearest weather station 10-20 km from study site; right). Trendlines are shown on all tests conducted (R^2=0.02; dashed line) and for those conducted by the same individual well operator (R^2= 0.78; black line).

A shallow water table ~0.6 m below ground surface (BGS; with +/- 0.3 m seasonal fluctuations) was identified by water monitoring wells hand-installed by the authors. The water table slope was consistent with an approximately southward groundwater flow direction. Slug and permeameter testing yielded a hydraulic conductivity at shallow depth (< 2 m) of $3x10^{-6}$ m s^{-1}. Fine silty-sand was observed down to two meters (the depth at which hand auger lithology samples were collected). Nearby water well records suggest unconsolidated sediments are present to about 10m depth, below which sedimentary bedrock occurs. Additional site details are reserved to protect site anonymity.

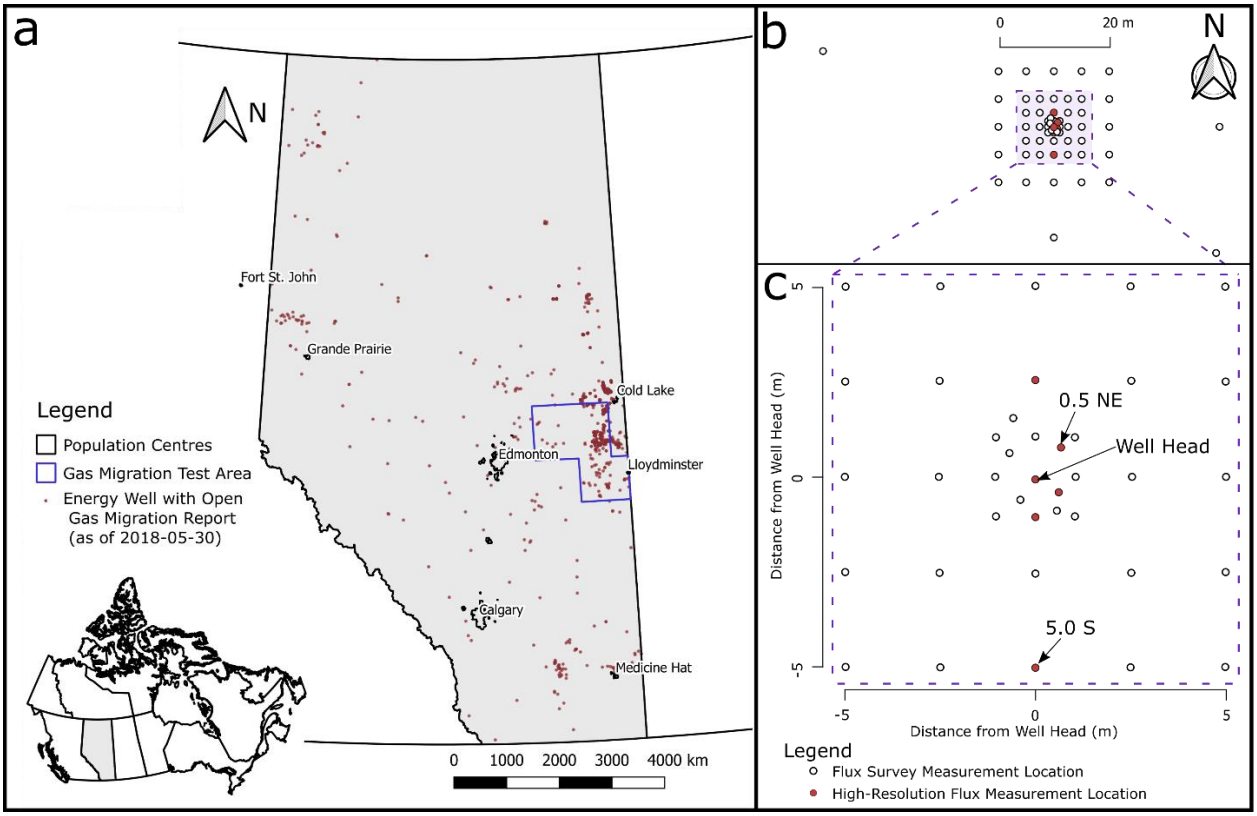

Figure 3 a) Overview of Alberta with all petroleum wells with open (i.e., detected but not repaired) reports of external gas migration as of 2018-05-30 (n = 1186), with the majority of these reported cases located on the eastern side of central Alberta in the region around Lloydminster and Cold Lake. The Alberta Energy Regulator Directive 20 gas migration Required Test Area outlined in blue is the only location provincially in which gas migration testing is currently mandated on all wells (Alberta Energy Regulator, 2021). Data from Alberta Energy Regulator (2018) and Statistics Canada (2016). b) Full scale and c) close-up plan view

schematic of the efflux monitoring network at the study well pad, showing locations of flux survey chambers (open circles). The location of repeat sampling and high-resolution efflux measurements over a two-week period (October 11th-27th 2019 are shown as red circles, labelled by distance and direction from the wellhead).

2.2 Methane concentration measurements using standard industry practices

Combustible gas concentrations were surveyed with a handheld detector (GT-43, Gas Measurement Instruments Ltd.) on soil surface (using a bell probe) and at 30 cm depth (with a slide-hammer gas vapor probe; Retract-A-Tip Gas Vapor Probe, AMS Inc.) on five separate occasions at recommended spacings (Alberta Energy Regulator, 2021). The handheld detector is representative of commonly available portable gas detectors in use, where multiple integrated sensors (thermal conductivity, semiconductor, catalytic bead) detect combustible hydrocarbon gases (CH_4, C_2H_6, etc.) across a wide range of concentrations (Szatowski et al., 2002). The sensors are calibrated to CH_4, and the sensor response to all combustible gases is reported in concentrations of CH_4 by ppm, % of the Lower-Explosive Limit (LEL) of methane (~5% v/v), or % gas by volume depending on sensed concentration (Gas Measurement Instruments, 2016). Using the three integrated sensors, the reported measurement resolution for CH_4 is 1 ppm in the <10,000 ppm range, 1% LEL in the <100% LEL range, and 1% gas by volume in the 1% to 100% volume range (Gas Measurement Instruments, 2016).

2.3 Soil gas sampling and analysis

Soil gas samples were collected from shallow soil vapor wells on five occasions (Feb 22, Jul 11, Aug 22-23, Sep 25, Oct 27, 2019). The soil vapor wells were constructed using 6.4 mm (1/4”) ID polyethylene plastic tubing with a Luer stopcock-valve fitting (Masterflex) and geotextile filter cloth covering a 10 cm perforated screen at the bottom. Vapor wells were installed at depths of 10 cm and 30 cm below ground surface by insertion of pre-constructed soil vapor wells into

diagonally drilled holes with soil allowed to collapse around the tubing. The 10 and 30 cm depths was selected based on inferred applicability to commercial gas migration testing procedures, with 30 cm being the maximum depth of observation permitted for subsurface sampling without the added expense of ground disturbance permitting (Province of Alberta, 2020). Previous attempts at installation of deeper soil vapor wells (0.5 and 1.0 m) resulted in saturation and clogging due to the shallow (0.3 to 0.8 m BGS over the observation period) water-table at the site. Prior to sampling, 20 mL of stale gas was purged from the vapor well tubing using a syringe (representing more than 3 tubing volumes removed). Following purging, a 60 mL soil gas sample was collected and injected through the butyl septa of a 30 mL helium-flushed and partially evacuated glass vial until the vial was overpressured. Syringe withdrawal rates were < 2 mL s^{-1} to limit atmospheric contamination and influx along the tubing. Soil gas samples were also obtained on Oct 21, 2018 using a slide-hammer probe (Retract-A-Tip Gas Vapor Probe, AMS Inc.) and stored in fully evacuated vials (in contrast to helium-flushed vials in other sampling events), permitting analysis of the He content of soil gas).

Major gas species were analysed by injecting a 5 mL gas sample aliquot into a Scion 450/456 four-channel gas chromatograph fitted with four separate sample loops, analytical columns, and detectors. The dedicated fourth channel separated and quantified argon-oxygen, with a lower detection limit of 50 ppm argon. The fourth channel used an MXT-Molsieve 5A analytical column (30m x 0.53mm, 50um film thickness) held at a constant temperature of 30°C, a 50µl sample loop, hydrogen carrier gas (constant flow 1.0 mL/min), and a Thermal Conductivity Detector (Filament Temperature 250 °C). Certified gas standards were used to calibrate the gas chromatograph immediately prior to analyses. Analytical precision and accuracy for all gases is typically better than ±2.5% of the reported concentration, and the reported lower detection limit

for alkanes (C1 to C5) is approximately 0.5 ppm. Isotope composition was measured using gas chromatography-isotope ratio mass spectrometry methods to determine $\delta^{13}C$ on CO_2, CH_4, and C_2H_6 (C2; ethane) on nine selected soil gas samples and six dissolved gas samples that met concentration thresholds (0.1% of the gas species of interest) (Humez et al., 2016). Two samples were analysed for $\delta^{2}H$ on CH_4 for additional gas source identification. Analyses were performed on a ThermoFisher MAT 253 isotope ratio mass spectrometer coupled to Trace GC Ultra + GC Isolink (ThermoFisher). All samples are reported in ‰ notation with respect to VPDB for $\delta^{13}C$ and VSMOW for $\delta^{2}H$. Lab reported accuracies are ±0.5 ‰ $\delta^{13}C$ and ±2 ‰ $\delta^{2}H$. All compositional and isotopic analyses were conducted at the University of Calgary Applied Geochemistry and Isotope Science Laboratories.

The composition and isotopic signatures of soil gases have previously been used to interpret the origins and near-surface interactions of migrating gases. Helium is routinely used as a noble trace gas associated with deep geologic origin, such as around natural CO_2 and CH_4 seeps, fault zones, and in gas migration leakage scenarios (Annunziatellis et al., 2008; Frederick et al., 2017; Wen et al., 2016). Similarly, elevated concentrations of higher alkanes (ethane, C2; propane, C3; etc.), are indicative of deeper gas origins since these gases are not considered to be co-produced during microbial methanogenesis that might occur in wetlands or surface aquifers (Bachu, 2017; Kang et al., 2014; Whiticar, 1999). Isotope ratios of $\delta^{13}C$ on CH_4, C2¸and CO_2 can also all be used to distinguish gas sources since diagnostic isotopic fractionation will occur during the source formation of these gases (Tilley & Muehlenbachs, 2012; Szatowski et al., 2002; Whiticar, 1999) and during their transport over geologic time (Hendry et al., 2017). In shallow groundwater and soil gas, argon can originate from both atmospheric sources, and the ultimate geogenic source of most argon on Earth, where ^{40}Ar is produced in the subsurface through the

radioactive decay of ^{40}K. However, any Ar in younger groundwater and soil gas systems (<20,000 years) can be presumed to originate from atmospheric sources due to the negligibly low abundance and long half life of the ^{40}K source (Almon and Magaritz, 1990). Therefore, Ar is used here as a noble gas tracer in shallow soil and groundwater systems, alongside other primarily atmospheric gases such as N_2 and O_2 (Almon and Magaritz, 1990; Martin et al., 1995; Frederick et al., 2017). Carbon dioxide can co-occur with CH_4 as a component of migrating subsurface natural gas, be produced during the microbial oxidation of methane, or during natural biologic respiration in soils (Romanak et al., 2014; Whiticar, 1999). Isotopic $\delta^{13}C_{CO2}$ values, and soil gas compositional trends, are used here to infer CO_2 origins (Risk et al., 2013; Romanak et al., 2014; Sandau et al., 2019).

2.4 Soil gas efflux measurements

Near-surface gas concentrations and effluxes were measured in two efflux survey and sampling events (Aug 20, 2019 and Sep 25, 2019) and one high-resolution long-term sampling event (Oct 11-27, 2019). Automated long-term and survey chambers measured spatial and temporal distributions of carbon dioxide and methane effluxes using the same equipment and approach previously described (Forde et al., 2018; Sihota et al., 2013). Soil efflux collars (20 cm tall, 200 mm internal-diameter SDR pipe segments) were installed in the soil to approximately 15 cm depth more than 24 hours before the initial survey measurements. During the two-week intensive measurements, a multiplexer (LI-8150, LI-COR Inc) switched between six long-term dynamic closed chambers (LI-8100-104, LI-COR Inc.) with chamber concentrations analyzed at 1 Hz with an infra-red gas analyzer (Li-8100, LI-COR Inc.) and an ultra-portable greenhouse gas analyzer (model 915-0011, Los Gatos Research Inc.). During each survey event, an efflux survey chamber (LI-8100-103, LI-COR Inc.) connected to the same two analysers was manually moved

between 51 different collar locations (Figure 3b). A custom wellhead collar (16 cm radius from the outermost well casing, total ground surface area 0.44 m^2) measured GM effluxes in the previously identified high-efflux zone immediately outside the surface casing (Figure S1). This custom collar fully encircled the well and was sealed against the intermediate casing below the wellhead. The long-term chamber closure times ranged from 15 to 90 seconds, switching sequentially between all 6 chambers with appropriate pre- and post-purge times, at around 18 minutes per cycle (Table S1).

Conservative CH_4 and CO_2 effluxes were calculated with linear curve fitting of chamber closure time vs. concentration in SoilFluxPro (LI-COR Biosciences; Forde et al., 2018; Sihota et al., 2013). The minimum detectable efflux (MDF) was calculated with conservative detector analytical accuracies taken to be $\Delta C = 0.2$ ppm for CH_4 and $\Delta C = 1$ ppm for CO_2, which is consistent with similar measurements at controlled injection gas migration study sites (Table S1; Christiansen et al., 2015; Forde et al., 2019a, 2019b). Manufacturer-reported instrumental accuracies are < 2 ppb for CH_4 (Los Gatos Research) and <1 ppm for CO_2 (LI-COR Inc).

The pre-closure concentrations of CH_4 and CO_2 within each chamber during each efflux measurement were taken as conservative estimates of the ground-surface concentrations at that moment and location. Use of these concentration 'initial values' from each automated efflux measurement as a proxy for measured concentrations using standard GM detection methods was validated by direct comparison between the two approaches using the same analyser. Immediately before each Aug 20, 2019 efflux survey measurement, the pre-closure concentrations were recorded within the chamber, and using the same gas analysers with a custom-fit bell-probe held against the soil surface adjacent to the outside of the collar. This procedure imitates standard industry practice for ground-surface concentration measurement

(e.g., DP-IR, Gas Measurement Instruments Ltd.; Irwin, INFICON; etc.). The moderately good positive correlation between the two methods (Spearman Rank R^2 = 0.48, m=0.85 on n= 48 measurement) at concentrations of < 3 ppm, validates use of initial chamber concentrations as a conservative estimate of ground-surface concentrations that would be obtained with industry-practiced detection techniques.

2.5 Environmental measurements

Soil moisture sensors (HydraProbe, Stevens Water Monitoring Systems Inc.) recorded hourly averaged temperature, electrical conductivity, water content, and apparent dielectric content to a datalogger (CR1000, Campbell Scientific Inc.) between July and November 2019 at six locations (depths of 5 and 30 cm, and distances of 1.0, 2.5, and 6.0 m East of the wellhead). Soil temperatures were also monitored using small sensors (TidbiT, Onset Computer Corporation) affixed with wire into countersunk holes in a softwood post at soil depths of 0, 0.1, 0.3, 0.5, 1.0 and 1.5 m BGS at locations 1.0 m East, and 6.0 m East of the wellhead between July 9 and November 18, 2019. Three additional temperature sensors were installed at 0.25 m North of the wellhead (immediately outside the wellhead efflux chamber) at depths of 0, 0.1 and 0.3 m for the duration of the October 11-27 measurement period. Water levels were recorded hourly in two piezometers with screens centered 1.0 m BGS, located 1.25 and 10 m South of the wellhead.

Precipitation and wind speed data were retrieved from the nearest public weather station (10 to 20 km away; exact distance withheld for confidentiality reasons) (Alberta Agriculture and Forestry). During this period, there was good regional correlation (averaging 0.86) between the 2 m height average wind speeds for the five nearest publicly available weather stations within a 50 km radius of the study site. Atmospheric pressures and temperatures were recorded hourly on-site (Barologger Edge, Solinst Canada Ltd.). Earth tide data (cm vertical displacement) over the

measurement period was estimated with site-specific coordinates using open software (Milbert, 2018). Change rates of water level and barometric pressure were calculated using a weighted five-hour central difference with three-hour rolling median smoothing (selected as the shortest window that eliminated hour-to-hour noise and produced visually smooth change rates).

2.6 Descriptive statistics of CH_4 and CO_2 concentration and efflux analysis

2.6.1 Regression modelling

Data processing and statistical analysis were conducted in the software package R (R Project version 4.0.2) with figures generated primarily using the ggplot2 package (R Core Team, Wickham, 2016). Linear interpolation was used to match the environmental data (typically recorded hourly) to times of efflux measurement. Thirteen environmental factors from the auxiliary data were considered for potential explanation of temporal variation in effluxes and concentration at each of the six chamber locations. These factors included: relative humidity, absolute barometric pressure, atmospheric temperature, approximate barometric pressure change rate, piezometer water level, approximate water level change rate, soil temperature at 0.05 m and 0.3 m BGS, soil water content at 0.05 m and 0.3 m BGS, temperature difference between the atmosphere and 0.3 m soil depth, vertical earth tide displacement, and wind speed.

Stepwise generalized additive regression models were used to identify the most important environmental predictors of temporal efflux and concentration variation by assessing the statistical relationships to the explanatory environmental factors (Hastie, 2019; Hastie & Tibshirani, 1990; Oliveira et al., 2018). Generalised additive regression models consider the combined (i.e., additive) linear or nonlinear (i.e., generalised) statistical relationships between multiple predictor variables (e.g., wind speed, atmospheric temperature, barometric pressure) and a response variable such as CH_4 efflux (Hastie & Tibshirani, 1990). In contrast to multivariate

linear regression, this method is advantageous for natural systems since it allows for nonlinear relationships between predictor and response variables to be described by a smooth function (Chen et al., 2019). In this analysis, parameter relationships could be represented as either linear, or a 2nd or 3rd order smoothed curve.

The relative statistical importance of each explanatory variable was assessed by building the model sequentially (i.e., in a forward stepwise fashion), with a single predictor variable being added at each step (Oliveira et al., 2018). Beginning with no explanatory factors, at each step the chosen algorithm sequentially added the single predictor variable which caused the largest increase to model performance. Continuous addition of all predictor variables may eventually lead to addition of irrelevant variables, overfitted models of excessive complexity, and weaker general predictive capacity. Excess model complexity was prevented here by optimising model performance towards the lowest possible Akaike Information Criterion (AIC) at each step (Akaike, 1974). A decreased AIC is produced by a model with better fit to the data, analogous to an increase in the model R^2. An increased AIC is produced by a model with greater complexity, such as a model with extraneous parameters or a statistical relationship described with a 2nd order curve when a linear fit is adequate (Hastie, 2019). Following this algorithm, the stepwise addition of model parameters stopped when further model fit would be achieved at the expense of excessive complexity. This type of statistical model analysis allows for identification of relationships between explanatory and response variables in complex data series with multiple potential interactions, however the results must be compared to existing scientific literature to ensure they are sensible (Chen et al., 2019).

2.6.2 Geostatistical interpolation

The relationship between flux magnitude and distance from the wellhead was first assessed through the Spearman rank correlation coefficient. The Spearman correlation describes non-linear relationships by correlating the relative rank rather than absolute magnitude. Total methane gas emissions from gas migration were then estimated by interpolating the CH_4 effluxes from August and September spatial surveys across the 20 m by 20 m measurement grid using Empirical Bayesian Kriging and Inverse Distance Weighting methods in ArcMap (ESRI). These two methods of spatial efflux interpolation were chosen for comparison based on their previous application in the related field of landfill gas emissions (Abichou et al., 2006; Börjesson et al., 2000; Spokas et al., 2003;), and elsewhere in the environmental geosciences (Annunziatellis et al., 2008; Cardellini et al., 2003). In this application, both kriging and IDW methods rely on the assumption that locations more closely spaced will have more similar effluxes than locations further apart (Börjesson et al., 2000). Inverse distance weighting is a deterministic method where the flux value at each interpolation location is calculated based on nearby measured values, weighted directly by the distance to the measurement points. Kriging can more optimally relate a predicted value to nearby measured points using a semi-variogram that most closely describes the site-specific distance-efflux relationship for all measured data. The predicted values in the kriged interpolation are based on both the distance and direction to the measured points, which may account for anisotropy and a non-uniform relationship between distance and efflux (Spokas et al., 2003).

The geospatial mean of the interpolated surfaces were used to generate an estimate of total methane emissions related to gas migration across the gridded area (Abichou et al., 2006), and the error associated with the interpolation using a 95% CI in the case of the kriged interpolation.

Emissions attributable to gas migration were also estimated with the previously published practice using the arithmetic mean efflux of all points measured within a 3 m radius of the wellhead, applied to the area within this radius (Erno & Schmitz, 1996). Finally, total emissions from directly within the wellhead chamber were calculated using the ground-surface area of the wellhead chamber, 0.42 m^2, multiplied by the mean efflux rate.

3. RESULTS

3.1 Methane concentration surveys:

Combustible gas concentrations measured using the handheld sensor were highest, and generally consistently detected, at ground surface only within one meter of the wellhead (Figure S. 2), while subsurface (30 cm depth) combustible gas was detected at higher concentrations and further distances (Figure S3). These gas concentrations had a similar spatial distribution and concentration range to the industry-provided GM test results (Figure 2), which also showed highest concentrations near the wellhead. Concentration measurements indicated that the only source of elevated combustible gas was from within the soil, with no indication of emissions from SCVF or other internal well integrity failure. During repeated site visits, there were no consistent sensory indications of the presence of GM, including an absence of visually obvious vegetation stress such as stunted, dead or discolored plants.

3.2 Gas efflux survey result

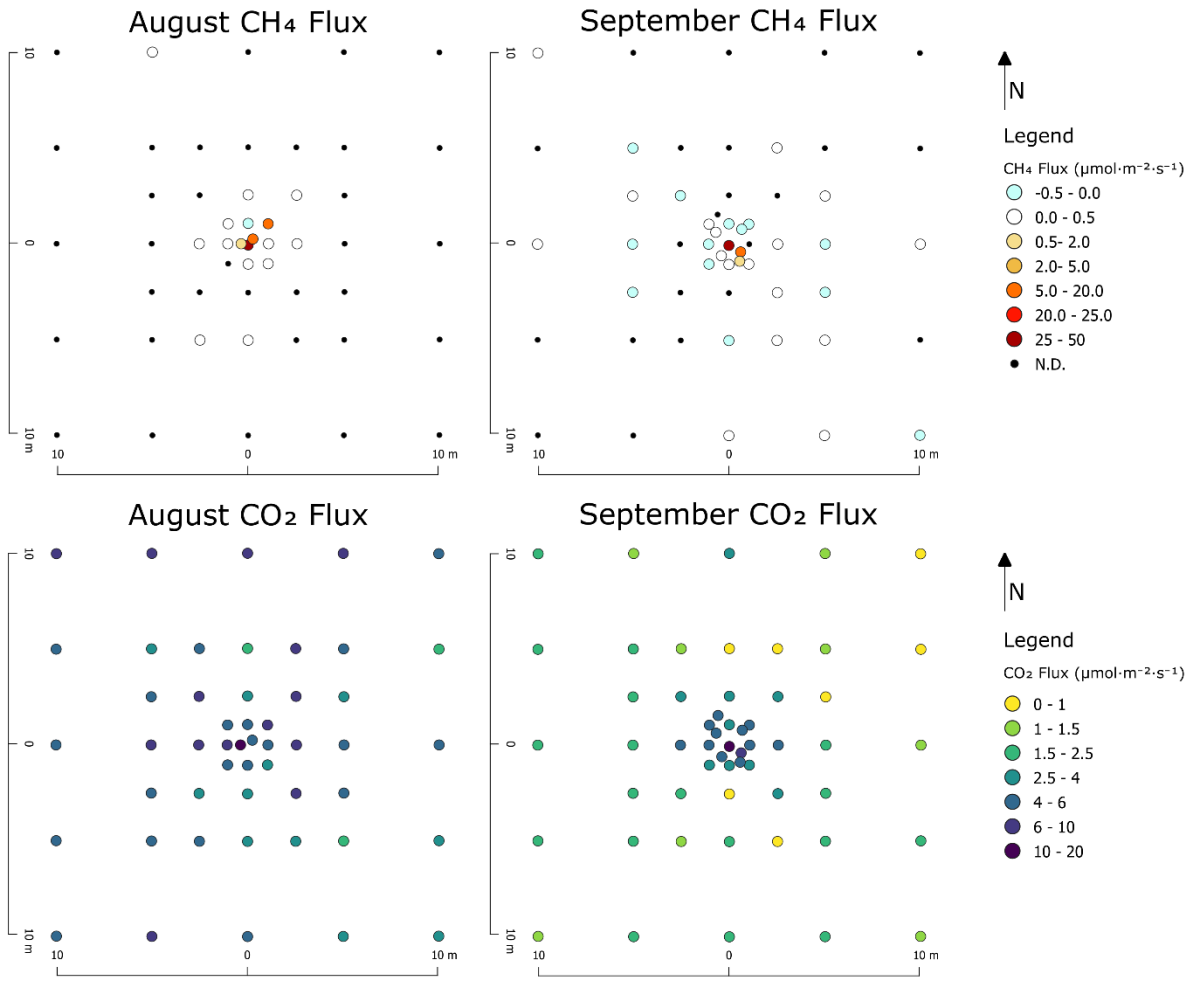

Figure 4 Plan view of efflux survey results for CH_4 (top row) and CO_2 (bottom row) measured in μmol m^2 s^{-1} on Aug 20, 2019 (PM; left hand side) and Sep 25. 2019 (AM; right hand side). Detection limits are generally 0.08 μmol m^2 s^{-1} CO_2 and 0.02 μmol m^2 s^{-1} CH_4. The horizontal distance from the wellhead is shown in scale bars.

Higher CO_2 effluxes were also observed around the wellhead, especially during the September efflux survey (Figure 4). Methane effluxes were substantially greater immediately around the wellhead, and some positive effluxes (emitting CH_4 from the soil into the atmosphere) were detected up to 10 m from the wellhead. Many effluxes (66% and 36% of measurements in August and September respectively), including some within meters of the wellhead, were less

than the detection limit (0.02 µmol CH_4 m^{-2} s^{-1}). Several sampling locations in September registered low-rate negative effluxes indicating CH_4 consumption occurred in the soil zone.

Considering data from both surveys, there was an inverse Spearman rank correlation with distance from the wellhead and CH_4 efflux across the entire measurement grid, and poor inverse correlation with distance and CO_2 efflux (r = -0.73, -0.17 for CH_4 and CO_2 respectively). Spearman correlation analyses were preferred to Pearson correlations since the former more appropriately described the nonlinear decline in effluxes with radial distance from the well. The estimated total CH_4 emissions from gas migration varied depending on measurement period and the method used (Table 4). There was a 62% increase in mean GM-related methane efflux in the wellhead chamber between the October dataset considering all measurements across the two-week measurement period (n=1215) and a subset when only considering times with wind speeds less than 3 km h^{-1} (< 0.83 m s^{-1}, thus reducing the observations to n =243; Table 4; Figure S12).

3.3 High frequency efflux measurement

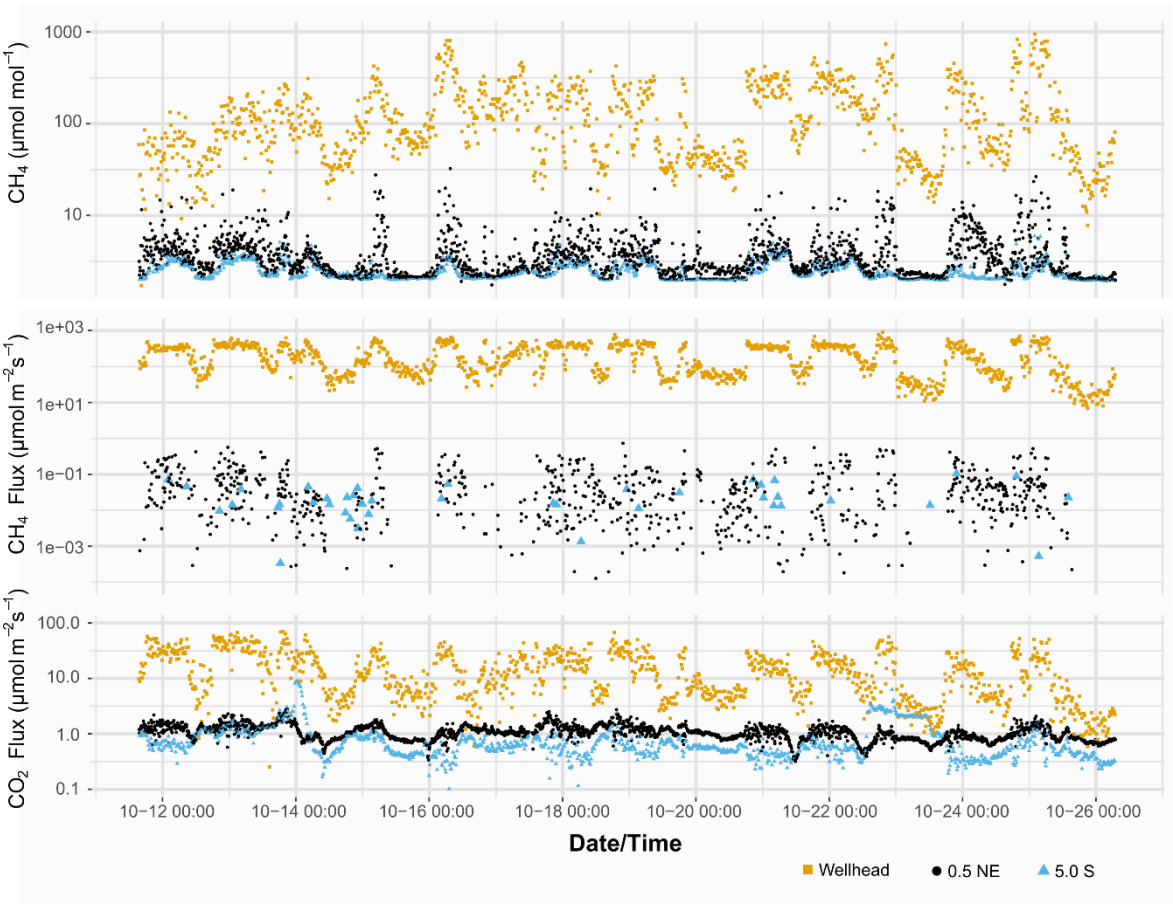

Figure 5 Time series of measured chamber pre-closure CH_4 concentrations (µmol mol^{-1}), CH_4 effluxes (µmol m^{-2} s^{-1}), and CO_2 effluxes (µmol m^{-2} s^{-1}) for three locations with high resolution measurement: at the wellhead (yellow squares), 0.5 m NE (black circles) and 5.0 m South of the wellhead (blue triangles).

The initial CH_4 concentrations at the wellhead chamber were always above the values at 5.0 m South of the wellhead, though the difference fluctuated from 10 to > 100 ppm CH_4 and the distinction was less clear during some periods (e.g. mid-day; Figure 5). Initial concentrations of CH_4 for other long-term chambers, including two located only 0.5 m from the wellhead, were approximately similar to the 5.0 South location, though slightly higher during peak flux periods (Table 1). Initial CH_4 concentrations at 5.0 South ranged between minimum and maximum values of 2.0 and 5.5 ppm CH_4, (5th percentile 2.07 ppm, 95th 4.33 ppm). Despite the higher CO_2

efflux at the wellhead, the pre-closure CO_2 concentration was not substantially different between chambers, ($R^2 > 0.9$) (Figure S5).

Table 1 Descriptive statistics of Oct 11-27th, 2019 high resolution efflux measurement series with chamber locations described in distance (m) and direction from the gas migration petroleum well. Confidence intervals calculated at 95% with bootstrapping methods and presented as (lower, upper).

	---------- CH_4 Efflux---------- ---			-- CO_2 Efflux --	CO_2 Efflux: CH_4 Efflux Linear Correl. Coeff (R)	CH_4 Concentration	Total Obs.
Chamber Location	Mean	SD	Detectable Obs.	Mean		Mean	n
	------- µmol m^{-2} s^{-1} ------		%	- µmol m^{-2} s^{-1} -	--	--- ppm ---	---
Wellhead	219 (210, 230)	197.2	100	16.4 (15.5, 17.3)	0.86	146 (138, 153)	1212
0.5 SE	1.25 (1.14, 1.35)	2.3	93	1.97 (1.93, 2.02)	0.51	6.22 (6.00, 6.42)	1216
0.5 NE	0.04 (0.04, 0.05)	0.8	47	1.08 (1.06, 1.09)	0.15	3.72 (3.62, 3.82)	2431
1.0 S	0.07 (0.06, 0.08)	1.0	40	1.27 (1.24, 1.30)	0.12	3.94 (3.74, 4.14)	1215
2.5 N	0.01 (0.00, 0.01)	0.3	11	0.87 (0.85, 0.89)	0.12	2.65 (2.60, 2.69)	1215
5.0 S	0.00 (0.00, 0.01)	0.3	8	0.84 (0.79, 0.89)	-0.19	2.48 (2.45, 2.51)	1214

3.4 Multivariate regression modelling of high-resolution methane efflux and concentration measurements

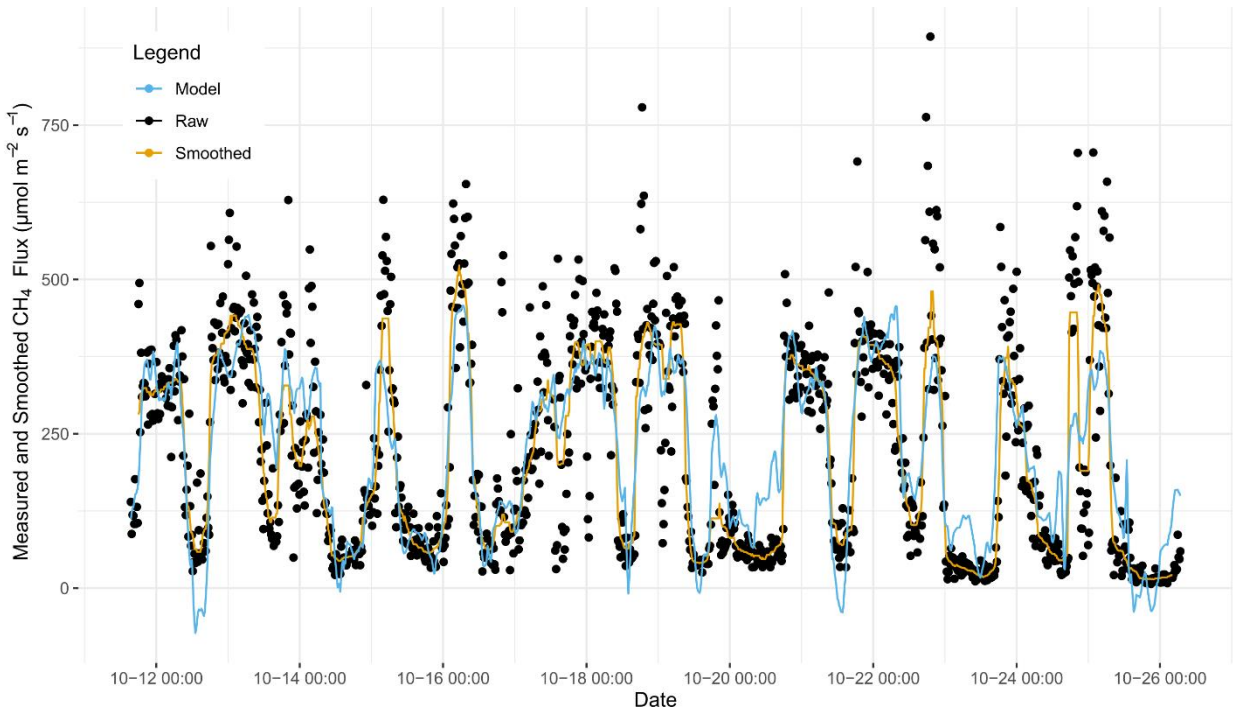

Figure 6 Wellhead chamber time series of CH_4 efflux from Oct 11-27th, 2019 with raw data (black dots), 20-point rolling median smoothing (yellow line) and multivariate regression modelling results (blue).

The two-week high resolution efflux monitoring period showed strong temporal variability, including diel variation with higher measured pre-closure concentrations and effluxes generally occurring overnight (Figure 5), and differences between consecutive measurements and stepped efflux behavior during chamber closure (Figure S6). Stepwise multivariate regression modelling results indicate that the quasi-diel patterns in observed gas migration concentrations and effluxes at the wellhead over the October 11-27th measurement period were most strongly related to varying wind speed and atmospheric temperature. Minor model contributions by other factors, including temperature at 30 cm depth, were considered in a final regression model including eight of the 13 possible environmental factors that explained 63% of the temporal variation in

wellhead CH_4 efflux (and 81% of smoothed efflux; Figure 6, Table S3). Wind speed was the most important parameter, and could explain 44% of the variation in measured CH_4 efflux at the wellhead (59% of smoothed efflux). Wellhead chamber CH_4 efflux was negatively correlated with wind speed (Pearson Correlation R = -0.72) and atmospheric temperatures (Pearson Correlation R = -0.49).

At all chamber locations, wind speed was the most important single predictor of temporal variation in CH_4 pre-closure concentration, and therefore first added factor to the stepwise model (Table 2). Wind speed was also the most important single addition to model R^2 at four out of the six chamber locations (Table S5). Other common relevant factors for CH_4 concentration models included change in barometric pressure, atmospheric temperature, and shallow soil water content or temperature. Compared to the CH_4 concentration regression models, the CH_4 efflux regression models (Table S3, Table S4) had less consistency in significant factors across all modelled chamber locations. However, wind speed and atmospheric temperature, or the differential in temperature between the atmosphere and soil, were assigned the highest priority by the model at 5 of 6 locations. Other lower priority (but statistically significant) factors included in the regression models for CH_4 efflux included groundwater levels and soil water contents (Table S4).

Table 2 Parameters most influencing the statistical model for the first three steps of forward stepwise multivariate generalized additive modelling of pre-closure CH_4 chamber concentrations at each long-term location. Model formulae are in the form: $[CH_4]$ = Parameter$_1$ + Parameter$_2$ …. The Akaike information criterion (AIC) is listed below the formulae at each step, with a decreasing AIC indicating an incrementally increasing goodness of fit. Environmental parameters abbreviations are: U_wind (windspeed), Wat.Cont_0.3 (30 cm depth soil water content), T_soil_0.05 (soil temperature at 5 cm depth), Baro_dP_dt (approximated barometric pressure change rate), T_atm (atmospheric temperature), E_tide (vertical component earth tide displacement).

Chamber Location	Model Step:1	Model Step:2	Model Step:3
Wellhead	U_wind ; 15200	Wat.Cont_0.3 + U_wind ; 15059	Baro_dP_dt + Wat.Cont_0.3 + U_wind ; 14985
0.5 SE	U_wind ; 6451	Baro_dP_dt + U_wind ; 6423	Baro_dP_dt + s(U_wind, df* = 2) ; 6405
0.5 NE	U_wind ; 11258	T_soil_0.05 + U_wind ; 11139	Baro_dP_dt + T_soil_0.05 + U_wind ; 11112
1.0 S	U_wind ; 6368	s(U_wind, df = 2) ; 6326	E_tide + s(U_wind, df = 2) ; 6308
2.5 N	U_wind ; 2816	T_soil_0.05 + U_wind ; 2708	T_soil_0.05 + s(U_wind, df = 2) ; 2676
5.0 S	U_wind ; 1789	T_atm + U_wind ; 1542	T_atm + Wat.Cont_0.3 + U_wind ; 1480

*df refers to the degrees of freedom of the smooth fitting function (1 if not indicated)

3.5 Soil Gas analysis results

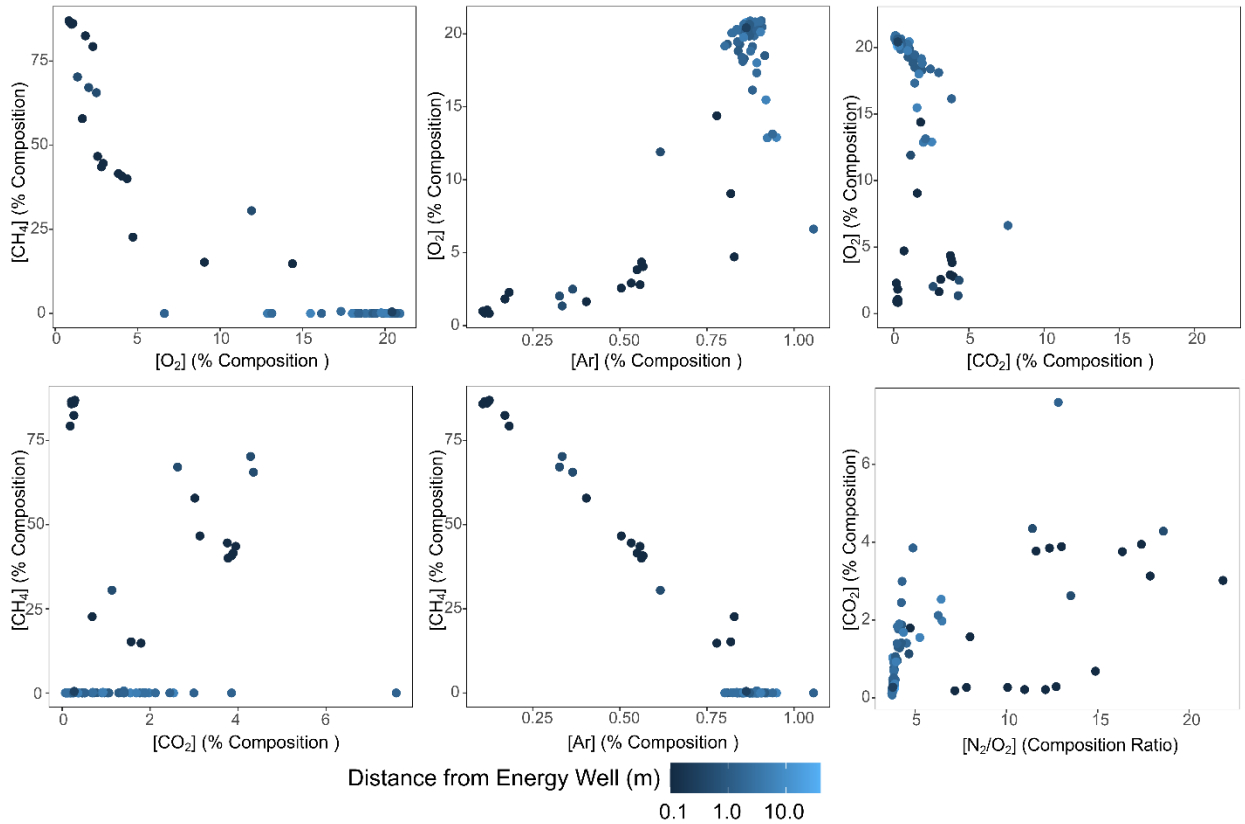

Figure 7 Selected scatterplot distributions of soil gas results at the 30 cm depth across five sampling events (% composition by volume), with lighter colors corresponding to increasing radial distance from the energy well.

Table 3 Pearson correlation matrix of soil gas compositions at the 30 cm depth around the gas migration test well.

	Ar	*N_2*	*O_2*	*CO_2*	*CH_4*
Ar	1	0.99	0.85	-0.12	-0.99
N_2		1	0.87	-0.15	-1.00
O_2			1	-0.51	-0.91
CO_2				1	0.21

The highest CH_4 concentration measured was 87% v/v, collected immediately outside the surface casing at a depth of 30 cm in November (i.e., early winter); this sample also contained CO_2 at 0.289 % v/v and He at 306 ppm. Across all samples, there was a relatively linear negative relationship between CH_4 and Ar (Figure 7). The O_2-Ar and O_2-CH_4 relationship was non-linear, with proportionally lower O_2 concentrations in most samples relative to direct mixtures of atmospheric and migrating gases. Further from the well, the soil gases contained generally lower concentrations of CH_4 and trace He, and higher concentrations of Ar, O_2, and N_2. Moderately positively correlations between CH_4 and CO_2 (Table 3) indicate CO_2 may be associated with migrating gases; however, the highest concentration CH_4 samples have lower concentrations of both CO_2 and Ar in comparison to samples with slightly lower CH_4 concentrations (Table S2). Several samples of soil CH_4 concentrations within < 5 m from the wellhead were as low as < 5 ppm CH_4. Some subsurface gas samples with deep gas signatures (including elevated CH_4, C2 and higher alkanes, and He) were detected up to 10 m from the well. Near the wellhead, soil gas samples had a high CH_4 content and low N_2 and Ar. CH_4 correlated very well with He (R^2 = 0.99) and the total concentration of higher alkanes, sum C_2-C_5, (R^2 = 0.87). Isotopic analyses of high concentration CH_4 samples nearest the wellhead had signatures of $\delta^{13}C_{CH4}$ = -60.7 ‰, $\delta^{13}C_{C2H6}$ = -45.0 ‰, $\delta^{2}H_{CH4}$ = -232 ‰, consistent with previous soil gas analyses conducted by the well owner (not shown). All soil gas samples (n=9) with CH_4 concentrations high enough for isotopic analysis (> 0.1% v/v CH_4) were within 0.5 m from the wellhead (Table S2). Analyses of $\delta^{13}C_{CO2}$ on these same gas samples ranged from -64.2 to -42.7 ‰. The $\delta^{13}C_{CH4}$ value rose as the concentration of CH_4 decreased relative to CO_2 (Figure S7).

4. DISCUSSION

4.1 Gas source and mixing implications

Trends and ratios in the isotopic composition and concentration of fixed gas indicators can be combined to infer mixing between two end-members soil gas sources and redox processes (Frederick et al., 2017; Romanak et al., 2014; Sandau et al., 2019). The presence of He and higher alkanes with methane, in addition to the carbon isotope ratios of $\delta^{13}C_{CH4}$, $\delta^{13}C_{C2}$ and $\delta^{2}H_{CH4}$, are diagnostic of migrating deeper or intermediate-zone thermogenic gases (Annunziatellis et al., 2008; Frederick et al., 2017). Isotopic and compositional 'fingerprints' of SCVF or GM gases can be compared with compositional depth profiles of gases sampled during drilling in nearby wells to estimate the stratigraphic source of the gas. Comparison of the isotope values of methane and ethane at this study well to four published isotope depth profiles in the region (Rowe & Muehlenbachs, 1999; Szatowski et al., 2002), indicate that the source of migrating gases at this study well may be ~300-400 m BGS.

While the saturated soils observed at the site provide conditions suitable for shallow natural (biogenic) CH_4 production (Romanak et al., 2014; Tokida et al., 2007; Whiticar, 1999), several results suggest there is not a significant biogenic CH_4 source at this site. Firstly, ethane, propane, higher alkanes, and helium are indicative of a deeper thermogenic methane, and gases are not co-produced during biogenic methane production (Kang et al., 2014). Similarly, the carbon isotope composition of CH_4 (and CO_2 near the wellbore) indicate a non-biogenic source (Kang et al., 2014; Szatowski et al., 2002; Romanak et al., 2014; Whiticar, 1999). Though the well pad is located near wetland areas, the maximum recorded methane efflux rates are higher than previously published rates in natural wetland settings (Tokida et al., 2007; Kang et al., 2014).

Considering the above observations and findings by previous authors, at this site CH_4, C2-C5, and He are interpreted to originate from a deeper gas migration source, while N_2, Ar and O_2 are interpreted to have primarily atmospheric origins (Annunziatellis et al., 2008; Frederick et al., 2017; Sandau et al., 2019). Since Ar is biologically inert, it provides a 'tracer' of atmospheric gases. The generally linear Ar-CH_4 relationship suggests a two end-member mixing model between methane and Ar, with dilution and displacement of atmospheric gas near the wellhead (Frederick et al., 2017). The non-linear correlations between O_2 and other gas species reflects its biological consumption and production.

4.2 Spatial distribution of migrating gases

Elevated CH_4 concentrations and efflux around the wellhead indicated a preferential migration zone. During the long-term measurements, the average CH_4 efflux at the 0.44 m^2 chamber encircling the wellhead was approximately two orders of magnitude greater than the next highest measured location at 0.5 m SE (Table 1). While the wellhead chamber extended > 15 cm beyond the edge of the surface casing, concentration surveys repeatedly indicated that the highest measured surface CH_4 concentrations (and therefore likely also the highest efflux) occurred immediately outside the casing (Figure S2). The observed spatial distribution supports the dominance of vertically acting buoyancy forces on gas transport in the saturated zone, and a higher gas permeability near the well in both the saturated and unsaturated zones (Van de Ven et al., 2020). Fracturing or disturbance of the rock within the formation during drilling, and the subsequent cementation challenges, are generally understood to result in micro-annuli between the cement and casing or cement and formation, causing the zone along the well casing to be a preferential migration pathway with lower capillary entry pressure to migrating free-phase gas (D'Aniello et al., 2020; Dusseault & Jackson, 2014).

Excluding the subset of highest effluxes and concentrations immediately adjacent to the wellhead, effluxes at ground surface, and surface and in-soil gas concentrations, were not uniformly lower with increasing radial distance (0.5 to 5 m) from the interpreted preferential migration pathway immediately outside the outermost casing. Spatial variability in gas effluxes and concentrations measured at the soil surface are known to exist due to subsurface heterogeneity and lateral migration underneath capillary barriers in the saturated zone (Forde et al., 2019a; Steelman et al., 2017; Van de Ven & Mumford, 2020) as well as preferential gas movement in the unsaturated zone (Chamindu Deepagoda et al., 2016; Mitton, 2018). This spatially variable distribution of migrating gases, with higher effluxes and concentrations closer to the well, rapidly decreasing to low or intermittently non-detectable values, confirms findings by several previous authors (Erno & Schmitz, 1996; Forde et al., 2019a; Lyman et al., 2020; Smith et al., 2019).

The rate and shape of concentration increase curves within the closed efflux chambers over time (Figure S6) varied spatially. Advective efflux was suggested by rapid linear concentration increases at high efflux locations, regardless of concentration gradients, while a low-rate exponential concentration increase indicative of diffusive efflux was observed at collars more distal to the preferential migration pathway (similar to finding by Forde et al., 2019a; Sihota et al., 2013). Occasional stepwise concentration increases suggest ebullition events (Figure S6).

The total number of CH_4 efflux measurements above the minimum detectable efflux ranged from 100% at the wellhead chamber down to 8% at 5.0 South (Table 1), suggesting that the gas migration pathway outside the outermost casing can be characterized as a relatively continuous transport pathway, while further away the transport of gas through the saturated zone shifted to a transitional or discontinuous flow regime, as was observed by Van de Ven et al. (2020) in lab

experiments. The spatial distribution of soil gas composition, detectable effluxes, and efflux curve behavior indicates primarily advection-driven gas transport from the gas source depth, along the well-casing preferential migration pathway to the atmosphere, with more intermittent and diffusive flow at greater distances from the wellhead (similar to observations by Chamindu Deepagoda et al., 2016).

Both heterogeneity in efflux patterns and short-term variation in effluxes over the two-hour spatial survey may have also introduced some apparent spatial variation since individual 90 second closures may have captured ebullition events or periods of higher efflux at some locations but not others. This spatial heterogeneity resulted in a poor spatial autocorrelation of CH_4 effluxes which introduced a large degree of uncertainty in the interpolated effluxes used to estimate total emissions (Table 4).

4.3 Total CH_4 emissions and other impacts

Total gas migration CH_4 emissions across the full measurement grid was estimated to be 466 g d^{-1} (non-detectable to 2590 g d^{-1} at 95% CI) in August and 229 g d^{-1} (non-detectable to 1750 g d^{-1} at 95% CI) in September using Bayesian kriging interpolation methods. Emissions averaged 129 g d^{-1} from the wellhead chamber over the 15-day high resolution measurement period (Table 4). While multi-day emissions directly around the wellhead reasonably predicted GM emission magnitude, the sum of low-rate diffusive effluxes applied across the 20 m by 20 m measurement area centered on the well did contribute significantly to the total estimated emissions from GM. Poor spatial autocorrelation of CH_4 effluxes resulted in substantial uncertainty in interpolation and therefore large total emissions estimate error through kriging methods (Figure S8). Emission estimates at the lower and upper 95% confidence intervals were non-detectable to 2590 and non-detectable to 1750 g CH_4 d^{-1} for August and September, respectively. This uncertainty indicates

the potential for error in estimates of total GM emissions at other sites when using point efflux measurements. Total GM emission estimates compared similarly when using Inverse Distance Weighting interpolation or the mean efflux applied to a three-meter radius around the well (after Erno & Schmitz, 1996), while Bayesian kriging estimates were higher (Table 4). High-resolution multi-day measurements were more likely than single sampling events to capture higher magnitude GM methane effluxes, which tended to occur over night during periods with low wind velocities, resulting in order of magnitude higher estimated effluxes for long-term chamber measurements compared to the snapshot survey measurements (Table 4).

Despite the uncertainty in emission estimates, the average of the two kriged spatial survey estimates, at 350 g CH4 d^{-1} (or 0.5 m^3 d^{-1}, 3.6 t CO2e y^{-1}), is within the range of values reported for energy wells with gas migration and comparable to other sources of anthropogenic methane emissions (Table 5). Direct comparison between these results and emission values presented in previous studies are complicated by differences in study design, since emissions measured through full-wellhead enclosures (e.g., Kang et al., 2014) or at cut-and-capped wells (Schout et al., 2019) may not be entirely due to GM, but also SCVF or other well integrity failures. There is also an expected variation between wells due to differences in geology and well design, and jurisdictional differences in wellhead configuration (where surface casings in Alberta are vented to the atmosphere; Dusseault & Jackson, 2014).

Table 4 Estimated total GM-related CH_4 emissions at this study site. Values are average effluxes (with upper, lower 95% confidence interval where available).

Data Description	Average Emissions		Method	Comments
	g d^{-1}	m^3 d^{-1}		
STUDY WELL				
August efflux survey	23	0.03	a	
	104	0.15	b	n=10 detectable efflux locations
	466 (0, 2590)	0.7 (0, 3.8)	c	
	118	0.17	d	
September efflux survey	15	0.03	a	
	84	0.12	b	n=8 detectable efflux locations
	229 (0, 1748)	0.34 (0, 2.6)	c	
	48	0.07	d	
October long-term measurement	129 (123, 135)	0.19 (0.18, 0.20)	a	Bootstrapped mean on n=1215 ground-surface emission measurements over 14 days
	1733	2.55	b	Mean of n=5 14-day long-term chamber mean efflux rates
Wind speed < 3 km h^{-1}	208 (199, 217)	0.31 (0.29, 0.32)	a	Mean wellhead ground-surface emissions, subset to times with wind speed < 3 km h^{-1}

[a] Ground-surface efflux in chamber directly around wellhead, [b] Arithmetic mean of all efflux measurements applied to a 3 m radius around the well (non-detectable and < 0 efflux treated as zero), [c] Bayesian Kriging Interpolation, [d] Inverse Distance Weighting Interpolation

Table 5 Previously reported literature values for emissions resulting from well integrity failure, and comparison with other anthropogenic and natural CH_4 sources/sinks. Unless otherwise stated, values are mean emissions (with upper, lower 95% confidence interval where available).

Data Description	Emissions		Method	Comments	Source
	g d^{-1}	m^3 d^{-1}			
GAS MIGRATION AROUND PETROLEUM WELLS					
Mean ground-surface emissions (Western Canada)	2350	3.5	b	N =29 shallow oil and gas wells in Eastern Alberta and Western Saskatchewan. Average 3 m CH_4 emission for all measurements at each well across n=29 wells reported in their Table 2. Median = 1052 g d^{-1}, 1.55 m^3 d^{-1}.	Erno & Schmitz, 1996
Mean ground-surface emission, natural gas storage wells (Utah)	100 (0, 300)	0.15 (0, 0.4)	b	Measurements conducted by Lyman et al., 2020. Dynamic efflux chamber measurement method	Smith et al., 2019
Mean wellhead emissions (Pennsylvania)	264	0.390	e	Measurements from 19 abandoned Pennsylvanian wells with existing above-ground wellhead. Median = 1.3 g d^{-1}, 0.0020 m^3d^{-1}	Kang et al., 2014
1 abandoned well (Netherlands)	10392		e	Only one of 29 abandoned (cut-and-capped) wells surveyed was leaking. Efflux at 2 m depth in soil.	Schout et al., 2018
Mean abandoned onshore oil and gas well (UK)	43 (35, 51)	0.06 (0.05, 0.08)	-	Emissions based on diffusive modelling of methane concentration measurements. Mean of 104 wells.	Boothroyd et al., 2015
SURFACE CASING VENT FLOWS IN PETROLEUM WELLS IN ALBERTA					
Mean Surface Casing Vent Flow (Alberta)	8860	013	-	April 2018 database records on n= 9493 open reports. Median = 136 g d^{-1}, 0.2 m^3 d^{-1}	Alberta Energy Regulator, 2018
NON-PETROLEUM SOURCES/SINKS					
Replacement/growing heifers/steers	183	0.27	-	Per-head direct emission through enteric fermentation, North America	IPCC 2019
Dairy cow	268	0.40			
Canadian landfill emissions to atmosphere, per capita	35	0.05	-	Based on the 2018 estimate of 12 Mt CO2e emitted to the atmosphere as CH4, with per-capita values calculated using July 1st, 2019 population of 37,589,262	Environment and Climate Change Canada, 2020.
Alberta soil consumption capacity	-124	-0.2	-	Per m^2 ground area. Ideal laboratory conditions. Up to 40-50% oxidation efficiency	Stein & Hetteriatchi 2001
Methane biofiltration	-1900	-2.8	-	Per m^3 bulk substrate. Actively aerated system	Gunasekera et al., 2018

[b] Arithmetic mean of all efflux measurements applied to a 3 m radius around the well (non-detectable and < 0 efflux treated as zero), [c] Bayesian Kriging Interpolation, [d] Inverse Distance Weighting Interpolation, [e] All efflux at and around the wellhead

Gas migration emissions are thought to typically represent only a small contribution of total emissions in the perspective of other vented and fugitive methane emission sources at the well pad scale, and more broadly within the upstream oil and gas industry (Schiffner et al., 2020; Schout et al., 2019; Smith et al., 2019). For example, an estimated 3.9 % of average per-well emissions at a gas storage facility measured by Smith et al. (2019) were due to emissions from

gas migration outside the surface casing. While likely comparatively low in the perspective of other sources within the upstream oil and gas industry, relatively poor quantification of the absolute number of wells with GM complicates quantification of industry-wide contributions of methane emissions through GM (Abboud et al., 2020). In addition, representative emission averages are difficult to obtain from limited measurements in an emission distribution that is characteristically heavily skewed by a small number of 'super emitters' (Brandt et al., 2014; Erno & Schmitz, 1996; Saint-Vincent et al., 2020; Zavala-Araiza et al., 2015). Nonetheless, GM at this study well was repeatably detectable using efflux and concentration-based approaches at varying time scales, despite a comparatively low emission rate in perspective of industry-wide sources. This indicates that 'super-emitting' GM wells most significant from an emissions standpoint will be reliably detected in similar field settings. Placed within the larger context of anthropogenic emissions, the annual methane emissions from this study well were equivalent to the operation of ~1 Canadian passenger vehicles (at 3.26 t CO_2e y^{-1}) or the direct emissions through enteric fermentation over the full-life of < 2 North American beef cattle (IPCC 2019; Natural Resources Canada).

Legal requirements for well decommissioning (abandonment) in Western Canada stipulate that GM (and other well integrity failures such as surface casing vent flow; SCVF) are repaired to non-detectable rates, at expense averaging at least $150 000 per well, and with an anecdotally high rate of unsuccessful repair attempts (Alberta Energy Regulator 2021; Dusseault et al., 2014). This repair cost is an economic disincentive for operators to repair and decommission non-producing wells with GM, therefore contributing to a backlog of suspended energy wells that may otherwise be decommissioned (Abboud et al., 2020; Alboiu & Walker, 2019; Schiffner et al., 2020). More widespread and increasingly rigorous testing approaches may provide insight

into the liability of suspended wells with GM, while remediation of all but super-emitter wells may contribute proportionally low reductions in overall methane emissions in the broader perspective of anthropogenic emissions.

From a GM detection perspective, surface efflux and concentration measurements most easily detect those wells which are more significant sources of atmospheric emissions, such that the highest impact wells will be most readily detected. This, however, may not be true of subsurface and groundwater impacts due to the complexity of subsurface migration pathways and geochemistry, and the potential for greater methane dissolution with lower rate or more episodic gas migration due to greater interfacial area between free phase gas and groundwater (Cahill et al., 2017; Van De Ven et al., 2020). The desired testing sensitivity and future standards of GM testing must consider desired risk mitigation, be it atmospheric emissions, groundwater impacts, or simply any presence of GM.

4.4 Temporal variability in measured effluxes and concentrations:

Measured CH_4 and CO_2 efflux and pre-closure concentrations of CH_4 at locations < 1 m from the well varied by up to 50% between individual measurements (taken ~18 minutes apart; Figure 5). Previous authors have found, both conceptually and experimentally, that the interaction of buoyancy and capillary forces of migrating free-phase gas in porous media will result in fingered and continuous or discontinuous migration pathways, causing spatially variable and potentially intermittent gas emission at the surface despite a continuous gas source at depth (Ahlfeld & Dahamani, 1994; Gorody, 2012; Van de Ven et al., 2020). This conceptual and laboratory understanding is supported by these field data of intermittently detectable observations, ‘stepped’ closed chamber concentration increases (Figure S6), and substantial variations in efflux

magnitude between measurements < 1h apart, as has been observed by other authors (Sihota et al., 2013; Forde et al., 2019a; Lyman et al., 2020).

In addition to this described irregular variation attributed to episodic ebullition and gas movement in the saturated zone, a quasi-diel cycle in efflux and concentration by up to one order of magnitude was identified with higher measured CH_4 and CO_2 initial chamber concentrations and effluxes occurring at night, and greater magnitude of variation nearest the wellhead (Figure 5). Decreased initial chamber concentrations during the daytime were correlated with periods of higher wind speeds, as suggested by the stepwise regression modeling results (Table 2), and as observed in previous gas migration studies at the well pad scale, and field-scale vadose zone gas injection experiments (Yin et al., 2014; Ulrich et al., 2019). Wind speed was also inversely correlated with historic gas migration concentration tests (Figure 1Figure 2) suggesting it has a similar effect in efflux chambers and the industry standard of practices. Increased wind velocity has been shown to erode the methane concentration boundary layer, thereby decreasing measured methane concentrations at and near the ground surface (Chamindu Deepagoda et al., 2016; Ulrich et al., 2019).

Regression models suggest multiple other factors were also related to varying initial CH_4 concentrations, including soil temperature and barometric pressure change for chambers near the well, and air temperature and absolute barometric pressure for chambers further away (Table 2). Despite the relatively thin vadose zone, the regression model also indicated a moderate relationship to changes in barometric pressure, particularly for suppressing higher modelled effluxes and higher concentrations during periods with the highest rate of barometric pressure increase, leading to a modest increase in the model R^2 for the CH_4 concentrations at several locations (Table S3, Table S5). This observation is consistent with pressure-differential induced

movements of soil gas within the unsaturated zone, as previously observed in multiple fields of research including artificial gas migration experiments, landfill gas emission, and natural methane-producing ecosystems such as peatlands (Börjesson, & Svensson, 1997; Forde et al., 2019b; Nachshon et al., 2011). There was no indication that falling barometric pressure triggered ebullition events as observed by Tokida et al. (2007).

Other observed statistical relationships to methane efflux and concentrations were to the water level and rate of water level change, and the related variable of soil water content. This is consistent with advective movement of gas during filling and emptying of pores, and altered gas movement pathways and lower effective gas permeability in the soil at higher soil water contents. Temperature-related factors included the atmospheric temperature, potentially leading to greater diffusion rates at higher temperatures, and the differential between soil and atmospheric temperatures since this may induce a convectively driven advective efflux (Nachshon et al., 2011).

4.5 Wind influences on variations in measured efflux

Regression modelling results also indicate that variation in wind speed was the most important predictor for the variation in the measured CH_4 efflux at the wellhead chamber, where it contributed to 11% of the final model R^2 fit. Measured CH_4 and CO_2 efflux and wind speed are negatively correlated at multiple chamber locations (Figure S11), where lower measured effluxes occur during times of higher wind speeds. These observations are similar to previous studies using dynamic closed chambers (e.g., Oliveira et al., 2018; Seo et al., 2020). This trend of lower measured efflux at higher wind speeds largely conflicts with conceptual understandings of greater ground-surface gas exchange at higher wind speeds caused by pressure pumping and a Bernoulli effect of reduced pressure (Poulsen & Møldrup, 2006; Poulsen et al., 2017; Redeker et

al., 2015). While these reported data may be due to a strong correlation to some unconsidered factor accounting for true variation in efflux at this site, lower observed efflux is most likely explained by measurement bias with site infrastructure and the equipment used (Maier et al., 2019). Experimental error involving flushing of gases within the chamber due to an imperfect isolation during chamber closure is considered unlikely. This wind-efflux relationship was observed across all six independent chambers, and spot-checked concentration increase curves did not indicate any air flushing during chamber closure (Figure S6; Figure S11).

Firstly, winds may flush soil gases around structures, removing the migrating soil gases from within the collars (5 cm depth at the wellhead, 15 cm depth elsewhere). Previous authors suggested that higher wind caused lower measured radon efflux and radon entry into structures due to flushing of the soil with atmospheric air, especially around above-ground structures that will induce pressure gradients within the soil (Kovach, 1945; Riley et al., 1996). This may present a potential problem for future use of chamber-based methods of CH_4 emissions through well pad soils. Larger flux collars (as used here), or larger or custom chambers or tents may be necessary to encircle the surface facilities (including the well casing or full wellhead) that are expected to represent preferential gas movement pathways (e.g., Kang et al., 2014; Lebel et al., 2020; Riddick et al., 2020).

Another explanation for the observed wind-efflux relationship is a bias towards under-estimating effluxes during high-wind periods due to more rapid breakthrough times at higher wind speeds and the closed chamber's attenuation of atmospheric pressure variations. In a laboratory experiment of gas breakthrough with varying wind speeds, Poulsen et al. (2017) noted that the breakthrough times of soil gas during windy periods was as low as 1 to 2% of wind-free conditions. Episodic arrivals of methane and other gases through ebullition at the water table will

therefore break through to the ground-surface boundary layer more rapidly in times of higher wind speed, increasing the chance that an ebullition event will not be captured by the discrete 90 second chamber measurements during higher-wind periods. At a shallow peatland, Redeker et al. (2015) observed that a high wind event of less than 10 minutes caused substantial gas exchange that temporarily raised peatland CO_2 effluxes until the soil had been flushed with atmospheric air, at which point the efflux was suppressed for several tens of minutes until pre-wind efflux rates re-established. The vents on the dynamic closed efflux chambers used in this study are specifically designed to limit any pressure fluctuations caused by wind under the intent to limit measured effluxes to those caused by diffusive mechanisms while avoiding the over-estimation of effluxes caused by a venturi-induced pressure drop within a chamber with open vents (Xu et al., 2006). Therefore, the vented chambers used in this study inhibit one of the primary modes of gas exchange across the ground surface. Since the effluxes at sites with shallow water tables are decreased after a higher wind event, the chamber measurements at this site may have been biased towards under-estimating the effluxes during periods of higher winds (Maier et al., 2019). This bias may have contributed to the 62% increase in average wellhead CH_4 efflux for low-wind (< 3 km h^{-1}) periods compared to the full time series (Table 4).

4.6 Methane oxidation in the unsaturated zone

Several previous authors have also suggested quasi-diel variations in CH_4 efflux may be explained by the strong, exponential dependence of CH_4 oxidation rates on higher temperatures, even when the magnitude of temperature variation in some previous studies were relatively small (Börjesson, & Svensson., 1997; Mikkelä et al., 1995; Stein & Hettiaratchi, 2001; Tang et al., 2008). During this field experiment, the magnitude of daily atmospheric temperature variation was up to 15 °C (from -5 to +10 °C), leading to soil temperatures variations of up to 4 °C (from 2

to 6 °C) at the 5 cm depth and <1 °C (around an average 3 °C) at the 30 cm depth (Figure S9). Variable oxidation rates caused by these diurnally fluctuating soil temperatures were unlikely to have caused a substantial proportion of the variation in observed efflux at the wellhead. The regression model fit indicated that soil temperature variation gave a relatively limited contribution to model performance at most chamber locations (Table S3, Table S5). In addition, there was no indication of increased CO_2 efflux coinciding with decreased CH_4 efflux at higher temperatures, as would be expected if the soil microbes were producing CO_2 at higher rates during higher daytime temperatures. This observed oxidation effect is expected to be more prevalent away from the primary gas transport zone. The relative importance of oxidation in decreasing measured concentrations would be lower along the high-efflux preferential flow pathway due to less contact time, lower surface area, and lower soil O_2 where atmospheric gases have been displaced (Forde et al., 2018; Gunasekera et al., 2018).

Although variable oxidation rates do not appear to contribute substantially to the diel variation in effluxes, there is good evidence that some CH_4 is being oxidized to CO_2 within the unsaturated zone, in support of observations of previous research at gas migration sites (Erno & Schmitz, 1996; Forde et al., 2018, Schout et al., 2018). Soil $\delta^{13}C_{CO2}$ averaged -53 ‰, indicating some CO_2 was being formed through biodegradation of thermogenically sourced CH_4, or a mixed thermogenic-biogenic source (Table S2, Figure S7; Risk et al., 2013; Romanak et al., 2014). Higher CO_2 effluxes and soil CO_2 concentrations are observed within meters of the wellhead preferential flow pathway (Figure 4; Figure 7). At the elevated concentrations observed, this CO_2 may be derived from some combination of natural in-soil biologic respiration, production of CO_2 during oxidation of CH_4, and transport of deeper CO_2 as a component of the migrating gases (Romanak et al., 2014). The samples with highest migrating gas concentrations of CH_4 and He,

collected from immediately outside the well casing, did not have the highest concentration of CO_2. In addition, the N_2/O_2 ratio is commonly higher than ten for samples near the well, compared to the atmospheric value of 3.7, which is consistent with the consumption of atmospheric O_2 (Figure 7; Romanak et al., 2014). Samples with O_2 concentrations that are depleted relative to atmospheric concentrations also have higher CO_2 concentrations. At the lower O_2 concentrations, the trend between O_2 and CO_2 is steeper than -1, indicating that methane oxidation is more important than natural biologic respiration in the production of CO_2 near the wellhead. More distal to the well, the N_2/O_2 ratio and the trend of O_2 to CO_2, are more consistent with a biologic respiration source (Figure 7; Sandau et al., 2019; Romanak et al., 2014). Biologic respiration is likely contributing to measured CO_2 concentrations and effluxes with a mixed or natural source, with increasing importance of biologic respiration further from the well. These combined compositional and isotopic indicators suggest that CH_4 oxidation within the unsaturated zone is leading to the elevated CO_2 concentrations and effluxes within meters of the wellhead.

While perturbations to the natural geochemical conditions, including anaerobic soils and inhibition of plant growth may develop, microbially mediated oxidation of CH_4 is favorable from an explosion hazard and emissions standpoint since these reactions will eventually yield CO_2, with substantially lower global warming potential (Hoeks, 1972; IPCC 2013). Systems to enhance this microbial methane oxidation may therefore be exploited as one potential option to decrease emissions from low-rate gas migration sources. Passively or actively managed in-soil oxidation or biofiltration systems could therefore be investigated as a medium or long-term strategy to address low-rate emission sources. However, the capacity of natural, actively, and passively managed systems to continue oxidizing CH_4 during soil conditions sub-optimal for

microbial growth (including low temperatures or low moisture contents) will need to be investigated further (Stein and Hettiaratchi. 2001; Gunasekera et al., 2018).

4.7 Implications for gas migration testing and future scientific study

Potential sensory indications of GM may include visual observations of bubbling through ponded water, vegetation impacts (including discolored, stunted, or dead plants), and "auditory, olfactory, or other evidence of possible gas migration" (BCOGC, 2019; Nooman et al., 2012). In Alberta, GM impacts on vegetation have been recorded historically and additional GM test points are recommended at locations of apparent vegetation stress surrounding a well (Alberta Energy Regulator, 2021; Bachu, 2017). Other sensory indications are not formally referenced by Alberta's provincial regulator. Throughout the field campaigns at this study site, conclusive sensory indications of GM were absent. Vegetation impacts were not observed despite soil oxygen contents at the 30 cm depth routinely approaching < 5% v/v O_2 (Figure 7). This may be explained in part by lessened requirements of soil O_2 by willow (Salix sp.) and other wetland vegetation at this site, with relevance to other sites with shallow water tables (Jackson & Attwood, 1996). These observations support previous arguments by Forde et al. (2019a) and Sandl et al. (2021) that reliance on sensory GM indications may be unreliable or insufficiently conclusive (especially at lower emission rates in similar field settings), and likely lead to under-quantification of the total number of wells with GM.

These high-resolution and survey efflux data document increased episodicity and less advection-driven gas movement further from the well casing, leading to increasingly lower and more irregularly detectable concentrations and effluxes (Figure S6; Chamindu Deepagoda et al., 2016; Van de Ven et al., 2020). Preferential flow pathways have often been observed along the well casing, as in this study, though Forde et al. (2019a) suggest that soil heterogeneity may, in some

cases, lead to undetectable GM nearby the well while gas is detectable at further distances. Spatiotemporal variability at this site caused intermittently non-detectable values of both surface concentration and measured efflux within meters of the casing. With application to GM detection, both efflux and concentration measurements were highly sensitive to measurement location, requiring measurement at sufficient spatial density to capture any preferential gas flow pathways both close to and further from the wellhead. Surface CH_4 concentrations, despite being in the % gas range in the shallow subsurface, were at times limited to 10's of ppm in the wellhead chamber, indicating that sensitive detectors in the ppm range are vital to distinguish the presence of wells with GM, especially if using surface detection methods (Ulrich et al., 2019). Wind speed was shown to be strongly inversely related to temporally variable pre-closure chamber CH_4 concentrations, a conservative proxy for ground-surface concentrations, and historic GM survey results. This suggests withholding GM testing during times of high wind speeds may increase the likelihood of detecting GM, especially if using ground surface measurements. The observed temporal change in maximum methane concentrations may also have implications for risk assessments of sites with GM near public structures or surface developments, such as where urbanisation has encroached on legacy infrastructure (Alberta Energy Regulator, 2014). Risk assessments could be improved by performing concentration-based measurements during circumstances that are expected to produce the highest possible concentrations at a site (e.g., low wind speeds), or through long-term measurements. Geological factors and soil heterogeneity may drive spatial variations at this site (e.g., Forde et al., 2019a; Steelman et al., 2017). Differences in well construction and operating practices, and local geology, may drive differences in spatiotemporal gas migration behavior and emission rates between this site and at other sites (Bachu, 2017; Forde et al., 2019b; Kang et al., 2014). Short-

term temporal variability in measured concentrations may have been caused by some combination of variable wind, temperature, episodic gas migration, and other factors, leading to a range in measured values of concentration or efflux at any one location over time. Despite this variation, methane concentration as a screening tool (i.e., pass/fail) for the presence of GM was resilient to temporal variability at this well with a thin unsaturated zone. Therefore, the concentration or efflux value from any 'snapshot' measurement may be a good indication of the presence of gas migration and relative magnitude of emissions only. Attempts, whether in industry or academia, to attribute a single efflux or concentration value to a well for the purposes of total emission quantification, risk classification, or assessment of trends in leakage rate over multiple years, must consider the error associated with estimates based on short-term measurements. In addition, the reported total emission rate depends substantially on the estimation method used (Table 4). Effluxes, like concentration measurements, were also shown to be spatiotemporally variable and impacted by a variety of environmental factors.

Accurate measurement of total gas migration emission rates may require multi-day measurements to account for variation induced by episodic gas movement and meteorological factors, including the apparent decrease in observed effluxes at higher wind speeds when using the dynamic closed chamber approach. While not considered in this work, soil frost and recent strong rainfall are currently listed in legislation as complicating factors for gas migration detection in Alberta, showing a precedent in regulations for recommending consideration of other environmental factors significant to gas migration detection work such as wind speed and barometric pressure change (Forde et al., 2019b; Alberta Energy Regulator, 2021). We recommend future work directly comparing the influences on measured gas efflux and

concentration by these various environmental factors, as well as assessing the resiliency of different testing methodologies to the observed spatiotemporal variation.

5. CONCLUSIONS

This study recorded multi-day shallow subsurface transport dynamics, and instances of spatial and temporal concentration and efflux variations for established conditions of gas migration around a petroleum well, where:

i) Efflux and concentration values varied spatially, with the highest CH_4 effluxes and concentrations focused within < 1 m of the wellhead. Gas species and isotopic composition, and efflux patterns, suggested deep gas (including thermogenic CH_4, C2-C5, and He) displaced atmospheric air and soil gas.

ii) Compared to measurements around the casing, detectable methane effluxes and concentrations as near as 0.5 m away from the wellhead were more temporally irregular. Methane effluxes 5 m South of the preferential migration pathway were routinely below detection limits.

iii) Two-week high-resolution efflux data recorded moderate temporal variability among individual measurements at a single location, and a diel variation with higher CH_4 and CO_2 initial concentrations and effluxes occurring at night. Multi-component stepwise regression modelling results show wind speed and atmospheric temperature were important predictors of temporal variation in surface concentration and measured efflux around the wellhead. Multiple factors were related to the observed temporal variation, and the correlated factors changed depending on measurement location.

Spatial variability, and short and medium-term temporal variability, may introduce error in estimates of total emissions and surface concentrations around sites with migrating gases. Although the presence of gas migration could be reliably determined at this site, despite observed spatiotemporal variability, quantifying the efflux rate was challenging. The range of total GM-related emissions at this site was 48-466 g CH_4 d^{-1} (0.07-0.69-m^3 CH_4 d^{-1}) using different emission estimation methods, with a mean efflux of 129 g CH_4 d^{-1}; (0.19 m^3 CH_4 d^{-1}) from the preferential migration zone encircling the well casing. At this site, total emissions from gas migration were largest around the well casing, though effluxes at this location also varied temporally. Variation in emission estimates introduced by different estimation methods, and spatiotemporal emission variability, suggests that measurement and estimation methods to account for spatiotemporal variation may need to be considered for accurate GM emission estimation. This well had comparatively low methane emission rates in the broader context of the upstream petroleum industry. Reliable detectability of migrating gas at this site indicates that higher-rate GM sources most important from an emissions standpoint will be detectable using common GM test methods in similar field settings. Relative gas species composition and shifts in the $\delta^{13}C$ value of CH_4 and CO_2 were consistent with near-surface methane oxidation, suggesting this process could be enhanced to further decrease emissions. Consideration of factors causing spatial and temporal variability of migrating gases may lead to more representative measurements of surface concentrations and effluxes, and therefore improved detection and quantification of the risks and impacts associated with migrating gases around energy wells.

We conclude that at this case-study site, short-term concentration or efflux surveys at sufficient spatial density will be resilient to temporal variability for the purposes of detecting the presence

of gas migration. GM detection surveys could be optimized by considering meteorological factors, and long-term assessment is required for accurate estimation of total emissions.

CREDIT AUTHOR STATEMENT

All authors contributed to study conceptualization. Cathy Ryan and Ulrich Mayer shared funding acquisition and supervision. Neil Fleming led the data acquisition and data analysis and wrote the initial draft. Tiago Morais assisted with data acquisition, visualization, and initial draft authorship. All authors contributed to editing and reviewing drafts.

DECLARATION OF COMPETING INTERESTS

The authors declare no competing personal or financial external interests that would have impacted the outcomes of this study.

ACKNOWLEDGMENTS

This work was co-funded by the Alberta Upstream Petroleum Research Fund (AUPRF), administered by the Petroleum Technology Alliance of Canada (PTAC), and the National Science and Engineering Research Council of Canada (NSERC), Grant no. CRDPJ/503367-2016, with additional funding by the Canada First Research Excellence Fund (CFREF). Funding for equipment utilized in this study was provided by the Canadian Foundation for Innovation (CFI), the BCKDF, the BCOGC, and NSERC through an RTI grant. We give thanks to the energy company that provided access to the study well, historic gas migration test data, and logistical support in field work.

APPENDIX A. SUPPLEMENTARY MATERIALS

Supplementary data for this article can be found as a separate document.

REFERENCES

Abboud, J. M., Watson, T. L., Ryan, M. C., 2020. Fugitive methane gas migration around Alberta's petroleum wells. Greenh. Gases: Sci. Technol. https://doi.org/10.1002/ghg.2029

Abichou, T., Powelson, D., Chanton, J., Escoriaza, S., Stern, J., 2006. Characterization of methane flux and oxidation at a solid waste landfill. J. Environ. Eng. 132(2), 220-228. https://doi.org/10.1061/(ASCE)0733-9372(2006)132:2(220)

Ahlfeld, D. P., Dahmani, A., & Ji, W., 1994. A conceptual model of field behavior of air sparging and its implications for application. Groundw. Monit. Remediat. 14(4), 132-139. https://doi.org/10.1111/j.1745-6592.1994.tb00491.x

Akaike, H., 1974. A new look at the statistical model identification. IEEE transactions on automatic control, 19(6), 716-723.

Alberta Agriculture and Forestry, Alberta Climate Information Service (ACIS) https://agriculture.alberta.ca/acis (retrieved January 2020)

Alberta Energy Regulator. 2014. Directive 79: Surface Development in Proximity to Abandoned Wells. Alberta, Canada. https://static.aer.ca/prd/2020-07/Directive079_0.pdf

Alberta Energy Regulator. 2020. Directive 009: Casing Cementing Minimum Requirements. Alberta, Canada. https://static.aer.ca/prd/2020-10/Directive009.pdf

Alberta Energy Regulator. 2021. Directive 20: Well Abandonment. Alberta, Canada. https://static.aer.ca/prd/documents/directives/Directive020.pdf

Alberta Energy Regulator. 2018. Vent Flow/ Gas Migration Report. Alberta, Canada. Accessed 2018-05-30 from http://www1.aer.ca/ProductCatalogue/365.html

Alboiu, V., & Walker, T. R., 2019. Pollution, management, and mitigation of idle and orphaned oil and gas wells in Alberta. Canada. Environ. Monit. Assess, 191(10), 611. https://doi.org/10.1007/s10661-019-7780-x

Almon, E., Magaritz, M, 1990. Dissolved common gases in groundwaters of the Appalachian region. J. Hydrol. 121(1-4), 21-32. https://doi.org/10.1016/0022-1694(90)90222-J

Annunziatellis, A., Beaubien, S. E., Bigi, S., Ciotoli, G., Coltella, M., Lombardi, S., 2008. Gas migration along fault systems and through the vadose zone in the Latera caldera (central Italy): Implications for CO2 geological storage. Int. J. Greenh. Gas Con. 2(3), 353-372. https://doi.org/10.1016/j.ijggc.2008.02.003

Bachu, S., 2017. Analysis of gas leakage occurrence along wells in Alberta, Canada, from a GHG perspective – Gas migration outside well casing. Int. J. Greenh. Gas Con. 61, 146-154. https://doi.org/10.1016/j.ijggc.2017.04.003

BCOGC. 2019. Oil & Gas Operations Manual. Chapter 9 Well Activity: Completion, Maintenance and Abandonment. Version 1.29. https://www.bcogc.ca/node/13316/download

Boothroyd, I, M, Almond, S, Qassim, S, M, Worrall, F, Davies, R, J, 2015. Fugitive emissions of methane fromabandoned, decommissioned oil and gas wells. Science of the Total Environment 547, 461–469. doi:https://doi.org/10.1016/j.scitotenv.2015.12.096.

Börjesson, G., Danielsson, Å., Svensson, B. H., 2000. Methane fluxes from a Swedish landfill determined by geostatistical treatment of static chamber measurements. Environ. Sci. Technol. 34(18), 4044-4050. https://doi.org/10.1021/es991350s

Börjesson, G., Svensson, B., 1997. Seasonal and diurnal methane emissions from a landfill and their regulation by methane oxidation. Waste Manag. Res. 15(1) 33-54. https://doi.org/10.1177/0734242X9701500104.

Brandt, A.R., Heath, G.A., Kort, E.A., O'sullivan, F., Pétron, G., Jordaan, S.M., Tans, P.,Wilcox, J., Gopstein, A.M., Arent, D., Wofsy, S., Brown, N.J., Bradley, R., Stucky, G.D., Eardley, D., Harris, R., 2014. Energy and environment methane leaks from North American natural gas systems. Sci. 343(6172), 733–735. https://doi.org/10.1126/science.1247045

Cahill, A., Steelman, C., Forde, O., Kuloyo, O., Ruff, S., Mayer, B., Mayer, K.U., Strous, M., Ryan, M.C., Cherry, J.A., Parker, B.L., 2017. Mobility and persistence of methane in groundwater in a controlled-release field experiment. Nat. Geosci. 10, 289.

Cardellini, C., Chiodini, G., Frondini, F., Granieri, D., Lewicki, J., Peruzzi, L., 2003. Accumulation chamber measurements of methane fluxes: application to volcanic-geothermal areas and landfills. Appl. Geochem. 18(1), 45-54. https://doi.org/10.1016/S0883-2927(02)00091-4

Chamindu Deepagoda, T.K.K., Smits, K. Oldenburg, C., 2016. Effect of subsurface soil moisture variability and atmospheric conditions on methane gas migration in shallow subsurface. Int. J. Greenh. Gas Con. 55:105–117. https://doi.org/10.1016/j.ijggc.2016.10.016

Chen, K., O'Leary, R. A., Evans, F. H., 2019. A simple and parsimonious generalised additive model for predicting wheat yield in a decision support tool. Agric. Syst. 173, 140-150. https://doi.org/10.1016/j.agsy.2019.02.009

Christiansen, J., Outhwaite J., Smukler, S., 2015. Comparison of CO2, CH4 and N2O soil-atmosphere exchange measured in static chambers with cavity ring-down spectroscopy and gas chromatography. Agric. For. Meteorol. 211, 48-57. https://doi.org/10.1016/j.agrformet.2015.06.004

D'Aniello, A., Fabbricino, M., Ducci, D., Pianese, D., 2020. Numerical Investigation of a Methane Leakage from a Geothermal Well into a Shallow Aquifer. Groundw. 58(4), 598-610. doi:10.1111/gwat.12943

Dusseault, M., Jackson, R., 2014., Seepage pathway assessment for natural gas to shallow groundwater during well stimulation, in production, and after abandonment. Environ. Geosci. 21(3), 107-126. doi: 10.1306/eg.04231414004

Dusseault, M., Jackson., R., MacDonald, D. 2014., Towards a Road Map for Mitigating the Rates and Occurrences of Long-Term Wellbore Leakage. University of Waterloo & Geofirma Engineering Ltd. (2014). http://geofirma.com/wp-content/uploads/2015/05/lwp-final-report_compressed.pdf.

Engelder, T., Zevenbergen, J., 2018. Analysis of a gas explosion in Dimock PA (USA) during fracking operations in the Marcellus gas shale. Process Saf. Environ. Prot. 117, 61-66. https://doi.org/10.1016/j.psep.2018.04.004

Environment and Climate Change Canada. 2020. National inventory report: greenhouse gas sources and sinks in Canada: executive summary. http://publications.gc.ca/pub?id=9.816345&sl=0

Erno, B., Schmitz, R. 1996. Measurements of soil gas migration around oil and gas wells in the Lloydminster area. J. Can. Pet. Tech. 35(07).

Fleming, N., Morais, T., Kennedy, C., Ryan, M.C., 2019. Evaluation of SCVF and GM measurement approaches to detect fugitive gas migration around energy wells. Presented at Geoconvention 2019. Calgary, Canada. May 13-17 2019.

Forde, O., Mayer, K., Cahill, A., Mayer, B., Cherry, J., Parker, B., 2018. Vadose zone gas migration and surface effluxes after a controlled natural gas release into an unconfined shallow aquifer. Vadose Zone J. 17, 1-16.

Forde, O. N., Mayer, K. U., & Hunkeler, D. 2019a. Identification, spatial extent and distribution of fugitive gas migration on the well pad scale. Sci. Total Environ. 652, 356–366.

Forde, O. N., Cahill, A. G., Beckie, R. D., & Mayer, K. U. 2019b. Barometric-pumping controls fugitive gas emissions from a vadose zone natural gas release. Sci. Rep. 9, 1-9.

Frederick, G., Wolfram, K., Eric, P., Gaëtan, B., Pierrick, D., Bernhard, M., & Eric, C. G., 2017. Natural CH4 gas seeps in the French Alps: characteristics, typology and contribution to CH4 natural emissions to the atmosphere. Energy Procedia, 114, 3020-3032. https://doi.org/10.1016/j.egypro.2017.03.1430

Gas Measurement Instruments Ltd. 2016. GT series user handbook. Accessed November 2020 from: https://www.manualslib.com/manual/1680676/Gmi-Gt-Series.html?page=2#manual

Gorody, A. W., 2012. Factors affecting the variability of stray gas concentration and composition in groundwater. Environ. Geosci. 19(1), 17-31. https://doi.org/10.1306/eg.12081111013

Government of Alberta. Reducing methane emissions. Accessed November 2020 from: https://www.alberta.ca/climate-methane-emissions.aspx

Gunasekera, S. S., Hettiaratchi, J. P., Bartholameuz, E. M., Farrokhzadeh, H., Irvine, E., 2018. A comparative evaluation of the performance of full-scale high-rate methane biofilter (HMBF) systems and flow-through laboratory columns. Environ. Sci. Pollut. Res. 25, 35845-35854. https://doi.org/10.1007/s11356-018-3100-1

Hastie, T., 2019. gam: Generalized Additive Models. R package version 1.16.1.

Hastie, T. J., Tibshirani, R. J., 1990. Generalized additive models, Vol. 43. CRC press.

Hendry, M. J., Schmeling, E. E., Barbour, S. L., Huang, M., Mundle, S. O., 2017. Fate and transport of shale-derived, biogenic methane. Sci. Rep. 7(1), 1-9. https://doi.org/10.1038/s41598-017-05103-8

Hoeks, J., 1972. Effect of leaking natural gas on soil and vegetation in urban areas. Report published by the Centre for Agricultural Publishing and Documentation, Wageningen, Netherlands.

Humez, P., Mayer, B., Ing, J., Nightingale, M., Becker, V., Kingston, A., ... Taylor, S., 2016. Occurrence and origin of methane in groundwater in Alberta (Canada): Gas geochemical and isotopic approaches. Sci. Total Environ. 541, 1253-1268.

IPCC. 2013. Climate Change 2013: The Physical Science Basis. Contribution of Working Group I to the Fifth Assessment Report of the Intergovernmental Panel on Climate Change [Stocker, T.F., D. Qin, G.-K. Plattner, M. Tignor, S.K. Allen, J. Boschung, A. Nauels, Y. Xia, V. Bex and P.M. Midgley (eds.)]. Cambridge University Press, Cambridge, United Kingdom and New York, NY, USA, 1535 pp.

IPCC. 2019. 2019 Refinement to the 2006 IPCC Guidelines for National Greenhouse Gas Inventories. Volume 4, Chapter 10. Accessed August 2020 from https://www.ipcc-nggip.iges.or.jp/public/2019rf/vol4.html.

Jackson, M., Attwood, P., 1996. Roots of willow (Salix viminalis L.) show marked tolerance to oxygen shortage in flooded soils and in solution culture. Plant and Soil, 187(1), 37-45.

Jackson, R. E., Gorody, A. W., Mayer, B., Roy, J. W., Ryan, M. C., Van Stempvoort, D. R., 2013. Groundwater protection and unconventional gas extraction: The critical need for field-based hydrogeological research. Groundw 51 (4), 488–510. https://doi:10.1111/gwat.12074.

Kang, M., Kanno, C. M., Reid, M. C., Zhang, X., Mauzerall, D. L., Celia, M. A., Chen, Y., Onstott, T. C., 2014. Direct measurements of methane emissions from abandoned oil and gas wells in Pennsylvania. Proc. Natl. Acad. Sci. 111(51), 18173-18177. https://doi.org/10.1073/pnas.1408315111

Kelly, W. R., Matisoff, G., Fisher, J. B., 1985. The effects of a gas well blow out on groundwater chemistry. Environ. Geol. Water Sci. 7(4), 205-213. https://doi.org/10.1007/bf02509921

Kovach, E. M., 1945. Meteorological influences upon the radon-content of soil-gas. Eos, Trans. Am. Geophys. Union, 26(2), 241-248. https://doi.org/10.1029/TR026i002p00241

Lebel, E. D., Lu, H. S., Vielstädte, L., Kang, M., Banner, P., Fischer, M. L., Jackson, R. B. 2020. Methane Emissions from abandoned oil and gas wells in California. Environ. Sci. Technol. 54(22), 14617-14626. https://doi.org/10.1021/acs.est.0c05279

Lyman, S. N., Tran, H. N., Mansfield, M. L., Bowers, R., Smith, A., 2020. Strong temporal variability in methane effluxes from natural gas well pad soils. Atmos. Pollut. Res. 11(8), 1386-1395. https://doi.org/10.1016/j.apr.2020.05.011

Maier, M., Mayer, S., Laemmel, T., 2019. Rain and wind affect chamber measurements. Agric. For. Meteorol. 279, 107754. https://doi.org/10.1016/j.agrformet.2019.107754

Martin, G. E., Snow, D. D., Kim, E., Spalding, R. F., 1995. Simultaneous determination of argon and nitrogen. Groundw. 33(5), 781-785. https://doi.org/10.1111/j.1745-6584.1995.tb00024.x

McMahon, P. B., Thomas, J. C., Crawford, J. T., Dornblaser, M. M., Hunt, A. G., 2018. Methane in groundwater from a leaking gas well, Piceance Basin, Colorado, USA. Sci. Total Environ., 634, 791-801. https://doi.org/10.1016/j.scitotenv.2018.03.371

Mikkelä, C., Sundh, I., Svensson, B. H., Nilsson, M., 1995. Diurnal variation in methane emission in relation to the water table, soil temperature, climate and vegetation cover in a Swedish acid mire. Biogeochem. 28(2), 93-114. https://doi.org/10.1007/BF02180679

Milbert, D., 2018. Solid Earth Tide. Accessed 2020 from: https://geodesyworld.github.io/SOFTS/solid.htm#link2

Mitton, M., 2018. Subsurface methane migration from natural gas distribution pipelines as affected by soil heterogeneity: field scale experimental and numerical study (Doctoral dissertation, Colorado School of Mines. Arthur Lakes Library)

Nachshon, U., Weisbrod, N., Dragila, M. I., & Ganot, Y., 2011. The importance of advective fluxes to gas transport across the earth-atmosphere interface: the role of thermal

convection. Planet Earth 2011-Global Warming Challenges and Opportunities for Policy and Practice. IntechOpen.

Natural Resources Canada. Greenhouse Gases Equivalencies Calculator- Calculations and References. Accessed 08-2020 from https://oee.nrcan.gc.ca/corporate/statistics/neud/dpa/calculator/refs.cfm

Noomen, M. F., van der Werff, H. M., Van der Meer, F., 2012. Spectral and spatial indicators of botanical changes caused by long-term hydrocarbon seepage. Ecol. Inform. 8, 55-64. https://doi.org/10.1016/j.ecoinf.2012.01.001

Oliveira, S., Viveiros, F., Silva, C., & Pacheco, J. E., 2018. Automatic Filtering of Soil CO2 Flux Data; Different Statistical Approaches Applied to Long Time Series. Front. Earth Sci. 6, 208. https://doi.org/10.3389/feart.2018.00208

Poulsen, T. G., Møldrup, P., 2006. Evaluating effects of wind-induced pressure fluctuations on soil-atmosphere gas exchange at a landfill using stochastic modelling. Waste Manag. Res. 24(5), 473-481. https://doi.org/10.1177/0734242X06066363

Poulsen, T. G., Pourber, A., Furman, A., Papadikis, K., 2017. Relating wind-induced gas exchange to near-surface wind speed characteristics in porous media. Vadose Zone J. 16(8), 1-13. https://doi.org/10.2136/vzj2017.02.0039

Province of Alberta. 2020. Pipeline Act. Accessed September 2020 from https://www.qp.alberta.ca/documents/Acts/p15.pdf Redeker, K. R., Baird, A. J., Teh, Y. A., 2015. Quantifying wind and pressure effects on trace gas effluxes across the soil-atmosphere interface. Biogeosci. 12(24), 7423-7434. doi:10.5194/bg-12-7423-2015

Riddick, S. N., Mauzerall, D. L., Celia, M. A., Kang, M., & Bandilla, K. 2020. Variability observed over time in methane emissions from abandoned oil and gas wells. Intern.J. Greenh. Gas Control. 100, 103116. https://doi.org/10.1016/j.ijggc.2020.103116

Riley, W. J., Gadgil, A. J., Bonnefous, Y. C., Nazaroff, W. W., 1996. The effect of steady winds on radon-222 entry from soil into houses. Atmos. Environ. 30(7), 1167-1176. https://doi.org/10.1016/1352-2310(95)00248-0

Risk, D., McArthur, G., Nickerson, N., Phillips, C., Hart, C., Egan, J., Lavoie, M., 2013. Bulk and isotopic characterization of biogenic CO2 sources and variability in the Weyburn injection area. Int. J. Greenh. Gas Control. 16, S263-S275. https://doi.org/10.1016/j.ijggc.2013.02.024

Romanak, K.D., Wolaver, B., Yang, C., Sherk, G.W., Dale, J., Dobeck, L.M., Spangler, L.H., 2014. Process-based soil gas leakage assessment at the Kerr Farm: comparison of results to leakage proxies at ZERT and Mt. Etna. Int. J. Greenh. Gas Control. 30, 42-57. https://doi.org/10.1016/j.ijggc.2014.08.008

Rowe, D., Muehlenbachs, K., 1999. Isotopic fingerprints of shallow gases in the Western Canadian sedimentary basin: tools for remediation of leaking heavy oil wells. Org. Geochem. 30(8), 861-871. https://doi.org/10.1016/S0146-6380(99)00068-6

Roy, N., Molson, J., Lemieux, J. M., Van Stempvoort, D., Nowamooz, A., 2016. Three-dimensional numerical simulations of methane gas migration from decommissioned hydrocarbon production wells into shallow aquifers. Water Resour. Res. 52(7), 5598-5618. https://doi.org/10.1002/2016WR018686

Saint-Vincent, P. M., Reeder, M. D., Sams III, J. I., Pekney, N. J., 2020. An analysis of abandoned oil well characteristics affecting methane emissions estimates in the Cherokee Platform in Eastern Oklahoma. Geophys. Res Lett. 47(23). https://doi.org/10.1029/2020GL089663

Sandau, C. D., Prokipchuk, M., Dominato, K. R., Mundle, S. O., 2019. Soil gas investigation of an alleged gas migration issue on a residential farm located above the Weyburn-Midale CO2 enhanced oil recovery project. Int. J. Greenh. Gas Control. 81, 11-20. https://doi.org/10.1016/j.ijggc.2013.02.024

Sandl, E., Cahill, A. G., Welch, L., & Beckie, R. 2021. Characterizing oil and gas wells with fugitive gas migration through Bayesian multilevel logistic regression. Sci. Total Environ. 769, 144678. https://doi.org/10.1016/j.scitotenv.2020.144678

Schiffner, D., 2020. Methane Emissions from Suspended Wells: Can Internalizing the Cost of Methane Leaks Incentivize Plugging and Reclamation of Petroleum Wells in Alberta? Proc. World Geothermal Congress, April 26 – May 2, 2020, Reykjavik, Iceland.

Schout, G., Griffioen, J., Hassanizadeh, S. M., de Lichtbuer, G. C., Hartog, N., 2019. Occurrence and fate of methane leakage from cut and buried abandoned gas wells in the Netherlands. Sci. Total Environ. 659, 773-782. https://doi.org/10.1016/j.scitotenv.2018.12.339

Seo, D., Han, W., Park, E., Jeong, J., Oh, Y. Y., Kim, H. J., ...Yun, S., 2020. Analyses and numerical evaluation of integrated time-series monitoring datasets including CO2 concentration and effluxes at controlled CO2 release site in South Korea. J. Hydro. 590, 125213. https://doi.org/10.1016/j.jhydrol.2020.125213

Sihota, N. J., Mayer, K. U., Toso, M. A., Atwater, J., 2013. Methane emissions and contaminant degradation rates at sites affected by accidental releases of denatured fuel-grade ethanol. J. Contam. Hydrol. 151, 1-15. https://doi.org/10.1016/j.jconhyd.2013.03.008

Smith, Ann P., Bowers, Richard L., Boyd, Victoria H., Lyman, S., 2019. Long-Term Methane Emissions Quantification and Alert System for Natural Gas Storage Wells and Fields. GSI Environmental, Inc., Austin, Texas. https://www.osti.gov/biblio/1526753

Spokas, K., Graff, C., Morcet, M., Aran, C., 2003. Implications of the spatial variability of landfill emission rates on geospatial analyses. Waste Manag. 23(7), 599-607. https://doi.org/10.1016/S0956-053X(03)00102-8

Statistics Canada, 2016. 2016 Census- Boundary Files. Accessed From: https://www12.statcan.gc.ca/census-recensement/2011/geo/bound-limit/bound-limit-2016-eng.cfm

Steelman, C. M., Klazinga, D. R., Cahill, A. G., Endres, A. L., Parker, B. L., 2017. Monitoring the evolution and migration of a methane gas plume in an unconfined sandy aquifer using time-lapse GPR and ERT. J. Contam. Hydrol. 205, 12-24. https://doi.org/10.1016/j.jconhyd.2017.08.011

Stein, V., Hettiaratchi, J. P., 2001. Methane oxidation in three Alberta soils: influence of soil parameters and methane efflux rates. Environ. Technol. 22(1), 101-11. https://doi.org/10.1080/09593332208618315

Szatkowski, B., Whittaker, S., Johnston, B., 2002. Identifying the source of migrating gases in surface casing vents and soils using stable Carbon Isotopes, Golden Lake Pool, West-

central Saskatchewan. Summary of Investigations 2002, Volume 1 Saskatchewan Geological Survey, Regina, SK, Canada. 2002(4.1) pp.118-125.

Tang, J., Bao, Z., Xiang, W., Gou, Q., 2008. Geological emission of methane from the Yakela condensed oil/gas field in Talimu Basin, Xinjiang, China. J. Environ. Sci. 20(9), 1055-1062. https://doi.org/10.1016/S1001-0742(08)62149-X

Tilley, B., Muehlenbachs, K., 2011. Fingerprinting of gas contaminating groundwater and soil in a petroliferous region, Alberta, Canada. Presented at Proceedings from International Network of Environmental Forensics Conference, 2011, Cambridge (UK) (2011) pp. 115-125.

Tokida, T., Miyazaki, T., Mizoguchi, M., Nagata, O., Takakai, F., Kagemoto, A., Hatano, R., 2007. Falling atmospheric pressure as a trigger for methane ebullition from peatland. Glob. Biogeochem. Cycles, 21(2). https://doi.org/10.1029/2006GB002790

Ulrich, B. A., Mitton, M., Lachenmeyer, E., Hecobian, A., Zimmerle, D., Smits, K. M., 2019. Natural gas emissions from underground pipelines and implications for leak detection. Environ. Sci. Technol. Lett. 6(7), 401-406. https://doi.org/10.1021/acs.estlett.9b00291

Van De Ven, C., Abraham, J., Mumford, K., 2020. Laboratory investigation of free-phase stray gas migration in shallow aquifers using modified light transmission. Adv. Water Resour. 103543.

Van De Ven, C., Mumford, K., 2020. Intermediate-Scale Laboratory Investigation of Stray Gas Migration Impacts: Methane Source Architecture and Dissolution. Environ. Sci. Technol. 54(10), 6299-6307.

Wen, T., Castro, M. C., Nicot, J. P., Hall, C. M., Larson, T., Mickler, P., Darvari, R., 2016. Methane sources and migration mechanisms in shallow groundwaters in Parker and Hood Counties, Texas- A heavy noble gas analysis. Environ. Sci. Technol, 50(21), 12012-12021. https://doi.org/10.1021/acs.est.6b01494

Whiticar, M. J., 1999. Carbon and hydrogen isotope systematics of bacterial formation and oxidation of methane. Chem. Geo. 161(1-3), 291-314. https://doi.org/10.1016/S0009-2541(99)00092-3

Wickham, H., 2016. ggplot2: Elegant Graphics for Data Analysis. Springer-Verlag New York.

Williams, G. M., Aitkenhead, N., 1991. Lessons from Loscoe: the uncontrolled migration of landfill gas. Q. J. Eng. Geol. Hydrogeol., 24(2), 191-207. https://doi.org/10.1144/GSL.QJEG.1991.024.02.03

Woods, A. W., Norris, S., 2016. Dispersion and dissolution of a buoyancy driven gas plume in a layered permeable rock. Water Resour. Res. 52(4), 2682-2697. https://doi.org/10.1002/2015WR018159

Xu, L., Furtaw, M., Madsen, R., Garcia, R., Anderson, D., McDermitt, D., 2006. On maintaining pressure equilibrium between a soil CO2 efflux chamber and the ambient air. J. Geophys. Res: Atmos. 111(D8). https://doi.org/10.1029/2005JD006435

Yin, J, Mayer, K.U., Sihota, N., 2014. Evaluation of gas migration near production wells in Northeastern BC- Results of a preliminary field survey. The University of British Colombia

Zavala-Araiza, D., Lyon, D. R., Alvarez, R. A., Davis, K. J., Harriss, R., Herndon, S. C., ... Hamburg, S. P., 2015. Reconciling divergent estimates of oil and gas methane

emissions. Proc. Natl. Acad. Sci. 112(51), 15597-15602. https://doi.org/10.1073/pnas.1522126112

2020. 4.02. https://www.R-project.org/.

6. SUPPLEMENTARY MATERIAL

Supplementary Material for: Spatiotemporal variability of fugitive gas migration emissions around a petroleum well https://doi.org/10.1016/j.apr.2021.101094

N.A. Fleming, T.A. Morais, K.U. Mayer, M.C. Ryan

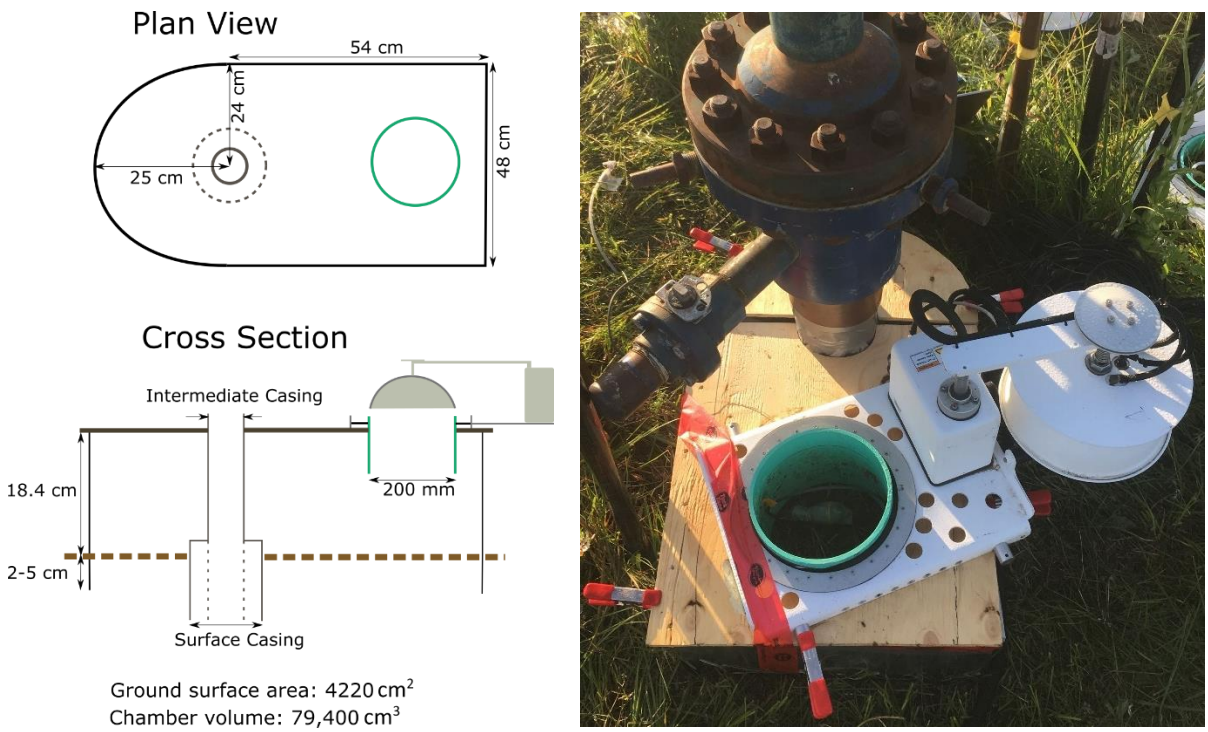

Figure S1 Custom wellhead collar construction schematic and field photograph showing the coupling of the automated dynamic efflux chamber to the custom collar. The collar base was constructed with thin sheet metal placed 2-5 cm into the ground surface around the well (the lateral segment of the surface casing preventing deeper installation). Rigid plastic sheeting formed an air-tight seal on the lid-portion of the chamber. A hole in the plastic sheeting accommodated a 200 mm PVC pipe, allowing for coupling with the automated chamber. A plywood external lid to the chamber provided structural support and prevented any pumping/chamber size modifications due to wind acting on the plastic. Note that the surface casing is vented to the atmosphere outside of the custom collar through a surface casing vent (not shown in schematic).

Minimum detectable efflux (MDF) was calculated using methods provided in Christiansen et al. (2015):

$$MDF = (\frac{A_a}{t_c})(\frac{VP}{SRT})$$

A_a is the instrument analytical accuracy, t_c is the closure time, V is the total volume (m^3), P is the atmospheric pressure (Pa), S is the chamber surface area (m^2), R is the ideal gas constant (8.314 m^3 Pa^{-1} K^{-1} mol^{-1}), and T is the temperature (K). The analytical accuracy is conservatively taken to be 0.2 ppm for CH_4 and 1 ppm for CO_2 (above reported instrumental accuracies (< 2 ppb CH_4, Los Gatos Research; <1 ppm for CO_2 LI-COR Inc.).

Table S1 Efflux measurement settings and parameters used for the October 11-26th measurement period, with calculated minimum detectable effluxes considering the average period temperature of 4.8 °C.

Chamber Location Name	Area (cm^2)	Total Volume (cm^3)	Chamber Closure Time (s)	Chamber MDF CO_2 (µmol m^{-2} s^{-1})	Chamber MDF CH_4 (µmol m^{-2} s^{-1})	Surface Area/Volume
Wellhead	4224.7	8 4260	15	0.54	0.11	0.05
1.0 S	317.8	6037	90	0.09	0.02	0.05
0.5 SE	317.8	6124	45	0.17	0.03	0.05
0.5 NE	317.8	5687	90	0.08	0.02	0.06
2.5 N	317.8	5878	90	0.08	0.02	0.05
5.0 S	317.8	6013	90	0.09	0.02	0.05

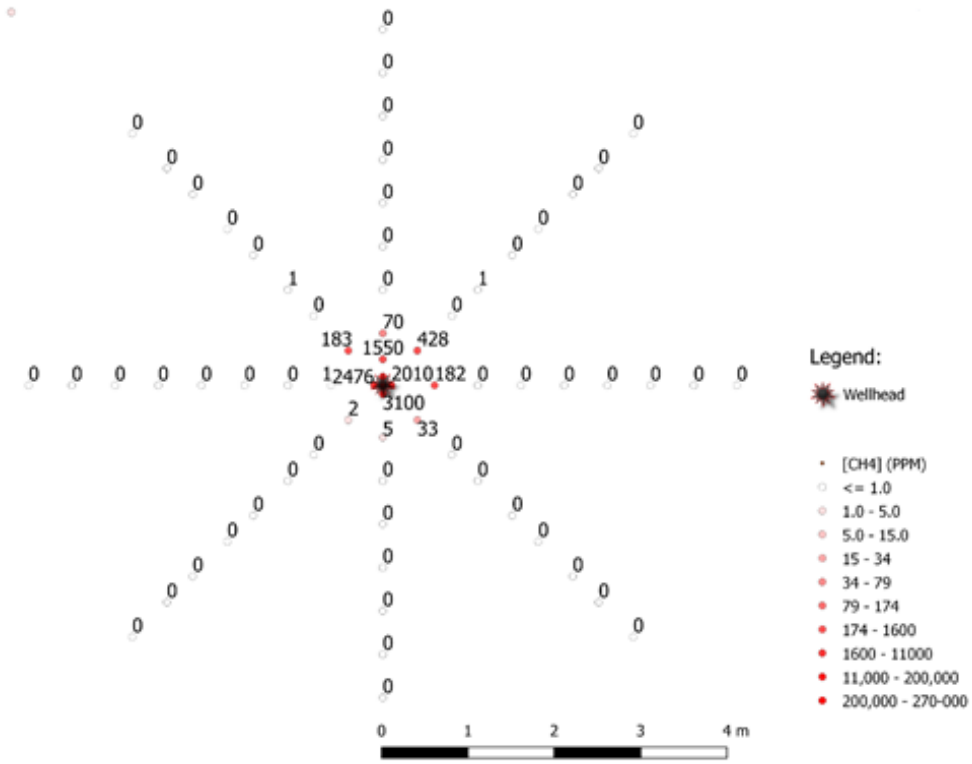

Figure S2 Close view of 2018-11-21 soil-surface methane gas concentrations as ppm CH_4 above background levels centered on the wellhead. Full survey extended to 20 m distance from well center.

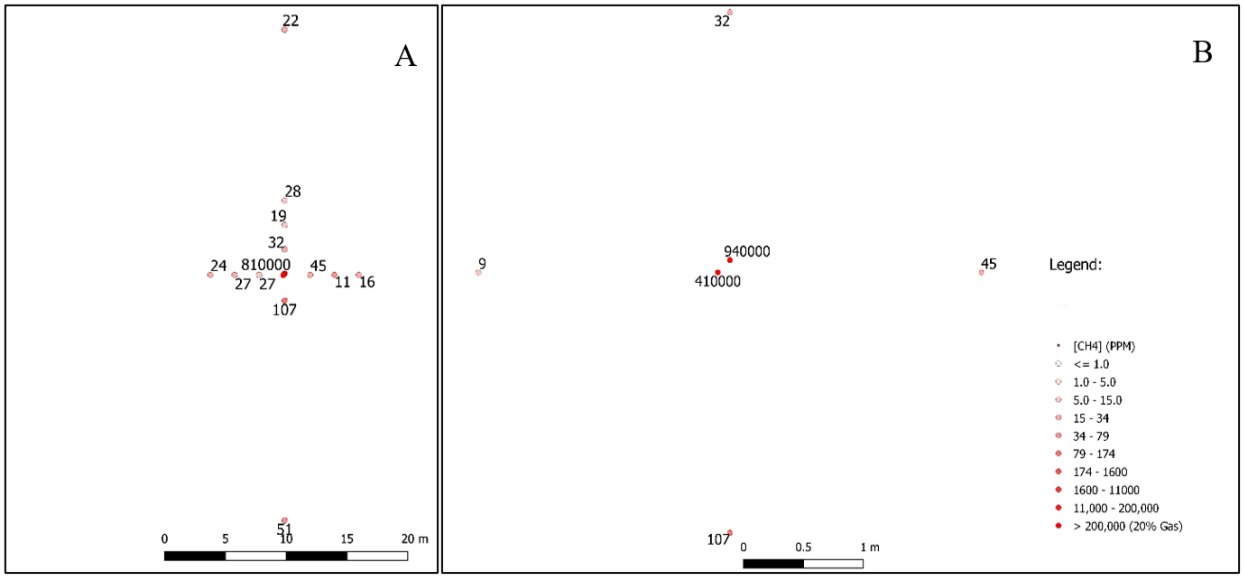

Figure S3 2018-11-21 30 cm depth methane gas concentrations as ppm CH_4 above background levels centered on the wellhead. A) shows full-site measurements, B) shows close-up on well center

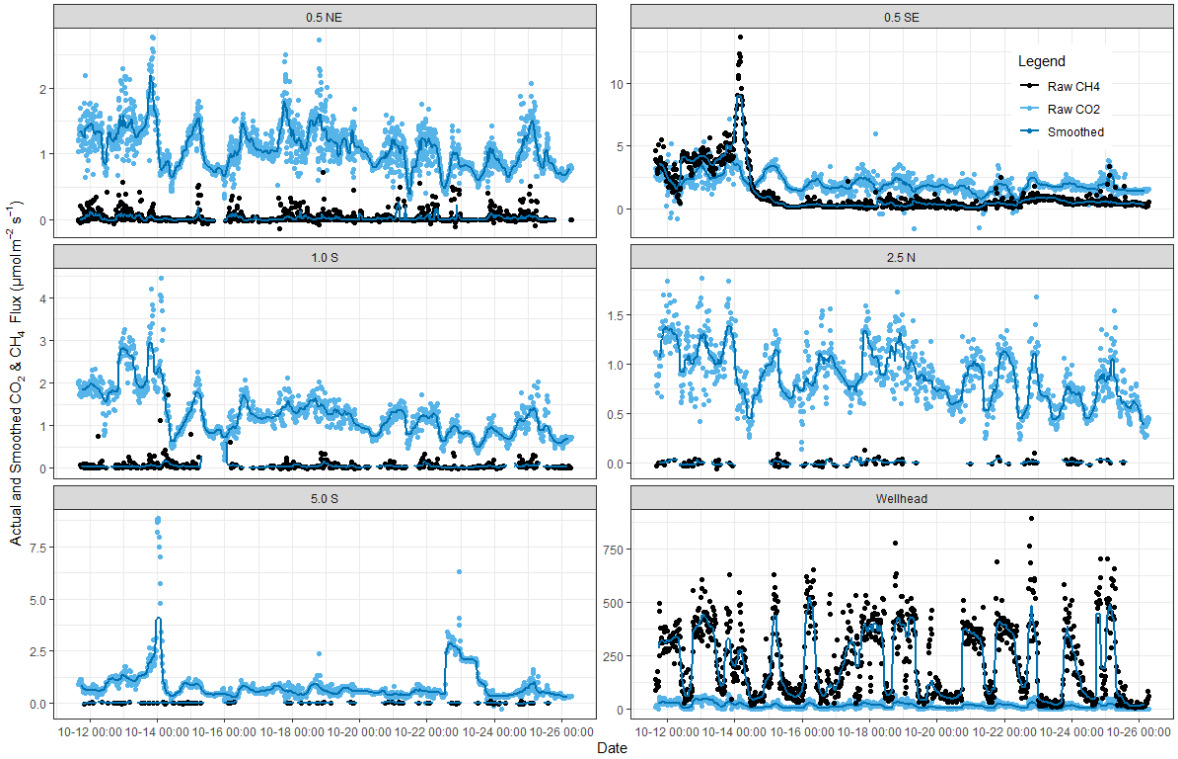

Figure S4 Two-week time series records showing all detectable linear calculated CO_2 and CH_4 effluxes in µmol m^{-2} s^{-1} at six locations. Raw efflux values presented with 20-point (~ 6 hour) moving median smoothing line for clarity in temporal variation.

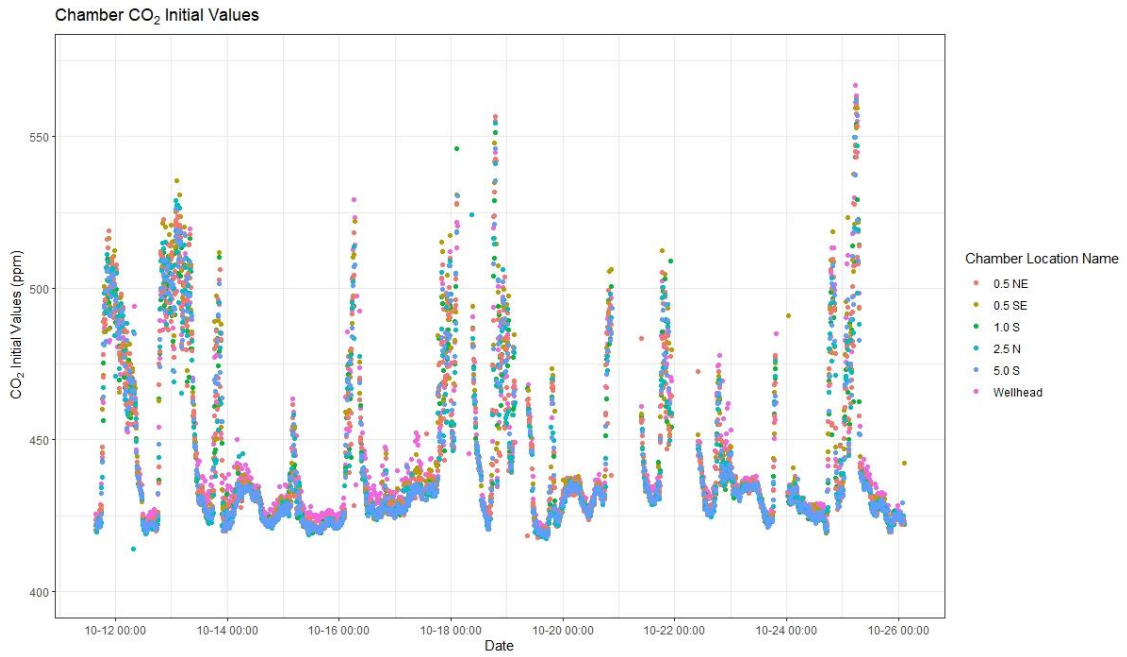

Figure S5 Initial chamber CO_2 concentrations in ppm for all six long term chambers over the long-term measurement period, showing quasi-diel variation between 420 and > 500 ppm and similarity in measured concentrations for all locations.

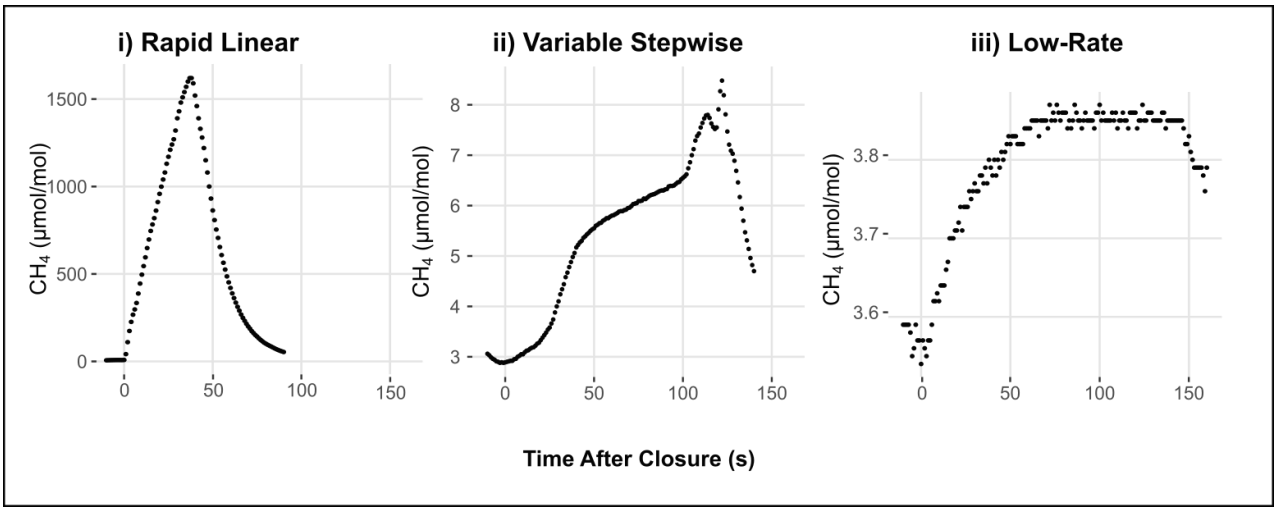

Figure S6 Representative typologies of methane concentration time series used to calculate efflux, shown as time after the beginning of chamber closure against the measured CH_4 concentration with the greenhouse gas analyzer (note different Y scales). i) Rapid linear increase (Wellhead), ii) Stepwise (0.5 NE), and iii) Low-rate exponential increase (5.0 m S).

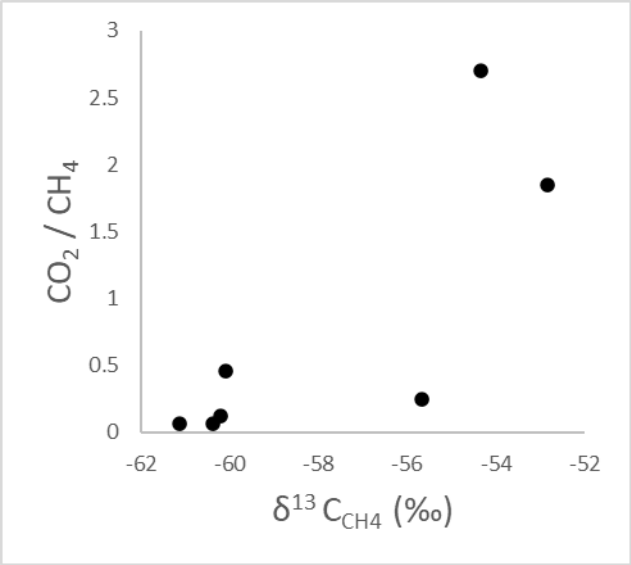

Figure S7 $\delta^{13}C_{CH4}$ (‰) with respect to the concentration ratio of CO_2/CH_4 for all analysed isotope samples, showing less depleted $\delta^{13}C_{CH4}$ (‰) with greater proportion of CO_2 to CH_4 in the gas samples.

Table S2 Soil gas and dissolved gas analyses showing distance in E-W (X), N-S (Y) and depth from ground surface (Z) in meters from well center.

X	Y	Z	Sample Date	Sample Type	Ar	O2	N2	CO_2	C1	C2	C3	>C3 *	Total	$\delta^{13}C_{CH4}$	$\delta^{13}C_{CO2}$	$\delta^{2}H_{CH4}$	$\delta^{13}C_{C2}$
0.0	0.1	0.3	2018-11-21	SVW	0.11	0.99	10.90	0.213	85.913	0.331	0.030	0.010	98.5	-60.4	-	-251.8	-
0.0	2.0	0.3	2018-11-21	SVW	0.89	17.33	78.44	1.404	0.635	0.002	0.000	0.000	98.7	-62.3	-	-213.5	-
0.0	0.1	0.45	2019-08-22	SVW	0.78	14.39	68.03	1.794	14.790	0.054	0.006	0.002	99.8	-60.2	-63.0	-	-
0.1	0.0	0.1	2019-08-22	SVW	0.79	18.12	73.70	1.237	5.064	0.020	0.002	0.001	98.9	-55.7	-64.2	-	-
0.5	0.0	0.3	2019-08-22	SVW	0.36	2.50	28.58	4.350	65.586	0.249	0.023	0.007	101.7	-61.1	-42.2	-	-45.3
0.5	0.0	0.1	2019-08-22	SVW	0.88	20.13	77.66	0.626	0.340	0.001	0.000	0.000	99.6	-52.8	-54.5	-	-
0.2	0.2	0.1	2019-08-22	SVW	0.88	20.25	77.16	0.561	0.208	0.001	0.000	0.000	99.1	-54.3	-53.4	-	-
0.5	0.0	0.3	2019-08-23	SVW	0.33	1.35	25.14	4.283	70.263	0.270	0.025	0.008	101.7	-60.4	-42.7	-	-44.8
-0.1	0.0	0.5	2019-08-23	WHC	0.79	20.11	77.09	0.187	0.407	0.002	0.000	0.000	98.6	-60.1	-47.6	-	-
0.0	-1.3	1	2019-08-21	DISS	1.15	13.16	63.97	13.983	5.917	0.011	0.001	0.001	98.2	-59.9	-36.5	-	-
1.3	0.0	1	2019-08-21	DISS	1.13	16.92	73.30	0.274	6.558	0.023	0.001	0.001	98.2	-61.1	-	-	-
0.0	-1.3	1	2019-08-23	DISS	1.38	13.91	64.67	11.475	7.033	0.014	0.002	0.011	98.5	-59.3	-35.5	-	-
1.3	0.0	1	2019-08-23	DISS	1.41	11.96	68.07	0.151	16.294	0.065	0.006	0.002	98.0	-62.3	-	-	-
0.0	-0.5	1	2019-08-21	DISS	1.02	13.65	61.37	0.393	21.529	0.092	0.006	0.001	98.1	-63.7	-	-	-
0.0	-6.0	1	2019-08-21	DISS	1.76	11.11	75.11	7.521	2.832	0.018	0.001	0.000	98.3	-57.3	-29.3	-	-

*iC4 + nC4 + neopentane +nC5 +iC5. DISS = Dissolved gas from a monitoring well 1m depth, SVW = soil vapor well sample, WHC = free air sample from within wellhead chamber. Precision and accuracy of $\delta^{13}C$ = ± 0.5 ‰ and $\delta^{2}H$ =± 2 ‰

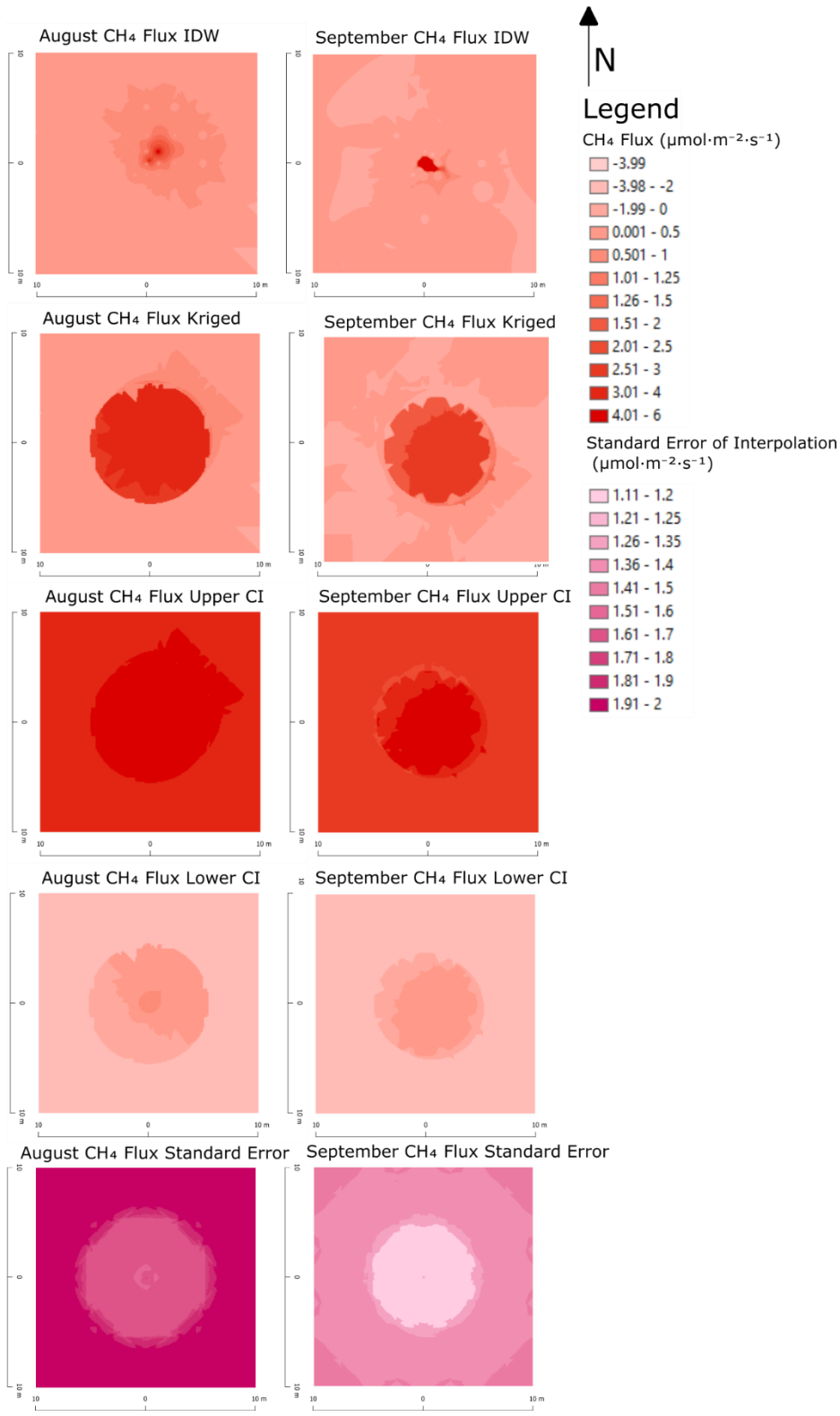

Figure S8 Spatial interpolation summary plots over the area of the dense well pad measurement grid (20 m X 20 m centered on the energy well).

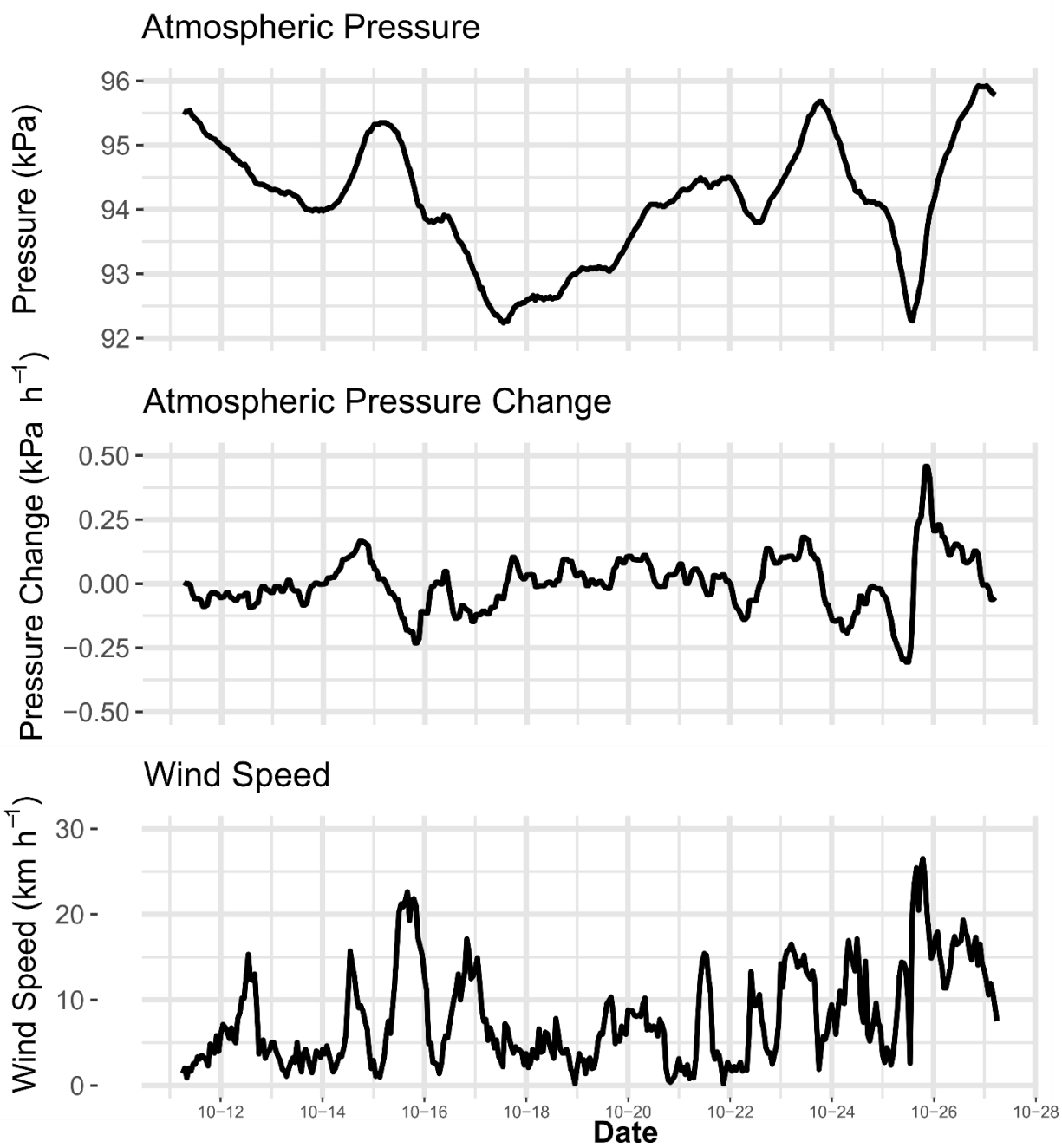

Figure S.9a Time series records of explanatory environmental factors considered in the stepwise general additive regression model

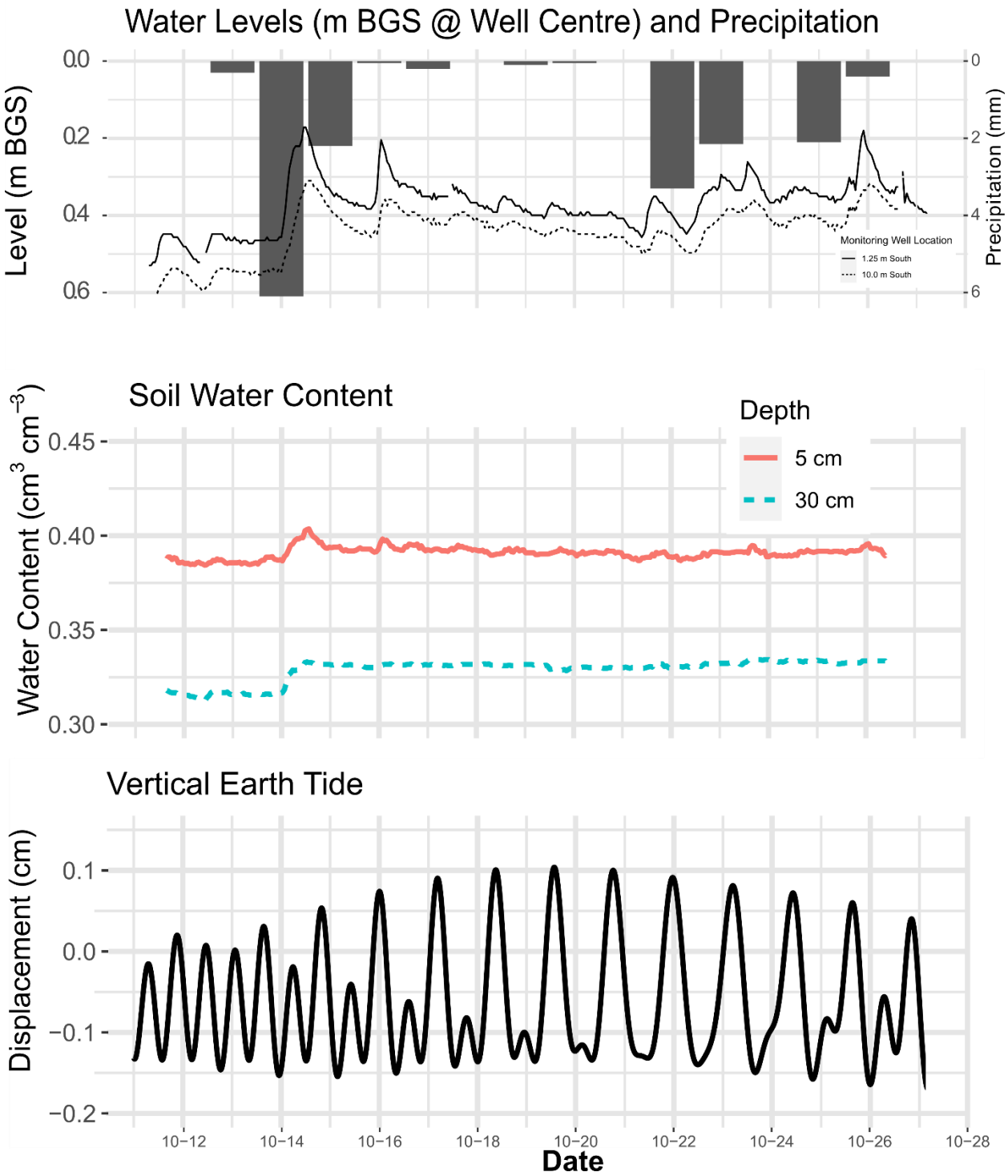

Figure S.9b Time series records of explanatory environmental factors considered in the stepwise general additive regression model

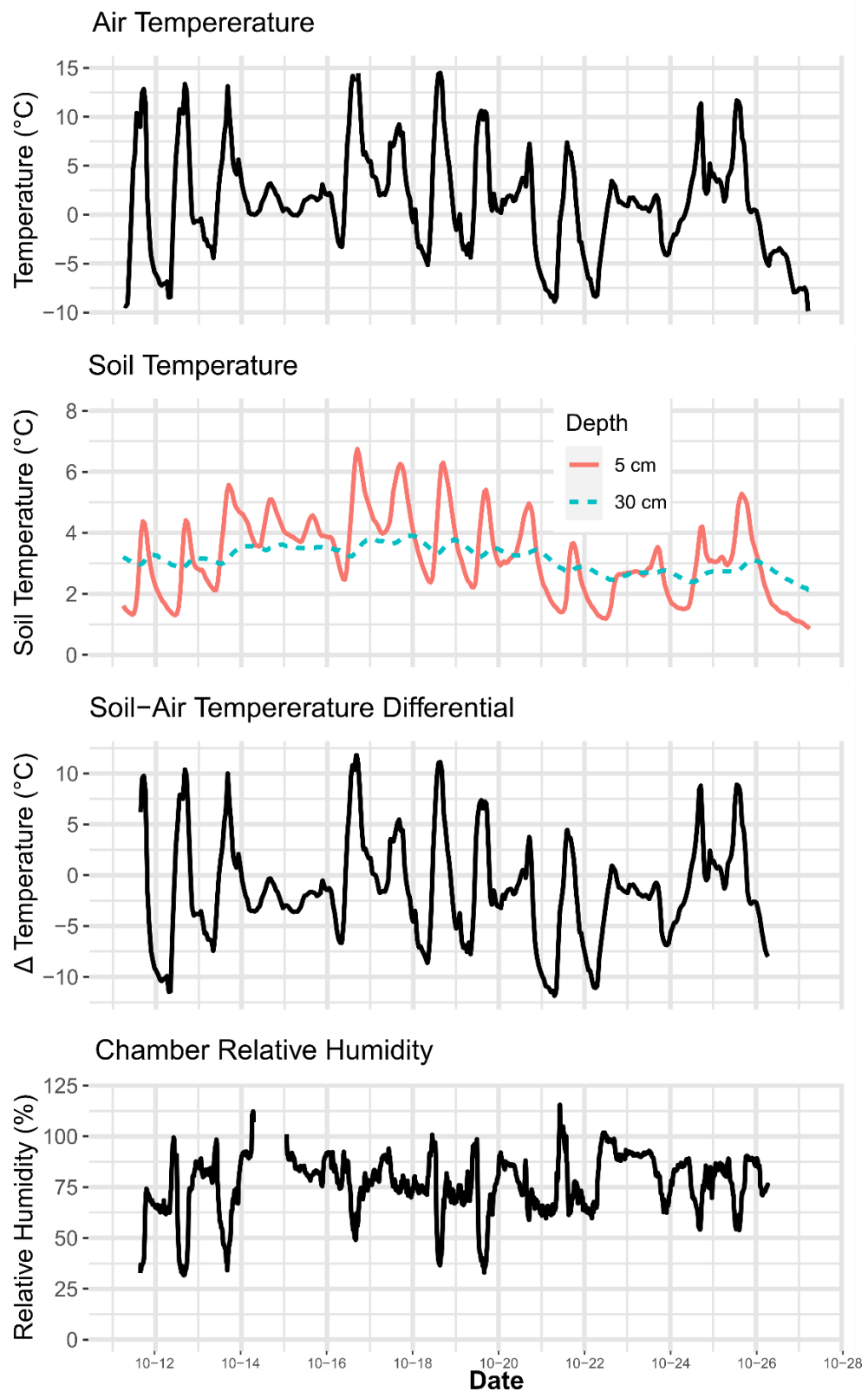

Figure S. 9c Time series records of explanatory environmental factors considered in the stepwise general additive regression model

Table S3 Summary of stepwise generalized additive modeling of raw CH_4 efflux for each long-term chamber location. ΔR^2 indicates the decrease in full model R^2 fit to raw flux data through removal of each factor. Blank parameters were not included in the full model, at significance of 0.001. Model parameters were Relative Humidity (RH), Absolute barometric pressure (Baro_P), atmospheric temperature (T_atm), approximate barometric pressure change rate (Baro_dP_dt), piezometer water level (Wat.Lev.), approximate change in water level (dWat.Lev_dt), soil temperature at 0.05 m (T_soil_0.05 m) and 0.3 m (T_soil_0.3) below ground surface (BGS), soil water content at 0.05 m (Wat.Cont_0.05) and 0.3 m (WC 0.3) BGS, temperature difference between the atmosphere and 0.3 m soil depth, vertical Earth tide displacement (E_tide), and wind speed (U_wind).

	Wellhead Chamber	**0.5 SE**	**0.5 NE**	**1.0 S**	**2.5 N**	**5.0 S**
	Full Model Fit R^2					
	0.63	0.86	0.15	0.11	0.19	0.19
	Single variable backward removal ΔR^2					
RH	0.02	0.01	0.01			
Baro_P	0.01					
T_atm	0.12		0.04			
Baro_dP_dt	0.02				0.08	
Wat.Lev.		0.01		0.01	0.00	
dWat.Lev.dt	0.01	0.09	0.02	0.02		
T_soil_0.05	0.01					0.04
T_soil_0.3	0.05	0.02	0.02	0.00		
Wat.Cont_0.05	0.01	0.01				
Wat.Cont_0.3	0.02	0.20	0.01		0.03	
Temp_Diff					0.00	0.12
E_tide	0.01		0.01	0.01		
U_wind	0.11	0.01	0.03	0.05		

Table S4 Parameters most influencing the statistical model for the first three steps of forward stepwise multivariate generalized additive modelling of CH_4 Efflux at each long-term chamber location. Model formulae are in the form: FCH4 ~ $Parameter_1$ + $Parameter_2$ …. The Akaike information criterion (AIC) is listed at each step as an indication of incremental goodness of fit. Factor abbreviations are: U_wind (windspeed), Temp_Diff (temperature differential between 30 cm depth soil and the atmosphere); Wat.Cont_0.3 (30 cm depth soil water content), T_soil_0.05 (soil temperature at 5 cm depth), Baro_dP_dt (approximated barometric pressure change rate), T_atm (atmospheric temperature), Wat.Lev (piezometer water level), dWat.Lev.dt (approximate water level change rate)

Chamber	Step:1	Step:2	Step:3
Wellhead	U_wind ; 15378	T_atm + U_wind ; 15248	T_atm + s(U_wind, df = 2) ; 15176
0.5 SE	Wat.Cont_0.3 ; 3876	Wat.Lev + Wat.Cont_0.3 ; 3575	Wat.Lev. + s(Wat.Cont_0.3, df = 2) ; 3423
0.5 NE	T_atm ; -2339	T_atm + U_wind ; -2368	T_atm + dWat.Lev.dt + U_wind ; -2385
1.0 S	U_wind ; -673	WL + U_wind ; -687	Wat.Lev. + dWat.Lev.dt + U_wind ; -695
2.5 N	Temp_Diff ; -587	Baro_dP_dt + Temp_Diff ; -591	s(Baro_dP_dt, df = 2) + Temp_Diff ; -594
5.0 S	Temp_Diff ; -462	s(Temp_Diff, df = 2) ; -465	T_0.05 + s(Temp_Diff df = 2) ; -468

df refers to the degrees of freedom of the smooth fitting function (1 if not indicated)

Table S5 Summary of stepwise generalized additive modeling of raw CH_4 pre-closure concentrations for each long-term chamber location. ΔR^2 indicates the decrease in full model R^2 fit to raw flux data through removal of each factor. Blank parameters were not included in the full model, at significance of 0.001. Model parameters were Relative Humidity (RH), Absolute barometric pressure (Baro_P), atmospheric temperature (T_atm), approximate barometric pressure change rate (Baro_dP_dt), piezometer water level (Wat.Lev.), approximate change in water level (dWat.Lev_dt), soil temperature at 0.05 m (T_soil_0.05 m) and 0.3 m (T_soil_0.3) below ground surface (BGS), soil water content at 0.05 m (Wat.Cont_0.05) and 0.3 m (WC 0.3) BGS, temperature difference between the atmosphere and 0.3 m soil depth, vertical Earth tide displacement (E_tide), and wind speed (U_wind).

	Wellhead Chamber	**0.5 SE**	**0.5 NE**	**1.0 S**	**2.5 N**	**5.0 S**
	Full Model Fit R^2					
	0.52	0.37	0.21	0.22	0.33	0.58
	Single variable backward removal ΔR^2					
RH	0.01	0.04	0.01			0.01
Baro_P	0.05	0.01		0.02	0.01	0.08
T_atm	0.03	0.01	0.00	0.02	0.02	0.06
Baro_dP_dt	0.05	0.05	0.02	0.01	0.03	0.03
Wat.Lev.	0.01	0.03	0.00			0.01
dWat.Lev.dt	0.03	0.03	0.02			
T_soil_0.05	0.01	0.08	0.01	0.01	0.01	0.01
T_soil_0.3	0.08		0.00			0.03
Wat.Cont_0.05	0.01		0.00	0.02		0.00
Wat.Cont_0.3		0.00	0.01	0.01	0.03	
Temp_Diff		0.01		0.02		
E_tide				0.00		0.01
U_wind	0.09	0.02	0.05	0.04	0.05	0.04

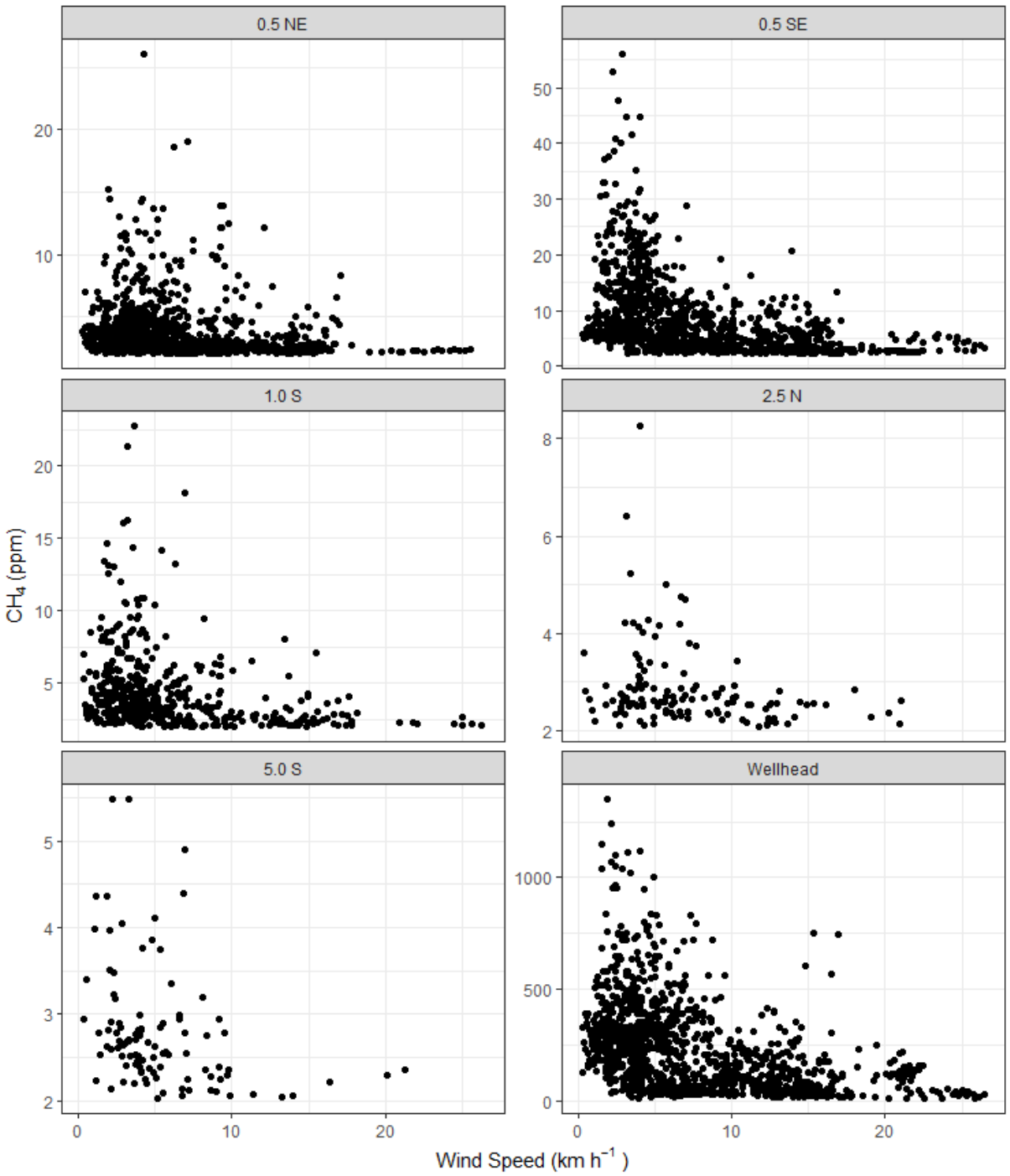

Figure S10 Wind speed from the nearest weather station (km h^{-1}) with respect to initial CH_4 chamber concentrations in ppm for all detectable efflux measurements over the full two-week long-term measurement period, showing higher measured initial concentrations during periods of lower wind speed.

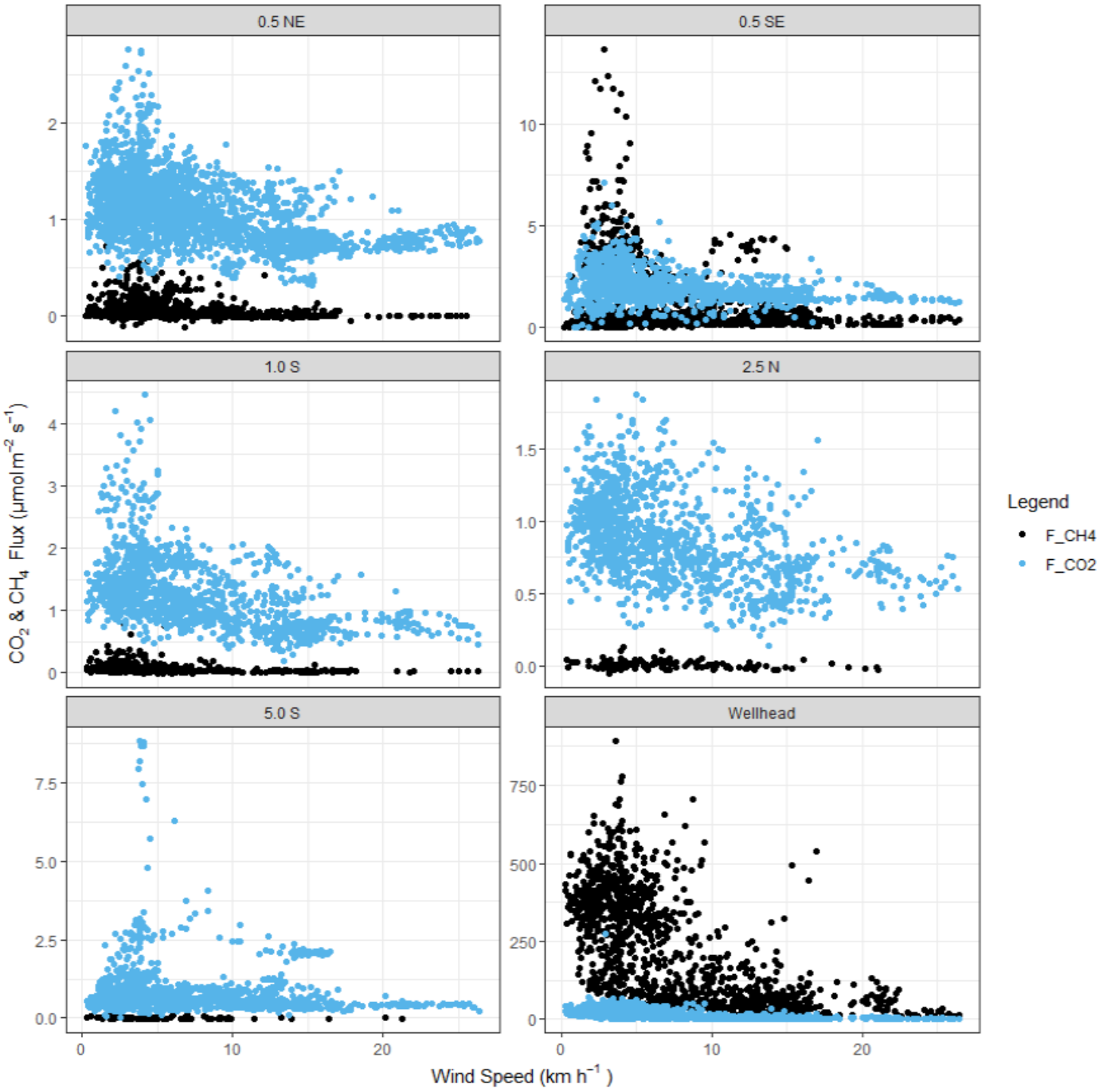

Figure S11 All detectable linear CH_4 (black) and CO_2 (blue) effluxes in µmol m^{-2} s^{-1} over the full two-week long-term measurement period with respect to wind speed from the nearest weather station (km h^{-1}), showing higher measured effluxes during periods of lower wind speed.

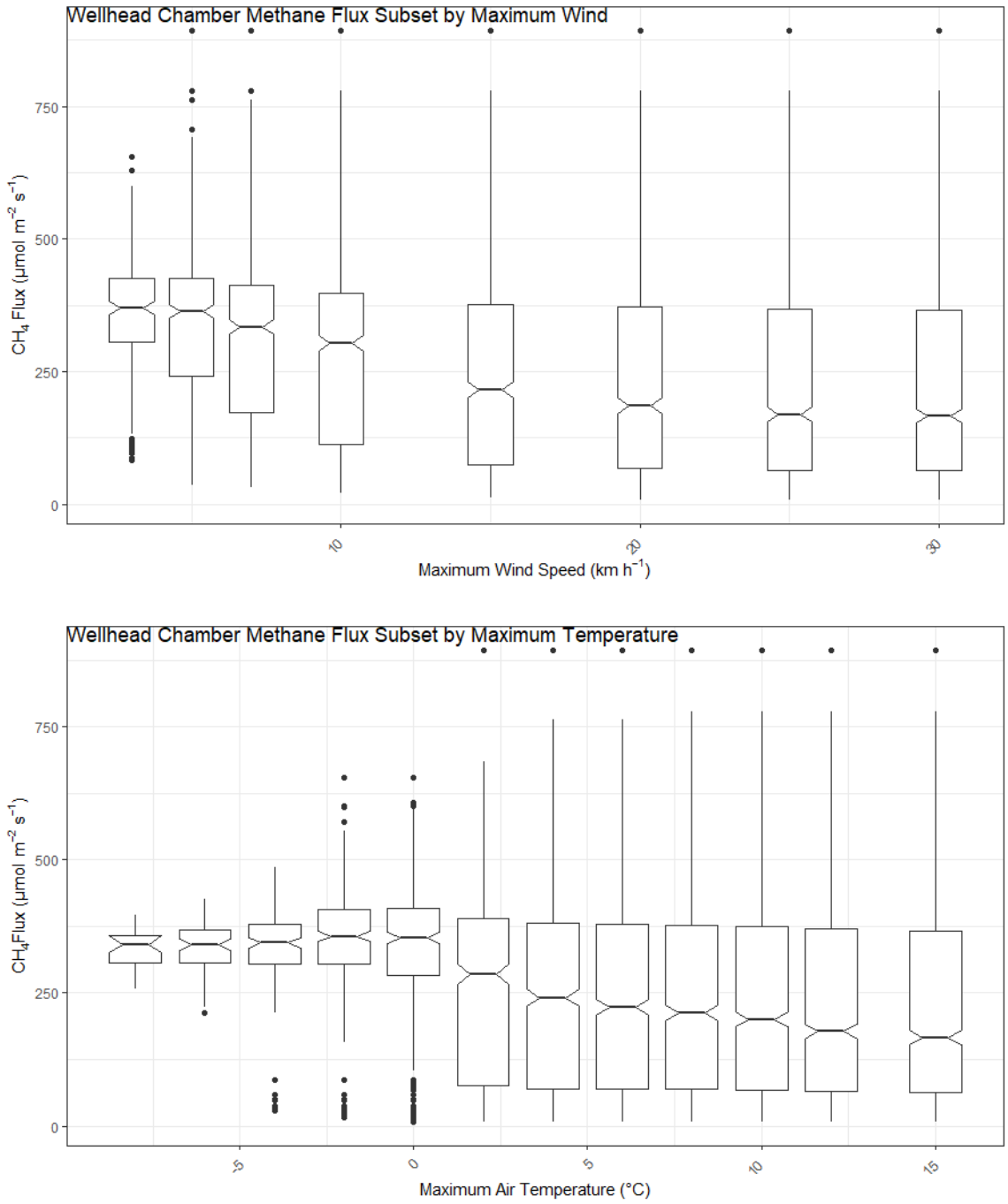

Figure S12 Boxplots of wellhead chamber methane efflux in µmol m^{-2} s^{-1} subset by maximum wind speeds (top) and maximum temperature (bottom). Boxplots illustrate the minimum, 1st quartile, median, 3rd quartile, and maximum. Outliers greater than 1.5 times the interquartile range above or below the 1st and 3rd quartile are marked as points.